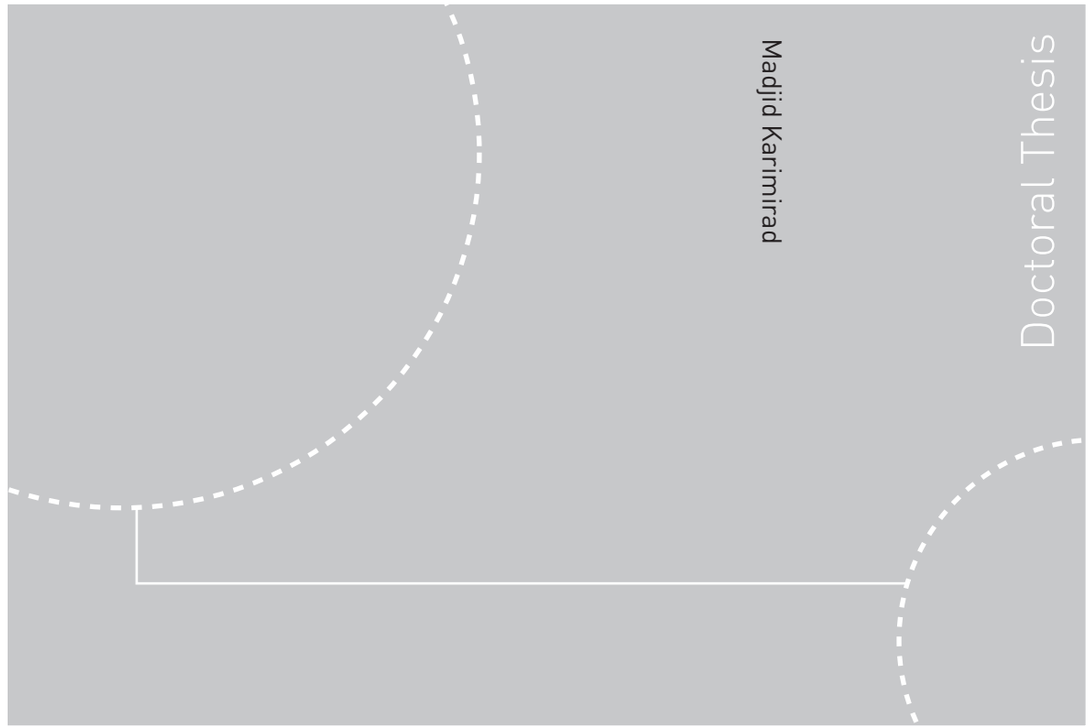

ISBN 978-82-471-2526-7 (printed ver.)
ISBN 978-82-471-2527-4 (electronic ver.)
ISSN 1503-8181

NTNU
Norwegian University of
Science and Technology

Doctoral theses at NTNU, 2011:8

Madjid Karimirad

Stochastic Dynamic Response Analysis of Spar-Type Wind Turbines with Catenary or Taut Mooring Systems

NTNU
Norwegian University of
Science and Technology
Thesis for the degree of
philosophiae doctor
Faculty of Engineering Science and Technology
Department of Marine Technology

Doctoral theses at NTNU, 2011:8

NTNU

NTNU
Norwegian University of
Science and Technology

Madjid Karimirad

Stochastic Dynamic Response Analysis of Spar-Type Wind Turbines with Catenary or Taut Mooring Systems

Thesis for the degree of philosophiae doctor

Trondheim, March 2011

Norwegian University of
Science and Technology
Faculty of Engineering Science and Technology
Department of Marine Technology

NTNU
Norwegian University of
Science and Technology

NTNU
Norwegian University of Science and Technology

Thesis for the degree of philosophiae doctor

Faculty of Engineering Science and Technology
Department of Marine Technology

ISBN 978-82-471-2526-7 (printed ver.)
ISBN 978-82-471-2527-4 (electronic ver.)
ISSN 1503-8181

Doctoral Theses at NTNU, 2011:8

Printed by Tapir Uttrykk

Dedicated to
my dear parents and my beloved wife

Abstract

Floating wind turbines can be the most practical and economical way to extract the vast offshore wind energy resources at deep and intermediate water depths. The Norwegian Ministry of Petroleum and Energy is strongly committed to developing offshore wind technology that utilises available renewable energy sources. As the wind is steadier and stronger over the sea than over land, the wind industry recently moved to offshore areas. Analysis of the structural dynamic response of offshore wind turbines subjected to stochastic wave and wind loads is an important aspect of the assessment of their potential for power production and of their structural integrity.

Of the concepts that have been proposed for floating wind turbines, spar-types such as the catenary moored spar (CMS) and tension leg spar (TLS) wind turbines seem to be well-suited to the harsh environmental conditions that exist in the North Sea. Hywind and Sway are two examples of such Norwegian concepts; they are based on the CMS and TLS, respectively.

Floating wind turbines are sophisticated structures that are subjected to simultaneous wind and wave actions. The coupled nonlinear structural dynamics and motion response equations of these turbines introduce geometrical nonlinearities through the relative motions and velocities. Moreover, the hydrodynamic and aerodynamic loading of this type of structure is nonlinear. A floating wind turbine is a multibody aero-hydro-servo-elastic structural system; for such structures, the coupled nonlinear equations of motion considering nonlinear excitation and damping forces, including all wave- and wind-induced features, should be solved in the time domain. In this thesis, the motion and structural responses for operational and extreme environmental conditions were considered to investigate the performance and the structural integrity of spar-type floating wind turbines. The power production and the effects of aerodynamic and hydrodynamic damping, including wind-induced hydrodynamic and wave-induced aerodynamic damping, were investigated.

Negative damping adversely affects the power performance and structural integrity. In this thesis, the controller gains were tuned to remove servo-induced instabilities. The rotor configuration effect on the responses and power production was investigated by comparing the upwind and downwind turbines.

To develop robust design tools for offshore wind power, the competencies of the offshore technology and wind technology must be combined. Both the offshore and wind energy industries have begun to extend their existing numerical codes to account for the combined aerodynamic and hydrodynamic effects on the structure. As a result verifications of extended codes by doing experiments and code-to-code comparisons are needed. One of the aspects of the present research was to fill this gap by performing hydrodynamic and hydro-elastic comparison between commercial codes. For both CMS and TLS concepts, the comparisons were carried out prior to using the tools to study the behaviour of the CMS and TLS under wave- and wind-induced loads.

Offshore structures encounter a variety of operational and harsh environmental conditions. Limit states such as ultimate, fatigue, accidental collapse and serviceability limit states (ULS, FLS, ALS and SLS) are defined as the design criteria for offshore structures. In performing realistic ultimate limit state analysis, the extreme responses of a floating wind turbine over its life should be estimated. This estimation requires detailed analysis of the extreme response. In the present thesis, extreme value analysis for spar-type wind turbines subjected to simultaneous wave and wind actions was preformed. The structural responses and the effect of modelled forces such as turbulence on these responses were investigated. The joint distribution of the environmental characteristics of the wave and wind was applied through the contour surface method.

Stochastic wave and wind analysis showed that, while rigid body modelling was sufficient for obtaining accurate motions, consideration of the elastic behaviour of the tower/support structure was necessary to predict structural responses. The blades structural responses were found to be significantly affected by the turbulent wind. However, the mean and standard deviation of global motion and structural responses were not affected by the turbulence. Thus, to reduce the simulation time in fatigue analysis, a constant wind speed model can be applied. The CMS and TLS wind turbines are inertia-dominated structures, and the hydrodynamic viscous drag did not affect their wave-induced responses, while an increase in viscous drag could effectively reduce the resonant responses of such turbines. Under operational conditions, aerodynamic damping was found to be active in reducing both wave frequency and resonant responses. The results showed that, for a floating wind turbine, extreme response could occur in survival conditions, while for a fixed wind turbine, the extreme response occurs in operational cases related to the rated wind speed. To estimate the extreme value responses, extrapolation methods were used to reduce the sample size in Monte Carlo simulations. The accuracy of methods to estimate the extreme responses as a function of sample size and methods applied was investigated. The normalized responses for both CMS and TLS offshore wind turbines were presented to draw more generalized conclusions.

Acknowledgements

First of all, I would like to thank my supervisor, Professor Torgeir Moan. He gave me the chance to be an independent researcher. During my Ph.D. studies, he helped me to overcome a number of scientific challenges and taught me to be the main director of the research. His great experiences in doing research for more than 35 years and handling the most sophisticated challenges in the field of offshore technology provided an invaluable outcome: he taught me the philosophy of science and technology. During my Ph.D. studies at the Centre for Ships and Ocean Structures (CeSOS/NTNU), I have learned many things, especially from Professor Moan. These includes trying and working hard, having overall picture of the research in mind, reviewing the theories and methodologies carefully, reading the works of others, being positive and helpful, communicating kindly, being patient, listening and answering gently, remembering important things, following the news about my professional carrier, increasing my knowledge day to day and being innovative and curious. I appreciate Professor Moan's supervision, teaching, invaluable advices and support during my study.

Many other people also supported and helped me during my Ph.D. studies. Dr. Zhen Gao, currently a postdoctoral fellow at CeSOS/NTNU, helped me through useful discussions from the first year of my research; he is also the co-author of two of my papers. I would like to thank Dr. Jason Jonkman, form NREL, for helpful discussions regarding the wind turbines and the FAST code. My thanks also go to Dr. Nilanjan Saha, currently a postdoctoral fellow at CeSOS/NTNU, for discussions about stochastic analysis. Special thanks go to Prof. Jørgen Amdahl from NTNU and Dr. Tore Holmas from Virtual Prototyping for discussions about the USFOS/vpOne code. I thank Mr. Quentin Meissonier for his close cooperation on the modelling of the TLS. I would like to acknowledge Prof. Sverre Haver from Statoil for discussions about environmental conditions and for providing the wave data, Prof. Finn Gunnar Nielsen from Statoil for discussions regarding hydrodynamics and floating wind turbine concepts and Dr. Ivar Fylling at Marintek for discussions about floating wind turbines. Thanks go to Dr. Rune Yttervik and Dr. Bjørn Skaare from Statoil for discussions about Hywind concept, mooring lines, power output and for providing some data for the spar platform. I would like to thank Prof. Jakob Mann, Torben J. Larsen and Dr. Anders Melchior Hansen for discussions about aerodynamics and the HAWC2 code, developed at Risø DTU.

It is my pleasure to complete my Ph.D. at CeSOS, the unique Centre for Ships and Ocean Structures; with its experienced director, Prof. T. Moan, this centre provides a dynamic, international and well-known research environment.

I also wish to acknowledge the financial support from the Research Council of Norway through CeSOS, NTNU.

I would like to thank all my professors and colleagues at CeSOS and at the Department of Marine Technology/NTNU for their excellent lectures and kind help in the past several years, including Profs. Odd M. Faltinsen, Carl M. Larsen, Arvid Naess, Bernt J. Leira and many other researchers and Ph.D. candidates, such as my office mate Giri Raja Sekhar Gunnu.

Finally, I am pleased to thank my family in Iran and my wife, Soosan, and our daughter, Dorsa, here in Norway.

Madjid Karimirad

24 January 2011
Trondheim, Norway

List of Appended Papers

The present thesis consists of an introductory part and nine papers (four journal papers and five conference papers).

The following nine papers are reported in the Appendix:

Paper 1:
Dynamic Motion Analysis of Catenary Moored Spar Wind Turbine in Extreme Environmental Condition
Madjid Karimirad, Zhen Gao and Torgeir Moan
Published in the proceedings of the European Offshore Wind Conference, EOW2009, September 2009, Stockholm, Sweden

Paper 2:
Wave and Wind Induced Dynamic Response of Catenary Moored Spar Wind Turbine
Madjid Karimirad and Torgeir Moan
Accepted for publication in the Journal of Waterway, Port, Coastal, and Ocean Engineering, ASCE

Paper 3:
Effect of Aerodynamic and Hydrodynamic Damping on Dynamic Response of Spar Type Floating Wind Turbine
Madjid Karimirad and Torgeir Moan
Published in the proceedings of the European Wind Energy Conference (EWEC2010), April 2010, Warsaw, Poland

Paper 4:
Extreme Structural Dynamic Response of a Spar Type Wind Turbine
Madjid Karimirad and Torgeir Moan
Published in the proceedings of the 29th International Conference of Offshore Mechanics and Arctic Engineering (OMAE2010), June 2010, Shanghai, China

Paper 5:
Extreme Dynamic Structural Response Analysis of Catenary Moored Spar Wind Turbine in Harsh Environmental Conditions
Madjid Karimirad and Torgeir Moan
Accepted for publication in the Journal of Offshore Mechanics and Arctic Engineering (JOMAE), ASME

Paper 6:
Hydro-elastic Code-to-Code Comparison for a Tension Leg Spar Type Floating Wind Turbine
Quentin Meissonnier, Madjid Karimirad, Zhen Gao and Torgeir Moan
Submitted to the Journal of Marine Structures (a revised-version of this paper will be published in the journal and as agreed among the authors, ***Madjid Karimirad*** will be the first-author in the final-paper)

Paper 7:
Ameliorating the Negative Damping in the Dynamic Responses of a Tension Leg Spar-Type Support Structure with a Downwind Turbine
Madjid Karimirad and Torgeir Moan
Accepted for an oral presentation and publication in the European Wind Energy Conference (EWEC2011), March 2011, Belgium

Paper 8:
Tension Leg Spar-Type Offshore Wind Turbine with Upwind or Downwind Rotor Configuration
Madjid Karimirad and Torgeir Moan
Accepted for an oral presentation and publication in the AWEA-WINDPOWER2011 Conference, May 2011, Anaheim, CA, USA

Paper 9:
Stochastic Dynamic Response Analysis of a Tension Leg Spar-Type Offshore Wind Turbine
Madjid Karimirad and Torgeir Moan
Submitted for publication

Declaration of authorship

Regarding the authorship of these nine papers and my contributions, I am the first author of eight of the papers, and I was responsible for establishing the models, performing the calculations, providing the results and writing all papers under the supervision of Prof. Torgeir Moan. He is the co-author of all the papers and made helpful corrections and comments to all my papers. Zhen Gao (the second author of the *Paper 1*) helped me in hydrodynamic comparison. Torgeir Moan initiated the *Paper 6*. Torgeir Moan and Zhen Gao, the third author of the *Paper 6*, made helpful comments for this paper. Quentin Meissonnier and I had very close cooperation in the modelling and performing the analysis for *Paper 6*. I am the second author and the corresponding author of the *Paper 6*; and I worked actively on the modelling, analysis, obtaining the results and writing of that paper.

Additional papers

The following two papers written during the study are not included in this thesis:

Other paper 1:
Wave and Wind Induced Motion Response of Catenary Moored Spar Wind Turbine
Madjid Karimirad and Torgeir Moan
Published in the proceeding of the Computational Methods in Marine Engineering Conference 2009, June 2009, Norway
(not considered as a part of the thesis because it is a short predecessor to *paper 2*)

Other paper 2:
Offshore Code Comparison Collaboration within IEA Wind Task 23: Phase IV Results Regarding Floating Wind Turbine Modeling
J. Jonkman, National Renewable Energy Laboratory (NREL), United States of America; T. Larsen and A. Hansen, Risø National Laboratory, Technical University of Denmark (Risø-DTU), Denmark; T. Nygaard, Institute for Energy Technology (IFE), Norway; K. Maus, Norwegian University of Life Sciences (UMB), Norway; ***Madjid Karimirad***, Z. Gao and T. Moan, Norwegian University of Science and Technology (NTNU), Norway; I. Fylling, Marintek, Norway; J. Nichols, Garrad Hassan & Partners Limited (GH), United Kingdom; M. Kohlmeier, ForWind, Leibniz University of Hannover (LUH), Germany; J. Pascual Vergara and D. Merino, Acciona Energia, Spain; W. Shi and H. Park, Pohang University of Science and Technology (POSTECH), Korea

Published in the proceeding of the European Wind Energy Conference (EWEC2010), April 2010, Warsaw, Poland
(not included in the thesis because my contribution to this paper is limited due to its multiple authorship)

Nomenclature

Abbreviation

ALS	Accidental Limit State
BEM	Blade Element Momentum theory
CB	Centre of Buoyancy
CFD	Computation Fluid Dynamic methods
CG	Centre of Gravity
CMS	Catenary Moored Spar
DLL	Dynamic Link Library
FEM	Finite Element Method
FLS	Fatigue Limit State
FWT	Floating Wind Turbine
HAWT	Horizontal Axis Wind Turbine
HSS	High Speed Shaft
IEC	International Electrotechnical Commission
IFFT	Inverse Fast Fourier Transformation
IFORM	Inverse First-Order Reliability Method
JONSWAP	Joint North Sea Wave Project
MW	Megawatt
MWL	Mean Water Level
NS	Navier-Stokes
PID	Proportional Integral Derivative
PM	Pierson-Moskowitz
SLS	Serviceability Limit State
STD	Standard deviation
TLP	Tension Leg Platform
TLS	Tension Leg Spar
ULS	Ultimate Limit State

Roman symbols

a_x	Water particle acceleration in x-direction (wave propagation direction)
A	Frequency dependent added mass

A_S	Swept area of wind turbine rotor
c_w	Scale parameter
C	Frequency dependent potential damping matrix
C_{aero}	Aerodynamic coefficient
C_P	Power coefficient
dT / dV	Slope of the thrust curve versus the wind speed
D	Characteristic diameter
D_{aero1}	Linear wave induced aerodynamic damping matrix
D_{aero2}	Quadratic wave induced aerodynamic damping matrix
D_{hydro1}	Linear viscous hydrodynamic damping matrix
D_{hydro2}	Quadratic viscous hydrodynamic damping matrix
E	Elastic modulus
EI	System bending stiffness
f	Frequency in hertz
f_{Thrust}	Thrust force
f_W	Weibull probability density function
F	Exciting force vector
$F_{Generalized}$	Generalized force vector
h	Mean water depth
h_{agl}	Height above ground level
H	Wave height
H_S	Significant wave height
I	Area moment of inertia
I_t	Turbulent intensity
k	Wave number
k_{ms}	Mooring system stiffness
k_w	Shape parameter
K	Position dependent hydrostatic stiffness matrix
K_{Pitch}	Pitch rigid body motion stiffness
$K_{\theta_{mooring}}$	Mooring stiffness in pitch motion
KG	Distance of the centre of gravity (CG) from the MWL
KB	Distance of the centre of buoyancy (CB) from the MWL
l	Length scale
L	System length
m	Body mass matrix

m_a	Added mass
$m_{nacelle}$	Mass of the nacelle
m_{rotor}	Mass of the rotor
m_{spar}	Mass of the spar
m_{top}	Mass of the nacelle and the rotor together at the top of the tower
m_{tower}	Mass of the tower
M	Frequency dependent mass matrix
P	Electrical generated power
r	Structural displacement vector
$\dot{r}$	Structural velocity vector
$\ddot{r}$	Structural acceleration vector
$R(t)$	Retardation function
R^D	Damping force vector
R^E	External force vector
R^I	Inertia force vector
R^S	Internal structural reaction force vector
t	Time
T	Total time
T_P	Wave peak period
S	Spectrum (wave or wind)
u	Water particle velocity in x-direction (wave propagation direction)
V	Wind velocity
V_{rel}	Relative velocity
V_{Annual}	Annual mean wind speed
$V_{10\,\mathrm{min}}$	10 minute averaged wind speed
x	Position vector including translations and rotations
z	Vertical coordinate axis (upward)
z'	Scaled vertical coordinate axis (upward)

Greek symbols

ς	Regular wave elevation
ς_a	Regular wave amplitude
λ	Wave length
ρ	Fluid density (water or air)
σ	Standard deviation
ω	Frequency (rad/sec)

ω_{eigen}	System elastic natural frequency
ω_n	Nth frequency (wave or wind)
φ_n	Phase angle
Δt	Time increment
∇	Submerged volume

Table of Contents

Chapter 1

Introduction

1.1 General background

Demand for renewable and reliable energy due to global warming, environmental pollution and the energy crisis deeply challenges researchers today. Wind, wave, tidal, solar, biological and hydrological forces are potential resources for generating the desired power. Among these sources, wind seems to be the most reliable and practical, with its annual increase rate of 25-30% (Sclavounos et al. 2010 and Henderson et al. 2002). The International Energy Agency (IEA) suggests that, with concentrated effort and technology innovation, wind power could supply up to 12% of global demand for electricity by 2050 (IEA 2008).

Wind has been used to generate power for many years on land and at sea. Its first use was propelling boats at sea. Milling grain and raising water from streams using wind energy was introduced with the first windmills in Persia in the tenth century (Spera 1998). It has been claimed that the Crusaders introduced windmills based on wood construction in Europe around the eleventh century (Ahlstrom 2005). Modern wind turbines that generate electricity were developed after the Industrial Revolution. The mega-watt scale wind turbine was started in the USA in late 1930 (Ahlstrom 2005).

For several decades, the land-based wind turbines have been used to generate green energy. Presently, the best onshore sites are already in use, and neighbours have been complaining aplenty in an overcrowded Europe. Land-based wind turbines are associated with visual and noise impacts that make it increasingly difficult to find appropriate and acceptable sites for future growth. Hence, wind engineering has moved offshore to find suitable sites for generating green electricity via ocean wind resources (Jonkman 2007 and 2009). Offshore wind turbines offer some advantages in that they cannot be seen or heard. Moreover, the offshore wind is steadier and stronger, which helps produce more electricity.

Following a number of large research projects, offshore wind turbines were mounted in Sweden, Denmark and the Netherlands in the early 1990s (Tempel 2006). Today, offshore wind power is approximately 1% of total installed capacity, but this capacity has been increasing very rapidly. By the end of 2007, 1100 MW capacities were installed offshore by five countries: Sweden, Denmark, Ireland, Netherlands and the UK (Twidell and Gaudiosi 2008).

Archer and Jacobson (2005) produced a worldwide wind atlas based on data from about 8000 locations. Wind speeds were calculated at 80 m. In the Figure 1.1, the wind atlas for Europe is illustrated (Archer et al. 2005); it clearly illustrates the potential of offshore wind resources for Europe.

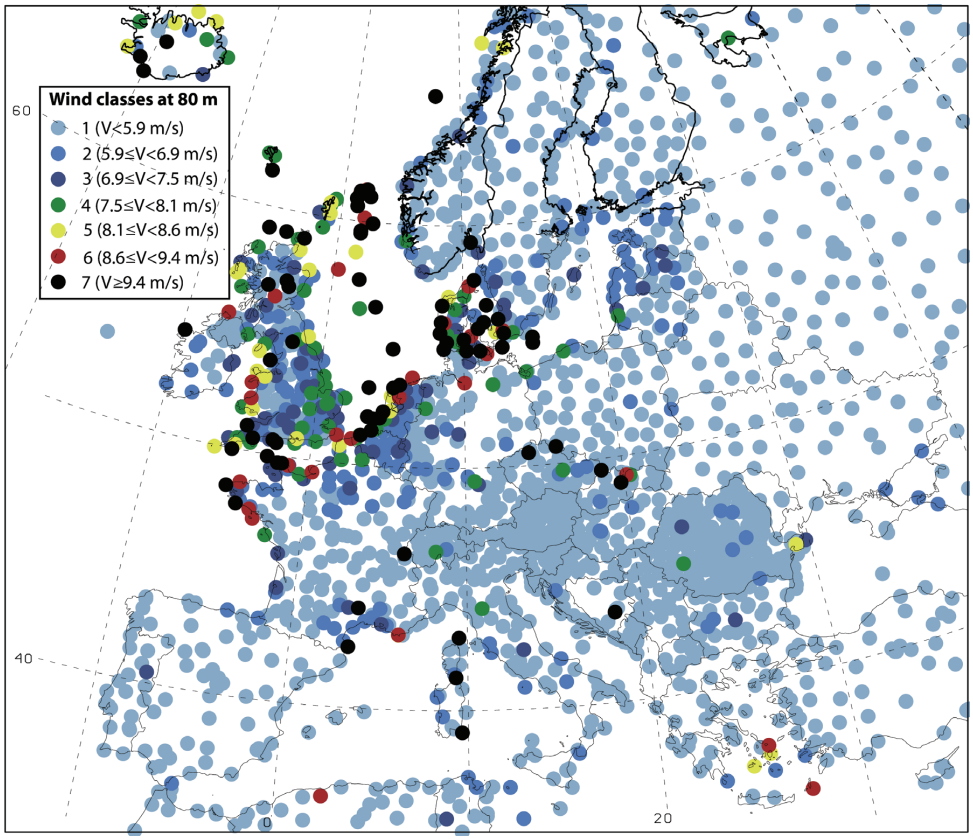

Figure 1.1: Europe wind atlas (Archer et al. 2005).

Offshore wind power will help alleviate some of the problems associated with land-based wind turbines, such as noise from turbine parks, visual pollution and lack of space. However, the practical fixed offshore wind power is limited by the following constraints (Twidell and Gaudiosi 2008):

- Cost

- Installation
- Distance from shore, grid connections
- Water depth
- Locations due to environmental considerations
- Conflicts with military and shipping routes and fisheries

In some countries, such as the USA, Norway and Japan, there is good wind power potential in deep water zones (Sclavounos et al. 2007). In recent years, the floating wind turbine (FWT) has been introduced as the most cost-effective solution for the production of wind energy in deep water zones. Further from the shore, the wind is more stable and stronger. Additionally, conflicts with tourism, military and naval forces, sailing and shipping are decreased when the turbines are placed a greater distance offshore.

1.1.1 Wind turbines

The wind turbine is simply an energy-converting structure that converts the kinetic energy of the wind to electrical power through a mechanical/electrical mechanism. Some features of wind turbine topologies, mentioned by Manwell (2006) are as following:

- Rotor axis orientation: horizontal or vertical
- Power control: stall, pitch, yaw and aerodynamic surfaces
- Rotor position: upwind or downwind of tower
- Yaw control: free or active
- Rotational speed: constant or variable
- Tip speed ratio and solidity
- Hub: rigid, teetering, hinged blades or gimballed
- Rigidity: flexible or stiff
- Number of blades
- Tower structure
- Design constraints such as installation and maintenance

According to the Rankine-Froude theory, the power (P) generated by a wind turbine can be written in the form of Equation 1.1, where C_P is the power coefficient, ρ is the air density, A_S is the swept area of the wind turbine rotor, and V is the wind velocity.

$$P = 0.5\, C_P\, \rho\, A_S\, V^3 \tag{1.1}$$

Based on the simple relation between the wind speed and the power in Equation 1.1, we can deduce that a 10% increase in the wind speed results in a 33% increase in power. This example shows the possibility of producing more power through offshore wind as the wind over the sea is stronger.

1.1.2 Horizontal axis wind turbines

A horizontal axis wind turbine (HAWT) usually consists of three blades connected to a hub. The low-speed shaft connects the hub to the gearbox and the gearbox connects the high-speed and low-speed shafts. The gear box and shafts are often called the 'drive train'. The high-speed shaft drives the generator to make power. The gearbox and generator are set in the nacelle on the top of the tower. In the pitch-regulated wind turbines, it is possible to turn the blades around a longitudinal axis to adjust the aerodynamic forces on the blades by changing the angle of attack. The yaw system aligns the rotor toward the incoming wind by rotating the nacelle around the tower axis. The blades have the shape of an airfoil, so that the airflow that passes the blades exerts aerodynamic lift and drag forces on the blade. These forces result in a torque on the gearbox. The gearbox raises the rotational speed and lowers the torque from the rotor to convert the mechanical energy into electrical energy (Kallesøe 2007).

1.1.3 Offshore wind turbines

As mentioned earlier, offshore wind energy is booming rapidly. The visual impact, acoustic noise, and electromagnetic interference (TV, microwave and radar) of land-based wind turbines are some of the impacts that can be reduced by moving offshore. Offshore wind power is still not a mature technology, and new concepts will appear. However, these concepts will only be appropriate and interesting if they can deliver low-cost energy. The DTU scenario calculates a cost reduction of 35% by 2050 compared to today for offshore power (Twidell and Gaudiosi 2008).

Large offshore turbines can be easily transported by barges or ships. Furthermore, the wind strength is stronger and less turbulent over the sea than over land. An array of sizes for a wind farm is available offshore while land ownership can be an obstacle to having a large land-based wind turbine park. Land-based wind farm capacity is limited to 50 MW while in offshore applications more than 100 MW farm capacities are possible. Despite these clear advantageous, it is necessary to keep in mind some of the challenges of developing offshore wind power, such as logistics and foundations, electrical connection (grids) and maintenance.

The cost of fixed mounted offshore wind turbines increases with water depth, so that their use is not economical in some locations. In deep-water areas, floating wind turbines can be the most cost-effective and reasonable solution. Relevant technology for support structures for floating wind turbines is available from the offshore oil industry. The offshore oil and gas industry has previously experienced technological development challenges similar to those currently faced by the offshore wind energy industry. Offshore oil and gas production began with the use of fixed structures such as jackets and jack-up platforms in shallow waters and continued with floating concepts such as semisubmersibles, buoys, spars and tension leg

platforms in deep water areas. The lessons learnt can be used to minimise the development needed for offshore wind turbines by starting from the most reliable and robust concepts. Nevertheless the differences between the oil and gas offshore industry and the offshore wind industry should be kept in mind. For instance, offshore structures are commonly one-of-a-kind while a floating offshore wind turbine park would require a large numbers of identical support structures, i.e., mass production of structures (Henderson et al. 2002).

The purchase price of offshore wind electricity may be higher than onshore generated electricity due to the need for support structures and additional electric infrastructure such as grids. However, higher average wind speeds and lower turbulence can increase the amount of electricity produced offshore and cover the initial greater investment. For floating wind turbines, a large platform is preferable to minimise the motion responses, and the weight of the wind turbine compared to the support floating platform is less. Hence, it is possible to install larger wind turbines with capacities of 5-10 MW to minimise the cost of generated electrical power (ISSC 2009).

A variety of concepts for fixed offshore wind turbines have been introduced; these include monopiles, tripods, guided towers, suction buckets, lattice towers, gravity-based structures, piled jackets, jacket monopile hybrids, harvest jackets and gravity pile structures (DNV 2007). Most of these concepts were developed in the past decade for water depths of 5-50 m and have been used to build structures that now produce electrical power. Figure 1.2 illustrates some fixed offshore wind turbine structures. As mentioned above, it is not feasible to go further based on fixed mounted structures, because the cost increases rapidly and practical issues such as installation and design are affected by depth. In deep-water zones, the use of floating wind turbines provides more options for a proper solution for a specific site.

Several concepts for floating wind turbines (FWT) based on semisubmersible, spar, TLP, and ship-shaped foundations have been introduced (Roddier et al. 2009). Each of these concepts has its benefits and disadvantages, which should be considered based on site specifications such as water depth, environmental conditions (Met-ocean), distance to shore, and sea bed properties. Figure 1.3 illustrates some of the floating wind turbine concepts. Floating wind turbine components include the following:

- Mooring system including mooring lines, tendons and clump masses
- Fairleads and anchors
- Platform (i.e., spar) and tower
- Blades, nacelle and hub
- Gear box, low speed shaft, high speed shaft with its mechanical brake
- Electrical generator and electronic controller
- Pitch and yaw mechanisms
- Hydraulics system and cooling unit

- Anemometer and wind vanes

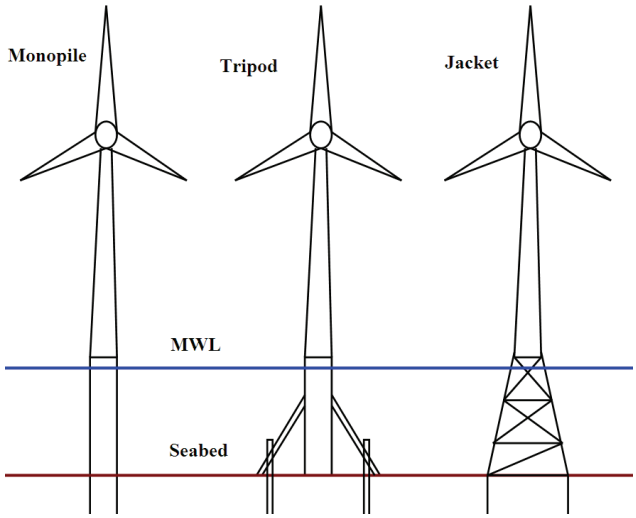

Figure 1.2: Fixed offshore wind turbines.

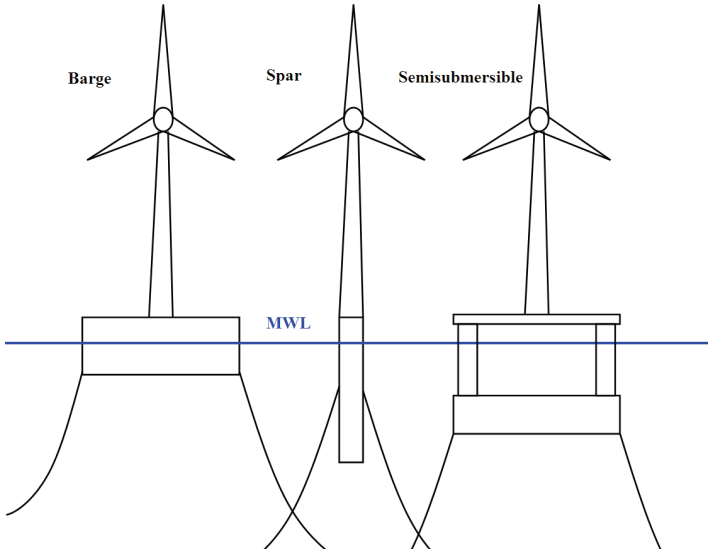

Figure 1.3: Floating offshore wind turbines.

Barge concepts are very simple and cheap to build, but their wave-induced response behaviour is weak. It is possible to use old, out-of-use ships as the base for wind turbines, but, like barges, ship-shaped structures are sensitive to wave loading. However, in calm seas such as the Persian Gulf and the Mediterranean, it is possible to use such a concept. Semisubmersible, TLP and spar-type FWTs are stabilized by water plane area, tension and buoyancy, respectively. The common characteristic of these types is that they are compliant in the horizontal plane, with surge and sway periods generally longer than 60 sec. In

conventional platforms, the natural period of the yaw motion is usually larger than 100 sec; this period is reduced to less than 10 sec in floating wind turbines to avoid turbulent wind excitation. The differences among these concepts are related to the motions in the vertical plane (DNV 2008), that is heave, roll and pitch. Mooring system, ballast and water plane area are the important design factors influencing the vertical motions. Combining these floating concepts into hybrid concepts by considering the required behaviour can provide a robust design with the advantages of different models (e.g., tension leg spar). The main challenge is to design an economically practical floating wind turbine. Butterfield et al. (2005) listed some key factors for finding the optimum platform as the support structure for a floating wind turbine:

- Requirements for design tools and methods
- Buoyancy tank cost
- Mooring line system cost
- Anchors cost
- Load out cost, complexity, options and requirements
- Onsite installation requirements
- Decommissioning and maintainability
- Corrosion resistance requirements: coatings, cathodic protection, etc.
- Depth dependence and depth range
- Required footprint (as a function of depth)
- System weight and central gravity sensitivity
- Induced tower top motions (wave sensitivity and allowable heal angle)
- Costs for candidate configurations

Of the concepts introduced for floating offshore wind turbines, the spar seems to be the most suitable concept for deep-water areas. The small water plane area and the deep draft of the spar reduce the heave excitation forces, which, in combination with the mass-dominated behaviour of this concept, provide very good heave motion performance. The spar concept is usually ballast-stabilised by setting the heavy ballast at the lower part of the structure and bringing down the centre of gravity, which has the most effective contribution to the pitch and roll motions. Mooring lines are used to keep the structure in position and reduce the surge and sway motions, a configuration that is suitable for power production purposes from wind turbines. It is possible to eliminate the wind-induced yaw motion by introducing the delta mooring lines for such a concept (Nielsen et al. 2006). Figure 1.4 illustrates the Hywind concept developed by Statoil, which was launched in 2009 and is located 10 km offshore of the Norway coast.

Figure 1.4: Hywind concept, 2.3 MW floating wind turbine (courtesy of Statoil).

The amount of available offshore energy depends on the site of the wind turbine park, the water depths and the diameter of the turbines, which is related to the installed power per wind turbine and the height of the turbine. Using offshore wind turbines in a location with 10 m/sec annual mean wind velocity it is possible to capture 5 MW from each km^2 of the ocean (ISSC 2006).

1.2 Dynamic response analysis

The entire structure composed of rotor, nacelle, tower, substructure (platform) and mooring system should be analysed using an integrated model. Gao et al. (2010) showed that for a fixed offshore jacket wind turbine, uncoupled dynamic analysis gives accurate results under certain conditions. However, this is not true for a floating wind turbine as the coupling of the top side and the floater is important (Karimirad et al. 2009a). For a floating wind turbine, the key issue is how to combine the highly nonlinear and dynamically responsive rotor, nacelle and tower with a dynamic substructure and mooring system. The model must include the gyroscopic loads of the wind turbine rotor on the tower and floater, the aerodynamic damping introduced by the rotor, the hydrodynamic damping introduced by wave-body interactions, and the hydrodynamic and the aerodynamic forces caused by wave and wind excitations (Wayman et al. 2006). Moreover, the nonlinear wave loading and nonlinear hydro-elastic response of the floater and the mooring system add to the complexity of the system (ISSC 2006). Accurate numerical tools that consider these complex aspects, including the flexibility and coupling of the turbine and platform, are needed (Butterfield 2007).

Model testing has been widely used in offshore engineering to determine the offshore platforms' wave-induced responses and to demonstrate feasibility of concepts and verify numerical tools. Unfortunately, it is not possible to build a scaled model of an operational wind turbine and attach it to a scaled floater. The behaviour of such a model wind turbine would not realistically mimic the response of a large-scale machine (Withee 2004). The reason for this is that the Froude scaling of the hydrodynamic and the Reynolds scaling of the aerodynamic loads cannot be simultaneously satisfied in a model. However, some useful data can be obtained by testing the scaled floating wind turbine in the ocean basin. Statoil tested a scaled model of the Hywind concept in the MARINTEK ocean basin before launching the full scale 2.3 MW floating wind turbine.

The time-domain/frequency-domain, uncoupled/integrated analysis, linear/nonlinear modelling, rigid/elastic body modelling, steady/turbulent wind simulation and linear/nonlinear wave theory are options for an integrated dynamic response analysis. For a floating wind turbine, nonlinear stochastic time-domain analysis tools that can be used with hydro-elastic-aero-servo simulations are needed. Because the hydrodynamic and aerodynamic loads vary over time and space, the equations of motions should be solved at each time step. The loads should be updated considering the instantaneous position of the structure at each time step.

Several numerical tools are available for the dynamic response analysis of wind turbines; these include Bladed, HAWC2, FAST, Flex5, Simo/Riflex and USFOS/vpOne codes. Benchmark studies are needed in order to improve and develop such codes for the analysis of floating wind turbines.

Hydrodynamic loads on the floater consist of nonlinear and linear viscous drag effects, currents, radiation (linear potential drag) and diffraction (wave scattering), buoyancy (restoring forces), integration of the dynamic pressure over the wetted surface (Froude-Krylov), and inertia forces. A combination of the pressure integration method, the boundary element method and the Morison formula can be used to represent the hydrodynamic loading. The linear wave theory may be used in deep water areas, while in shallow water the linear wave theory is not accurate as the waves are generally nonlinear. Agarwal et al. (2009) showed that, for offshore wind turbines, nonlinear (second-order) irregular waves can better describe waves in shallow waters. Linear and nonlinear hydrodynamic loading based on the linear wave theory has been studied for a catenary moored spar wind turbine (*Paper 2*). Considering the instantaneous position of the structure in finding the loads adds some nonlinearity. These hydrodynamic nonlinearities are mainly active in the resonant responses, which influence the power production and structural responses at low natural frequencies.

The aerodynamic loads are highly nonlinear and result from static and dynamic relative wind flow, dynamic stall, skew inflow, shear effects on the induction and effects from large deflections. The complex methods for calculating the aerodynamics are based on solving the Navier-Stokes (NS) equations for the global compressible flow in addition to accounting for the flow near the blades. The extended blade element momentum theory can be used to consider advanced and unsteady aerodynamic effects for aero-elastic time-domain calculation. Approaches of intermediate complexity, such as the vortex and panel methods, can also be applied (Hansen et al. 2006). Computational fluid dynamics methods (CFD) are the most accurate but are very time consuming. The advanced blade element momentum (BEM) theory is fast and gives good accuracy compared to CFD methods. The BEM method relies on airfoil data; therefore, the results obtained using this method are no better than the input. Hansen et al. (2006) proposed using NS methods to extract airfoil data and applying them in less advanced methods (e.g., BEM theory).

The aerodynamic loads and the time-dependent structural behaviour of the system are strongly coupled. For a floating wind turbine, the structural behaviour is wave- and wind-induced. A blade might change its twist and thus its angle of attack when deflected. Additionally, the angles of attack are changed when the blades have a velocity relative to the fixed ground. For instance, if the tower of a floating wind turbine is moving upstream due to wave-induced surge motion, it will be seen by the blades as an increased relative wind speed; thus, higher angles of attack will be present along the blades (Hansen et al. 2006). In *Paper 3*, the effect of the aerodynamic and the hydrodynamic damping on the dynamic response of a catenary moored spar wind turbine is presented.

Wind- and wave-induced motions directly affect the nacelle motion and its velocity, which can influence the relative velocity. The relative wind velocity contains motion response frequencies (resonant and wave frequency responses). The magnitude/frequency of the platform's rigid body motion influences the dynamic structural responses and power production and its quality through the relative wind velocity. In *Paper 1*, it is shown that for survival cases, the dynamic motion responses can be found accurately by assuming a rigid body formulation of a floating wind turbine. However, it was found that the structural responses were sensitive to the elastic body formulation and that it was necessary to model the elastic body to capture accurate structural responses (*Paper 4*). Ahlstrom (2005) showed that large blade deflections have a major influence on power production and that the resulting structural loads must be considered in the design of very slender turbines. Finite element modelling (FEM) with multi-body formulation and substructure approach is commonly used to model the wind turbines (e.g., HAWC2 code). In such modelling, the gravitational, centrifugal and gyroscopic forces are accounted for through the mass matrix. On the other hand, it is possible to describe the structural motion of a turbine by a finite series of structural eigen-frequencies (mode shapes); the accuracy of such a model is highly dependent on the

modes chosen to describe the wind turbine (e.g., FAST code). This approach is not appropriate for floating wind turbines because the mode shapes of the tower are, in reality, affected by the platform (spar) through the elasticity and added mass contribution.

The tower and the blades are slender structures. The geometrical nonlinearities in their physical behaviour are primarily introduced by large deflections and should be accounted for by subdividing the structure into several linear structural elements (e.g., Timoshenko beam) or by applying nonlinear elastic theories. It was found that the beam modelling of the slender structures, such as the tower, can be sufficiently accurate compared to shell modelling (*Paper 5*). Wind turbines suffer from low structural damping, which can become critical under certain operational conditions (Hansen et al. 2006). Because offshore wind turbines are large in size compared to land-based wind turbines, investigation of their aero-elastic stability is even more required. Bir et al. (2007) studied the aero-elastic instabilities of large offshore and onshore wind turbines and showed the potential of aero-elastic instability in some modes of motion for a barge-type floating wind turbine.

A proportional-integral-derivative (PID) controller is commonly used to control wind turbines. The PID controller is a generic control loop feedback mechanism that attempts to minimise the error (the difference between the measured and desired value of a process variable) by adjusting the process control inputs. The three constants (proportional, integral and derivative constants) should be tuned in the PID controller algorithm to provide the needed control action for a specific process according to the nature of the system. The control algorithm of the turbine limits the power taken from the wind to keep the drive train torque constant when the wind speed is higher than the rated speed. The control algorithm shuts down the wind turbine when the wind speed is above a certain cut-off value of around 25 m/sec. Pitching the blades, controlling the generator torque, applying the high speed shaft (HSS) brake, deploying the tip brakes and yawing the nacelle are the basic methods of controlling the wind turbine (Jonkman et al. 2005). Usually, the wind turbine control is applied as a dynamic link library (DLL) interface to the aero-hydro-elastic code (e.g., the Bladed, HAWC2 and FAST codes). By tuning the land-based control algorithm, it is possible to use such a controller for an offshore wind turbine. For a floating wind turbine, changing the controller target from constant power to constant torque can reduce the aerodynamic loads on the structure. Larsen and Hanson (2007) showed a method for avoiding negatively damped low-frequency motion of a floating pitch-controlled wind turbine (spar buoy concept). Jonkman (2008) studied the influence of the control on the pitch damping of a barge-type floating wind turbine. The blade pitch control of an operating turbine can introduce negative damping in a floating wind turbine. For example, if the relative wind speed experienced by the blades increases due to the rigid body motion of the system, then, if a conventional controller is used, the blades will feather to maintain the rated electrical power. In this research, the controller gains were modified to tune the controller to get rid of

negatively damped responses for over-rated wind speed cases (*Papers 7*). The results showed that modifying the controller gains is efficient to remove the servo-induced instabilities. This method was applied to ameliorate the negative damping in the dynamic responses of tension leg spar-type wind turbine with both downwind and upwind rotors (*Paper 8*).

The effect of the presence of the turbine tower on the flow field is modelled by the tower shadow. The rotor configuration effects on the power performance and responses accounting for the tower shadow models proper for each concept were studied (*Paper 8 and 9*). The potential flow and jet wake models were used to represent tower shadow effect of upwind and downwind rotors, respectively. The results showed that the tower shadow does not significantly affect the global responses. However, the tower shadow effects on the blade responses were notable (*Paper 9*).

The dynamic behaviour of floating wind turbines is highly dependent on the environmental conditions. Unlike other offshore structures in which wave loads usually dominate, offshore wind turbines may be equally loaded by wind and waves (Argyriadis et al. 2006). The wave-induced and wind-wave-induced reposes of spar-type wind turbines were compared (*Papers 2 and 8*). The mean values of the dynamic responses are primarily wind-induced and the standard deviations of the responses are mainly wave-induced. The maximum of the responses under operational and survival conditions are wind-induced and wave-induced, respectively (*Papers 2 and 8*).

The correlation of wave and wind should be considered when dealing with offshore wind turbines. The waves are wind-generated. However, at a given site, it is possible to have a combination of wind-generated waves and swell. Site assessments that include met-ocean data are needed to develop the joint distribution of the wave and wind for such analysis. Johannessen et al. (2001) studied the joint distribution of wind and waves in the northern North Sea. The 25-year recorded wave and wind data have been smoothed and fitted to analytical functions. The contour surface of the joint distribution of significant wave height, wave peak period and mean wind speed can be used to represent the environmental conditions for the response analysis. This method was used in *Paper 5* to estimate the 100-year response of a floating wind turbine utilising the contour surface method.

Limited work has been done regarding the coupled aero-hydro-servo-elastic time-domain dynamic response analysis of floating wind turbines, especially under harsh environmental conditions. IEA Wind Task 23 deals with the offshore wind turbine computer code comparison carried out by a number of research centres and universities. A study of spar-type floating wind turbine modelling was recently completed (Jonkman et al. 2010). Sclavounos et al. (2010) considered the dynamic response analysis of tension leg platform and taut leg buoy floating wind turbines. Roddier et al. (2009) introduced the WindFloat as a semisubmersible-

type offshore wind turbine. Utsunomiya et al. (2009) carried out tests in a scale model of a spar-type floating wind turbine. Their study focused on the wave-induced responses and the viscous hydrodynamic effects. Jonkman (2007) studied the dynamic response analysis of barge concepts. He developed the FAST code to include the hydrodynamic forces for floating wind turbines. Larsen and Hanson (2007) presented a method for avoiding negatively damped low-frequency motion of a floating, pitch-controlled spar-type wind turbine. Their work is related to the Hywind concept from Statoil. Nielsen et al. (2006) studied the dynamic response analysis of a catenary moored spar buoy wind turbine, the Hywind concept from Statoil. A comparison of model tests and numerical simulations was presented in their work. Withee (2004) studied the coupled dynamic response analysis of TLP-type floating wind turbines.

The operational and survival conditions should be considered for a floating wind turbine. The fatigue limit state can be governed by operational cases, and the ultimate limit state can be governed by survival cases. However, the limit states are concept-dependent and should be investigated using integrated response analysis. The operational case is the power-generating status of the wind turbine, in which the control is active. However, in the survival case, the wind turbine is parked with the blades feathered and locked in order to minimise the aerodynamic loads and the control is inactive. It is common to shut down the turbines at high wind speed, typically at wind speeds in the range from 20 to 25 m/sec. Ultimate loads on parts of the wind turbine can occur during shutdown conditions at very high wind speed (Hansen et al. 2006). It has been shown that the extreme responses for spar-type floating wind turbines occur in survival conditions (*Papers 2, 5, 8 and 9*). The maximum of the structural response for the survival case was found to be almost two times greater than its value for operational conditions.

The stochastic nature of the wind makes the dynamic response analysis complicated and time demanding. The results presented in *Paper 2* and *Paper 9* showed that the turbulent wind does not significantly affect the global motion and structural responses; thus, it is possible to use the constant wind model in fatigue and ultimate limit state analyses with an acceptable accuracy. However, the blade structural responses are significantly affected by the turbulence and a proper turbulent model to investigate the blade response behaviour is needed.

Because the nature of the turbulent wind input is highly stochastic, the calculated extreme loads of a wind turbine are random with significant variation. For a floating wind turbine, the stochastic wave adds more randomness to the response. *Paper 5* presented an efficient and robust method for capturing the extreme value response of a floating wind turbine based on extrapolation methods. The extrapolation methods are used to estimate the extreme value responses under operational and survival conditions for both the CMS (*Paper 2*) and TLS (*Paper 9*) offshore wind turbines. Extrapolation of the response events will give much higher

ultimate loads than will the extreme wind gusts (Madsen et al. 1999). The IEC 61400-3 recommends the use of ultimate strength analysis of parked wind turbines in harsh conditions (design load case, DLC 6) in the design of offshore wind turbines. For fixed offshore wind turbines, several standards and guidelines, such as the IEC 61400-3, GL Wind Offshore, Danish Recommendation and DNV-OS-J101 exist. Standards for assessing floating offshore wind turbines are expected in the near future.

1.3 Objectives and scope of the thesis

This thesis is written in article-based format. It consists of collection of articles, including four journal papers and five conference papers, as listed in the Appendix. The stochastic dynamic motion and structural responses to investigate the power production and structural integrity of the system are discussed in the papers. The aero-hydro-servo-elastic coupled response analysis of floating wind turbines is one of the key issues in the present thesis. Several aspects of this topic are studied in the papers. The main objectives of the thesis are listed below. They include:

- Modelling
  - Catenary mooring and tension leg mooring systems
    - Nonlinear spring model
    - Physical model of the lines
    - Structural damping of the mooring lines
  - Environmental conditions
    - Joint distribution of the wave and wind
  - Stochastic wave and wind modelling
    - Avoiding repetition of the wave and wind time series
    - Number of frequencies, cut-in and cut-out frequencies
    - Effect of the sample size
  - Damping
    - Structural damping effects of the tower/support structure
    - Aerodynamic damping
    - Hydrodynamic damping
  - Negative damping
    - Constant torque control algorithm
    - Modifying the controller gains and tuning the controller
  - Tower shadow effects
    - Upwind (potential tower shadow model)
    - Downwind (jet tower shadow model)

- Comparative studies
  - Hydrodynamic and hydro-elastic code-to-code comparison
  - Parked versus operational conditions
  - Wave-induced versus wind-wave-induced responses
  - Constant and turbulent wind speeds
  - Rigid and elastic body
  - Rotor configuration

Extreme value estimation
- Monte Carlo simulations
- Up-crossing rates
- Extrapolation methods

In the following paragraphs, the scope and objectives of the papers are listed separately. Figure 1.5 shows the main topics and the interconnection between the papers.

Paper 1:
Dynamic response analysis was conducted by focussing on the motion responses of a parked wind turbine. Two parked rotor configurations, blades parallel to wind and blades perpendicular to wind (a fault condition), were discussed. Rigid and elastic body modelling were compared.

Paper 2:
The hydrodynamic code-to-code validations were performed for catenary moored spar-type floating wind turbines. The Simo/Riflex (DeepC) and HAWC2 codes were compared through wave-induced responses. The panel method and the Morison formula were applied to the CMS to investigate the hydrodynamic features of such a concept. The turbulent and constant wind modelling was compared for the motion response, power production and structural responses for several load cases. The wave- and wind-induced responses of an operating and parked wind turbine were investigated.

Paper 3:
Power production and the effect of aerodynamic and hydrodynamic damping on the performance of a wind turbine were discussed. The wave-induced and wave- and wind-induced responses of a CMS in operational conditions with a rotating and parked rotor were compared to illustrate the aerodynamic damping. A simplified formula for addressing the hydrodynamic and aerodynamic damping was presented. Power production and motion response in below-rated, rated and over-rated wind speeds were studied.

Paper 4:
The structural response of a catenary moored spar-type floating wind turbine was investigated. The contour surface method was used to perform extreme response analysis. The operational and survival cases were compared. It was shown that for a floating wind turbine, it is possible to have extreme structural responses in survival conditions.

Paper 5:
The extreme value analysis and the sensitivity study of the ultimate limit state were studied and discussed. Extrapolation methods for estimating the extreme value responses were used to reduce the sample size in the Monte Carlo simulations. The accuracy of methods to estimate the extreme responses as a function of sample size and methods applied was investigated.

Paper 6:
Hydro-elastic analysis of a tension leg spar-type wind turbine was performed to establish the basis for coupled integrated analysis. The USFOS and HAWC2 codes were compared using a wave-induced analysis of a TLS wind turbine. Different hydrodynamic methods, such as the displaced volume method and pressure integration method, were compared. Tension leg spring and damping effects, rigid versus elastic modelling, and simulation convergence are studied. The effects of wave elevation sampling and total simulation time on the stochastic dynamic response were studied.

Paper 7:
The servo-induced instabilities for a tension leg spar-type wind turbine were investigated. Dynamic responses of a TLS with downwind turbine configuration subjected to wave and wind loads under different operational conditions were studied to highlight the negative damping. The controller gains were modified to remove servo-induced negative damping. The responses obtained using tuned and untuned controllers were compared. It was shown that the tuning of controller gains can help to reduce the structural responses and to increase the power production.

Paper 8:
The wave-induced and wave-wind-induced responses of a TLS with both downwind and upwind rotor configurations were studied. The effect of the rotor configuration on the dynamic responses of tension leg spar-type wind turbine was discussed. The results showed that the responses under operational and survival conditions are wind-induced and wave-induced, respectively.

Paper 9:
The effect of turbulence and tower shadow on the dynamic responses of a tension leg spar-type wind turbine subjected to stochastic wave and wind loads was investigated. The dynamic response of the downwind TLS subjected to simultaneous wave and wind actions was compared for both constant and turbulent wind with and without tower shadow. Extrapolation methods were used to estimate the maximum responses and the normalized responses for both the operational and survival conditions were presented to make more generalized conclusions.

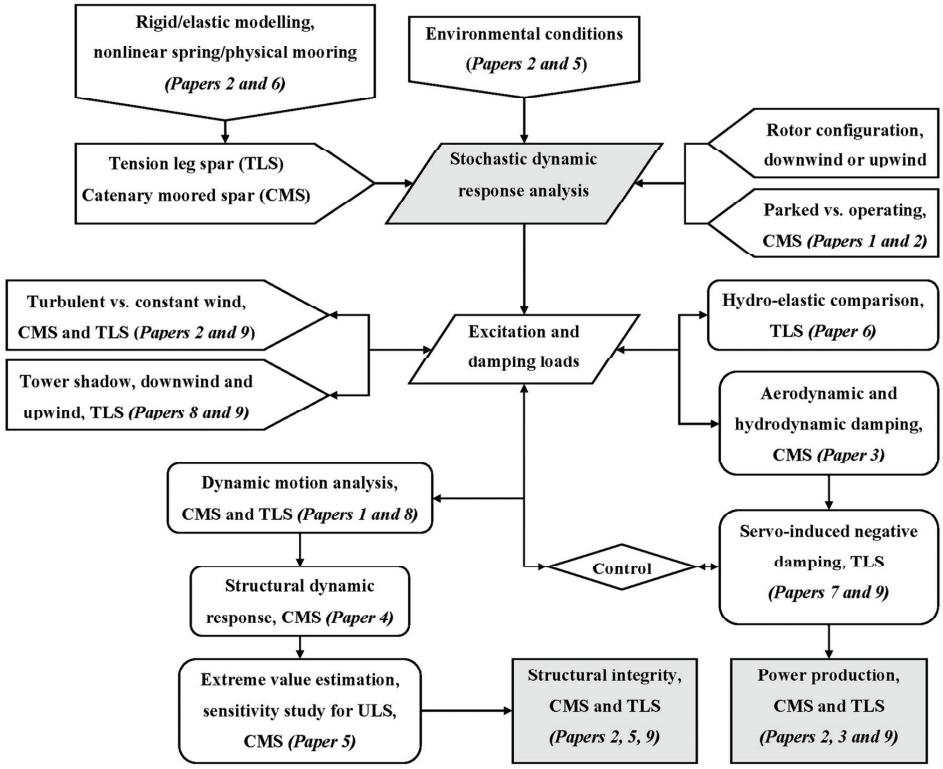

Figure 1.5: Scope of the thesis and interconnection between the appended papers. CMS is a catenary moored spar wind turbine with an upwind rotor configuration. TLS is a tension leg spar wind turbine primarily with a downwind rotor unless it is explicitly mentioned to be upwind.

Chapter 2

Analysis for the Design of Floating Wind Turbines

2.1 Floating wind turbine configurations

Based on offshore oil and gas experiences, several floating wind turbine configurations are possible that utilise different foundations and mooring systems. In Figure 2.1, some of the floating wind turbine concepts suitable for deep water applications are presented. The spar concept moored by catenary (CMS) or taut mooring lines gets stability by using ballast at the bottom of the spar. The tension leg platform (TLP) achieves stability through the use of tendons and the excess buoyancy in the platform. Hybrid concepts such as the tension leg spar (TLS) can be used to obtain the advantages of both concepts (*Paper 6*).

Floating offshore wind turbines may be located in intermediate to deep water depths, a region of the seas where relatively few structures have been built. The offshore oil and gas industry has considerable experience in the design and construction of platforms for deep waters. Coastal engineering has focused on the design of fixed structures for use in shallow water regions. The design objectives for both these branches of engineering are different from those of the offshore wind energy industry. In the former, cost has a lower priority compared to other aspects such as time scale, reliability and safety (Henderson 2003). Although much useful knowledge can be gained through study of the offshore and coastal engineering experiences, the design methods used in these industries may need to be modified for offshore wind turbine design in order to avoid an extremely costly or possibly even unreliable structure. To develop a robust offshore wind power design, competency in both offshore technology and wind industry application is needed.

The stability of a floating structure is affected by the restoring forces/moments that come from hydrostatic and mooring system effects. Moreover, the restoring forces/moments have important effects on dynamic responses. As an example, the pitch stiffness (K_{Pitch}) of a spar is given in Equation 2.1 (K_{Pitch} is calculated with an axis origin at the centre of gravity).

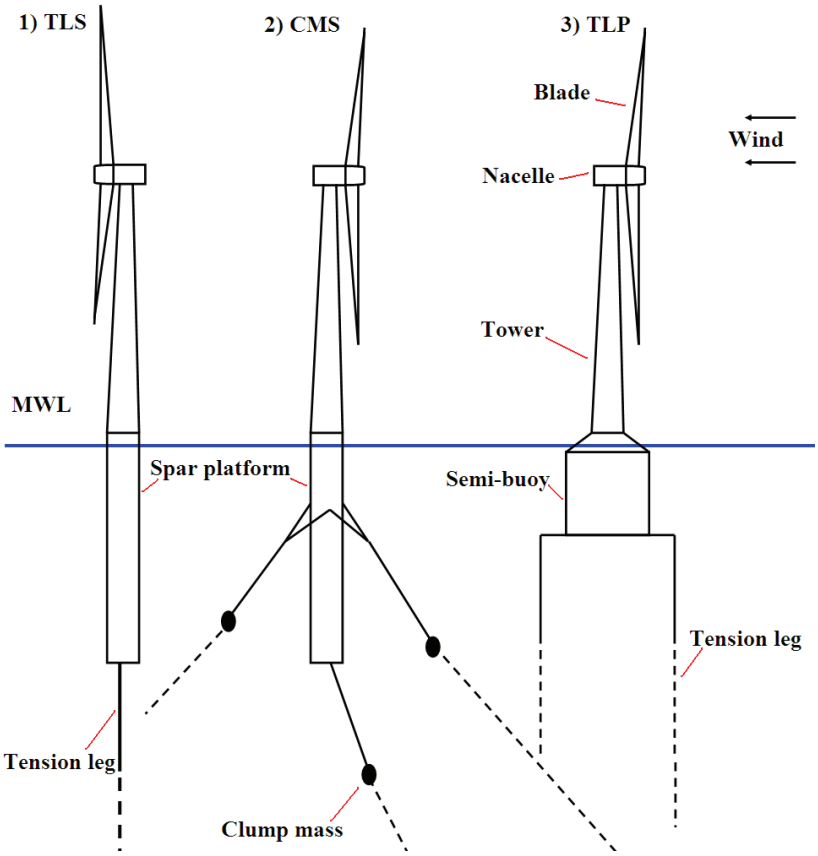

Figure 2.1: Floating wind turbine concepts for deep water.

$$K_{Pitch} = \rho g \nabla GM + K_{\theta_{mooring}}$$
$$GM = (KB - KG + \frac{I}{\nabla}) \tag{2.1}$$

where ρ is the water density, ∇ is the submerged volume, $K_{\theta_{mooring}}$ is the mooring stiffness in pitch motion, and GM is metacentric height, connected to the stability of the platform and should be positive in order to have a stable system (Usually, $GM \geq GM_{LIMIT}$). KG is the distance of the centre of gravity (CG) from the bottom of the spar, KB is the distance of the centre of buoyancy (CB) from the bottom of the spar and I is the area moment of inertia.

For a catenary-moored spar, $K_{\theta_{mooring}}$ is given by the following expression:

$$K_{\theta_{mooringCMS}} = K_{Surge}(KG - KF)^2 \tag{2.2}$$

where K_{Surge} is the mooring stiffness in surge and KF is the distance of the fairlead from the bottom of the spar.

For a tension leg spar $K_{\theta_{mooring}}$ is given by the following expression:

$$K_{\theta_{mooringTLS}} = \frac{T_0}{L}(KG + L)KG \tag{2.3}$$

where T_0 is the pretension and L is the tension leg length.

For a spar platform, the area moment of inertia is negligible. For a semisubmersible and ship-shaped structures (i.e., barges), however, it is the main source of stability. For a TLP concept, the mooring system is the main restoring part. In a spar concept, the difference between the CB and CG assures the stability (ballast-stabilised).

To give an idea of the effect of the platform motions and the performance of the wind turbine, a simple relation of the thrust force (f_{Thrust}) is presented in Equation 2.4. Through the relative velocity (V_{rel}), the platform motion induces some extra aerodynamic loading which directly affects the power production. C_{aero} is the aerodynamic coefficient.

$$f_{Thrust} = \frac{1}{2} C_{aero} \rho V_{rel}^2 A \tag{2.4}$$

For a fixed wind turbine (offshore or land-based), the relative velocity is very close to the wind velocity. The elastic deflections of the blades, tower and substructure have limited effect. However, for a floating wind turbine, motion-induced velocities are comparable to the wind velocity. In fact, both the hydrodynamic and aerodynamic loads are coupled through the instantaneous position. This coupling illustrates the importance of coupled wave- and wind-induced dynamic analysis for a floating wind turbine.

Another important point regarding the floating wind turbine is the variety of characteristic frequencies involved. The main frequencies are listed below:
Natural frequencies:

- Surge and pitch natural frequencies: 0.05-0.2 rad/sec
- Heave natural frequencies (i.e., TLS, depends on many factors such as water depth and system mass): 3-6 rad/sec
- First flexible eigen-frequencies for tower and blade modes: 2-4 rad/sec

Excitation frequencies:

- Wave frequencies (first order): 0.2-0.8 rad/sec and sum frequencies: 0.4-1.6 rad/sec
- Wind frequencies: 0.01-1 rad/sec with slowly varying peaks
- Rotor frequencies i.e., the first, second and third rotor harmonics (three-blades rotor)
- Motion-induced excitation frequencies: accounting for instantaneous position of the structure introduces nonlinear hydrodynamics (*Paper 2*). The nonlinear effect of the tension leg introduces the sum and difference of the pitch, surge and wave frequencies for the heave and tension responses (*Paper 6*).

The wide range of characteristic frequencies of a floating wind turbine makes it difficult to design a robust concept. In so doing, one must ensure that the system frequencies, such as the structural rigid and elastic frequencies, are out of the range of the wave and wind excitation frequencies. In Figure 2.2 the main characteristic frequencies in a floating wind turbine are illustrated.

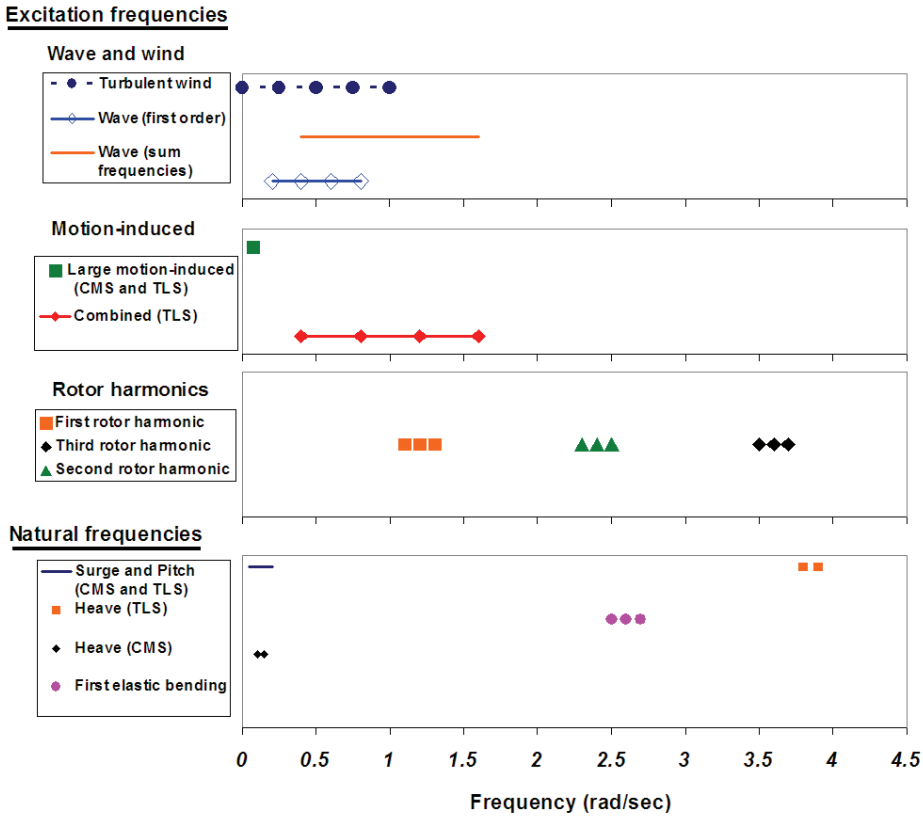

Figure 2.2: Frequencies involved for spar-type wind turbines: excitation and natural frequencies.

As an example, for the NREL Offshore 5MW baseline wind turbine (Jonkman 2007), the rotor harmonics can be calculated in the following manner. The rated rotational speed of rotor is 12.1 rpm. Therefore, the first and third rotor harmonics are given as follows:

$$1P_{rotor} = 12.1\frac{2\pi}{60} = 1.26 \quad rad/\sec \qquad and \qquad 3P_{rotor} = 12.1\frac{2\pi}{20} = 3.80 \quad rad/\sec \tag{2.5}$$

The first elastic natural frequency of a floating wind turbine (i.e., a catenary-moored spar-type wind turbine) is a function of the mooring system stiffness, the added mass, the mass of the system and the structural elastic stiffness (Equation 2.6). To find the elastic eigen-frequencies, modal analysis using finite element analysis is usually performed.

$$\omega_{eigen} = f(EI, k_{ms}, L, m_{top}, m_{tower}, m_{spar}, m_a) \tag{2.6}$$

where ω_{eigen} is the system elastic natural frequency, EI is the system bending stiffness (E is the elastic modulus and I is the area moment of inertia), k_{ms} is the mooring system stiffness, L is the system length, $m_{top} = m_{nacelle} + m_{rotor}$ is the mass of the nacelle and the rotor together at the top of the tower, m_{tower} is the mass of the tower, m_{spar} is the mass of the spar and m_a is the added mass.

In this design, the goal is to set the natural frequencies between, above or below the harmonic frequencies to avoid resonance. If the first structural mode is between the first and third rotor harmonics then the system is soft-stiff. A very stiff structure has a first natural frequency that is greater than the third rotor harmonic. It is possible to design a soft system whose first structural mode is below the first rotor harmonic. The softest structure has the least cost because the cost increases with the tower mass.

2.2 Spar wind turbines

In oil and gas offshore technology, the Spar platform is being considered the next generation of deep water offshore structures. Such a platform consists simply of a vertical cylinder that floats vertically. Strakes (finlike structures) can be attached in a helical fashion around the exterior of the platform act to break the water flow against the structure for further enhancement of stability (Agarwal et al. 2003).

2.2.1 Spar with catenary mooring

A catenary-moored spar wind turbine (CMS) is a moored spar platform supporting a wind turbine. By wind turbine we mean the tower, nacelle and rotor. The dynamic behaviour of the integrated structure is complicated as we are dealing with an aero-servo-hydro-elastic multi-body system. The wind and wave motions induced through time- and geometry-dependent loading can excite the rigid and elastic modes. Coupling is inevitable in such structures because the aerodynamic and hydrodynamic damping and excitation forces are highly affected by each other through the relative motions. The elasticity of the structure shows its effects mainly on the structural responses. The first elastic mode excited by wave- and wind-induced loading makes a clearly defined contribution to the structural responses (*Paper 4*). In harsh environmental conditions the wind turbine is parked with blades parallel to wind to reduce the loads. In such a situation the control is inactive. However, for operational cases, the role of the control in decreasing the structural loads, reducing fluctuations in the output power, and increasing the mean value of power is significant.

Spar platforms are slender compared with the wave length, and the past work has shown that for such a structure, the extended Morison formula accounting for the instantaneous position

of the structure is suitable if the pressure integration method is used to account for the heave excitation. The heave motion of the spar is reduced due to the small water plane area and deep draft. The surge and sway rigid body motions are very low responses governed by catenary mooring line stiffness. The mooring lines keep the structure in position by allowing it to smoothly surge with less influence on the electrical power production. The pitch and roll motions are mainly ballast-stabilised. The hydrostatic restoring forces due to high righting moment provided by the low centre of gravity stabilise the structure in pitch and roll motions. There is no hydrodynamic yaw excitation force for the spar, but the wind excites the yaw motion which should be stabilised by introducing delta mooring. If the spar motions are small enough, the taut system can be used instead of catenary mooring lines. The taut mooring systems save a significant length of wire and chain. The schematic of such a system is shown in Figure 2.3.

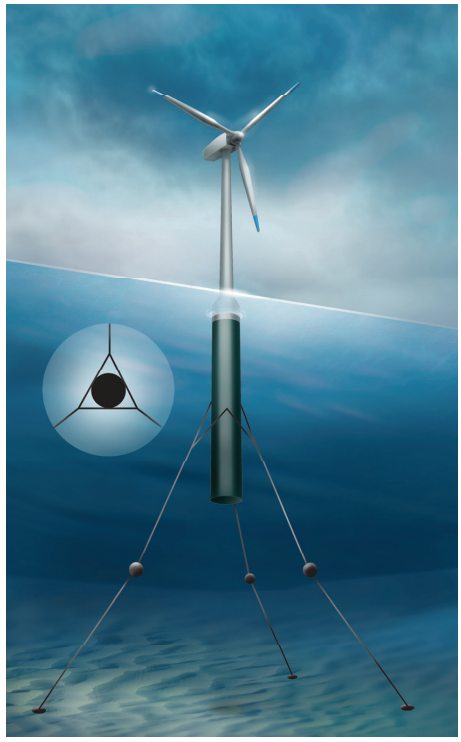

Figure 2.3: Moored spar wind turbine (CeSOS Annual Report 2009).

Mathieu instability for a spar platform arises when there is harmonic variation in the pitch restoring coefficients caused by large heave motion. Moreover, the period of the heave motion and the pitch natural period have a special ratio of 0.5 (Koo et al. 2004). The pitch restoring coefficient can be represented by a function of the displaced volume and the metacentric height of the spar platform. Due to heave motion, the displaced volume and the metacentric height of the spar platform change in time and this heave/pitch coupling can be represented by Mathieu's equation. It is possible to have this instability for other ratios of

heave/pitch natural frequency. Haslum et al. (1999) showed that for a system with no damping, no excitation, and no coupling between pitch and surge, these ratios are 0.5, 1, 1.5 and 2. The Mathieu instability has been avoided in the present study by considering the criteria mentioned by Haslum et al. (1994) and Koo et al. (2004).

For analysis of the dynamic behaviour of floating wind turbines, comprehensive numerical tools are needed. The hydrodynamic loads based on panel methods, the Morison formula and pressure integration methods should be accounted for when considering the geometrical updating. The position-dependent terms of the hydrodynamic loading add nonlinearities, which can excite the natural frequencies.

The aerodynamics of a floating wind turbine can be treated similarly to that of a fixed bottom-mounted wind turbine, keeping in mind the large rigid body motions of the structure, which induce the additional aerodynamic damping and excitation forces through relative velocity. These additional forces can affect the survival cases, as the wave-induced motions in harsh conditions are significant. These wave-induced motions can influence the wind-induced motions and vice versa. For operational cases, the relative velocity can cause negative damping through the constant power application of conventional controllers. As an example, if the structure surges toward the coming wind for an over-rated wind speed, the controller pitches the blades to decrease the aerodynamic forces due to increased wind velocity. For over-rated wind speed zone, the slope of the thrust curve versus the wind speed (dT / dV gradients) is therefore negative (*Papers 7 and 9*). However, this is not the case for fixed wind turbines because the pitch controller is normally slow compared to the changes in wind speed induced by structural vibrations (Larsen et al. 2007). The remedy for this error when using conventional control algorithms is to set a constant torque instead of constant power for over-rated wind speeds and tune the gains so that the controller frequency is less than the low rigid body natural frequency (*Paper 7*). The constant torque control algorithm for over-rated wind speed helps to reduce the loads in higher wind speeds as well.

The low rigid body natural frequencies of the structure can be excited by the wind. However, these frequencies are kept below the wave frequencies. Because the wind covers a wide range of frequencies, avoiding the wind-induced resonances of low rigid body motions is not possible. Wave-induced aerodynamic damping has been shown to be active in both over- and below-rated wind speed (*Paper 3*). The hydrodynamic damping of a spar wind turbine can be increased by introducing pins and strakes on the circumference of the spar platform. The damping is the key issue for resonant responses. Because the structure is inertia-dominated, increasing the hydrodynamic damping does not affect the wave response, but it reduces the resonances. Some of the options for reducing the resonant responses are discussed in Section 4.4.2.

As mentioned above, turbulent wind excites the rigid body modes associated with low natural frequencies. Moreover, the modes corresponding to these natural frequencies are also excited in the steady (constant) wind case. The reason for this is that the platform motion frequencies show themselves in the relative wind velocity and hence in the excitation forces. Thus, for a floating wind turbine the motion of the platform can be "self-excited" through the aerodynamic forces. Although wave-induced aerodynamic damping reduces the resonant responses, this excitation can still be important.

The mooring line inertia and damping can be neglected because the velocity of the lines' motion is small and the wet weight of the lines compared to the whole system weight is negligible. However, if mooring system responses are to be determined, a detailed model of the mooring system is necessary and the coupled dynamic responses should be performed. In some cases, the lines effects can be handled in a quasi-static manner for simplification of the problem. FE modelling of the mooring line system, including the delta lines and clump masses considering the large deflections, can be performed to capture the mooring line force-displacement relations. This approach was used in *Paper 1* to carry out the coupled analysis in the HAWC2 code. The mooring line's position-dependent forces at each time increment were imported into the HAWC2 code through a dynamic link library (DLL).

2.2.2 Spar with tension leg mooring

The tension leg spar wind turbine (TLS) is a spar platform with a pre-tensioned mooring line that supports a wind turbine. Actually this line is a tubular member with a diameter of e.g. 1.0 m. The dynamic behaviour of the TLS can be more complicated compared that the CMS due to additional nonlinearities from tension leg effects. The wind- and wave-induced motions can excite the rigid and elastic modes through time- and geometry-dependent loading. The motions are strongly coupled because of the tension leg (*Paper 6*).

In the single-leg TLS concept, a pre-tensioned vertical tension leg connects the bottom of the spar to the seabed. The torsional stiffness provided by one leg is not very high; consequently an upwind turbine is much less convenient in yaw compared to a downwind configuration. To create a more stabilised yaw motion, the downwind rotor configuration is recommended for a TLS floating wind turbine. The simplest way to make a downwind turbine is to hang the rotor behind the tower; thus, the downwind turbine has its rotor behind the tower. Therefore, in the downwind turbine, the wind faces the blades in the same manner as in the upwind turbine. This ensures that the aerodynamic properties of the blades and airfoils are correct (*Paper 8*). An upwind turbine has a shaft tilt and hub cone angle designed to avoid the blades' hitting the tower due to large aeroelastic deflections. In a downwind turbine, these values can be set to zero because the rotor is behind the tower (*Papers 7, 8 and 9*). The effect of rotor configuration on the dynamic responses has been investigated for a TLS-type wind

turbine in *Paper 8*. The tower shadow model proper for modelling the tower wake deficit (potential model for upwind and jet model for downwind) is applied. It is found that the tower shadow does not significantly affect the global responses (*Paper 9*). However, the tower shadow effect on the blade responses is notable (*Paper 9*).

As with the CMS, the extended Morison formula accounting for the instantaneous position of the structure is suitable for the TLS if the pressure integration method is applied to deal with heave excitation forces. The TLS has very small heave motion due to large tension leg stiffness. The surge and sway rigid body motions are very low responses that are governed by tension leg stiffness. The single tension leg keeps the structure in position, allowing it to smoothly surge with less influence on electrical power production. The pitch and roll motions are stabilised due to ballast and tension leg effects; the tension leg provides restoring moments for pitch and roll motions. Moreover, the hydrostatic restoring forces due to the up righting moment provided by the low centre of gravity help to stabilise the structure in pitch and roll. There is no hydrodynamic yaw excitation force for the spar, but the wind excites the yaw motion, which should be stabilised by introducing a proper yaw mechanism and individual blade pitch control. Moreover, a downwind rotor configuration helps reduce the aerodynamic yaw moments. An artistic impression of such a system is shown in Figure 2.4.

Figure 2.4: Tension leg spar wind turbine (CeSOS Annual Report 2009).

Because the heave motion is very small for the TLS due to the effective tension leg stiffness, the Mathieu instability is not possible for a tension leg spar. However, for this concept other instabilities can appear in poor designs. Some of these instabilities are given below:

1) Yaw instability
   The yaw instability can occur because the single tension leg has limited yaw stiffness. To reduce the effect of this instability, one must ensure a robust yaw mechanism (at the top of the tower, the spar-leg connection or the spar-tower connection) and provide an individual blade pitch controller
2) Heave instability
   The tension leg spar has a high heave natural frequency, which can be close to rotor harmonics or the first tower eigen-frequency. This can cause extraordinary heave resonance.
3) Pitch instability
   The servo-induced negative damping can present and affect the structural responses and power production. The negative damping and its effect on the performance and structural integrity is studied in *Papers 7 and 9*. The controller gains have been tuned to remove the pitch motion instability (*Paper 7*).

By accounting for the instantaneous position of the TLS in calculating the forces, some hydrodynamic nonlinearity is introduced due to the nonlinear hydrodynamic excitation. In addition, the TLS is more sensitive to the numerical discretisation of the wave spectrum (*Paper 6*). All the motions are highly connected through the tension leg. The governing mode is the pitch response, which affects all the other responses through the tension leg. The nonlinear effect of the tension leg introduces sum and difference of pitch, surge and wave excitation frequencies for heave and tension responses (see Figure 2.2). It is necessary to design the system so that the pitch natural frequency is outside the wave spectrum. However, the nonlinear hydrodynamic loading can cause excitation at the natural frequencies.

2.3 Limit states and safety

A floating wind turbine (FWT) is designed to produce power from offshore wind resources. The dynamic behaviour of the system is important for the survivability in severe sea states and for its ability to resist high loads over a long period of time with respect to fatigue (FLS). When survivability is to be assessed, it is the most severe conditions that are of interest (ULS). When the power absorption is to be estimated, it is the most probable conditions that are the most important. In other words, the structure and all structural members should be verified according to four limit states: a) ultimate limit state (ULS, the structure is checked against extreme loads); b) serviceability limit state (SLS, the maximum deflections are checked for a safe operation); c) accidental limit state (ALS, structural damage caused by accidental loads will be checked); and d) fatigue limit state (FLS, the structure is checked

against failure due to fatigue damage) (DNV 2007). The different limit states help the designers determine the survivability of the structure in extreme and operational conditions and assess the ability of the concept to produce power. The first three limit states represent the wind turbine's integrity over its lifetime. The serviceability limit state (SLS) corresponds to tolerance criteria applicable to normal use (e.g., acceleration at the nacelle).

Three safety classes are considered for structures in an offshore wind park. A low safety class is used when the failures imply low risk for personal injuries and pollution, low risk for economic consequences and negligible risk to humans. A normal safety class is used for structures for which failures imply some risk for personal injury, pollution or minor societal losses, or significant economic consequences. A high safety class is used when failures imply large possibilities for personal injuries or fatalities, for significant pollution or major societal losses, or very large economic consequences (DNV 2007).

The safety level of a floating wind turbine is acceptable when the design load effect does not exceed the design resistance. In this respect, the following design approaches can be used (DNV 2007):

- Design by the partial safety factor method
- Design by direct simulation of the combined load effect of simultaneous load processes

Because floating wind turbine structures are subjected to several simultaneous loads, design by direct simulation of the combined load effect may be more accurate than design by the linear combination model of the partial safety factor method. The linear combination model of the partial safety factor method may be insufficient where the load effect associated with one of the applied load processes depends on the other load effects. For instance the wave-induced aerodynamic forces (damping or excitation) are aerodynamic load processes dependent on wave-induced motions.

2.3.1 Load cases

The IEC (International Electrotechnical Commission) issued the 61400-3 standard, which describes 35 different load cases for design analysis (IEC 2008). An appropriate combination of wind and wave loading is necessary for design purpose in an integrated analysis. In the IEC standard, different load cases are introduced for offshore wind turbines to assure the integrity of the structure in installation, operation and survival conditions. The defined load cases are given below:

- Power production
- Power production plus fault condition
- Start-up

- Normal shutdown
- Emergency shutdown
- Parked
- Parked plus fault condition
- Transport, assembly, maintenance and repair

The power production case is the normal operational case in which the turbine is running and is connected to an electrical load with active control. The power production plus fault condition involves a transient event triggered by a fault or loss of electrical network connection while the turbine is operating under normal conditions. If this case does not cause immediate shutdown, the resulting loads could affect the fatigue life. Start-up is a transient load case. The number of occurrences of start-up may be obtained based on the control algorithm behaviour. Normal shutdown and emergency shutdown are transient load cases in which the turbine stops producing power by setting to the parked condition. The rotor of a parked wind turbine is either in the standstill or idling condition. The ultimate loads for these conditions should be investigated. Any deviation from the normal behaviour of a parked wind turbine resulting in a fault should be analyzed. All the marine conditions, wind conditions and design situations should be defined for the transport, maintenance and assembly of an offshore wind turbine. The maximum loading of these conditions and their effects should be investigated.

When combining the fault and extreme environmental conditions in the wind turbine lifetime, the realistic situation should be proposed. Fatigue and extreme loads should be assessed with reference to material strength, deflections and structure stability. In some cases, it can be assumed that the wind and waves act from one direction (single-directionality). In some concepts, multi-directionality of the waves and wind can be important. In the load case with transient change in the wind direction, it is suggested that co-directional wind and wave be assumed prior to the transient change.

For each mean wind speed a single value for the significant wave height (e.g., expected value) can be used (IEC 2009). This method has been used to analyse the wave- and wind-induced response of a catenary-moored spar wind turbine in operational and survival cases (*Papers 2 and 9*).

2.3.2 Operational versus parked condition

The pitch-regulated variable-speed wind turbine is the state-of-the-art wind machine device. Depending on the wind speed, the status of the wind turbine is divided into four regions (e.g., Kallesøe 2007):

- The wind speed is too low for cost-effective operation of the wind turbine, so the rotor is parked.
- The wind speed is greater than the cut in wind speed, but still less than the maximum capacity of the generator. Therefore, the turbine should extract as much energy from the wind as possible. The rotation speed of the rotor is kept below the rated rotor speed to optimise the efficiency of the turbine. The blade pitch is constant in this region.
- The wind speed is above the rated wind speed. The pitch controller turns the blades towards less aerodynamic torque such that the energy extracted from the wind fits the capacity of the generator. The rotation speed of the rotor is constant.
- The wind speed is too high for safe operation of the wind turbine. After passing the cut-out wind speed, the rotor is parked.

In operational conditions, the wind turbine produces electricity, and the control is active. During survival conditions the wind turbine is parked (shut down) and the control is inactive. In parked configuration, the blades are feathered and set parallel to the wind to decrease the aerodynamic loads on the blades. Figure 2.5 shows, the power curve for a 5 MW wind turbine is shown.

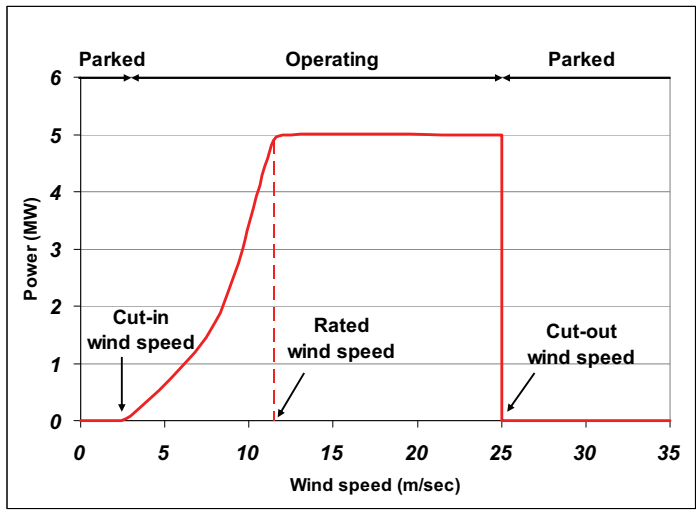

Figure 2.5: Schematic illustration of power production as a function of wind speed for a 5 MW bottom-fixed wind turbine.

2.3.3 Wind turbine in harsh environmental conditions

In a storm conditions (harsh environmental conditions), the turbine is shutdown and placed in parked (stationary) position with the blades parallel to the wind. In this situation, the mechanical brake prevents the blades from rotating. This is done in order to reduce the loads on the wind turbine to help it withstand hurricane conditions.

Appropriate extreme value analysis of these types of environmental conditions is needed for investigation of the reliability and safety of a wind turbine structure during hurricanes. The mechanical brake keeps the blades from rotation. If the brake fails because of extreme wind and corresponding forces, the blades will over speed, creating extreme loads. The blades, tower or, in the worst case, the whole structure can be damaged. Below a certain critical wind speed, the yaw system can prevent the blades from over speeding if the mechanical brake fails.

In the operational cases, the rotor follows the incoming wind by using the yaw system to produce maximum power. The nacelle along the axis of the tower rotates. However, in survival cases, the wind turbine is parked with the blades parallel to the wind to reduce the loading. If the yaw system fails, the rotor rotates so that the blades are no longer parallel to the wind, which may cause large aerodynamic forces. The yaw system may fail for a variety of reasons:

- Failure of the anemometer (error in showing the wind direction)
- Grid failure
- Failure of the yaw system electric motors

If the yaw system fails, the mechanical brake is the only system to keep the blades from over speeding in harsh environmental cases.

Chapter 3

Equations of Motion for Offshore Wind Turbines

3.1 General

The equations of motions can be written in the form of Newton's second law $M\ddot{x} = F_{Generalized}(t, x, \dot{x})$, in which the generalised force vector $F_{Generalized}(t, x, \dot{x})$ includes all the environmental forces, inertial and gravitational forces, mooring system and soil interaction (if applicable), and all kind of stiffness and damping forces (including aerodynamic, hydrodynamic and structural stiffness and damping). M is the mass matrix, and x is the position vector including translations and rotations.

The equations of motion for a floating wind turbine are nonlinear and can be solved in the time domain using direct step-by-step integration techniques. Time domain analysis allows the handling of nonlinearities involved in hydrodynamic and aerodynamic loading and finite wave amplitude effects as well as nonlinear material and geometrical effects.

The rigid body equations of motion for a floating structure, such as a floating wind turbine in regular waves, can be written as follows:

$$M\ddot{x} + C\dot{x} + D_{hydro1}\dot{x} + D_{hydro2}g_{hydro} + D_{aero1}\dot{x} + D_{aero2}g_{aero} + Kx = F(t, x, \dot{x}) \tag{3.1}$$

$$\begin{aligned} &M = m + A(\omega), \\ &A(\omega) = A_{\infty} + a(\omega),\ A_{\infty} = A(\omega = \infty), \\ &C(\omega) = C_{\infty} + c(\omega),\ C_{\infty} = C(\omega = \infty) \end{aligned} \tag{3.2}$$

where M is the frequency-dependent mass matrix, m is the body mass matrix, A is the frequency-dependent added mass matrix, C is the frequency-dependent potential damping matrix, D_{hydro1} is the linear viscous hydrodynamic damping matrix, D_{hydro2} is the quadratic viscous hydrodynamic damping matrix, D_{aero1} is the linear aerodynamic damping matrix, D_{aero2} is the quadratic aerodynamic damping matrix, g_{hydro} and g_{aero} are vector functions

where each element is given by $g_i = \dot{x}_i \left| \dot{x}_i \right|$, K is the position-dependent hydrostatic stiffness matrix, x is the position vector including translations and rotations, and F is the exciting force vector given by Equation 3.3.

$$F = F_{Hydrodynamic} + F_{Aerodynamic} + F_{Mooring\ System} + F_{Gravitational} + \ldots \tag{3.3}$$

In Equation 3.3, other forces, such as earthquake forces, current and tidal forces, ice loading and others, can be added depending to the offshore site and the concept.

The frequency-dependent coefficients make it difficult to solve Equation 3.1. One of the most-used methods for solving Equation 3.1 is based on a convolution integral. Considering the radiation part of the problem and applying the inverse Fourier transform, the radiation part is related to the retardation function ($R(t)$), which can be calculated using either potential damping or added mass (Equations 3.4 and 3.5), see e.g. Falnes (2005).

$$\begin{aligned}(m + A_\infty)\ddot{x} + D_{hydro1}\dot{x} + D_{hydro2}g_{hydro}(\dot{x}) + D_{aero1}\dot{x} \\ + D_{aero2}g_{aero}(\dot{x}) + K(x)x + \int_0^t R(t-\tau)\dot{x}(\tau)d\tau = F(t,x,\dot{x})\end{aligned} \tag{3.4}$$

$$R(t) = \frac{2}{\pi}\int_0^\infty [c(\omega) - C_\infty]\cos(\omega t)d\omega = -\frac{2}{\pi}\int_0^\infty \omega[a(\omega) - A_\infty]\sin(\omega t)d\omega \tag{3.5}$$

Equation 3.4 is known as the Cummins equation and contains the memory effect of the generated waves (radiation part). As the potential damping and added mass is almost frequency-independent for the spar, the retardation function (Equation 3.5) converges to zero. However, for large-volume structures, such as semisubmersible and ships, the added mass and potential damping are highly frequency-dependent. The rigid-body equations of motion for a spar-type floating wind turbine can be written without the convolution integral as Equation 3.6, which is consistent with the Morison formula. In the present thesis, the potential damping and added mass of the spar are assumed to be frequency independent.

$$(m + A_\infty)\ddot{x} + D_{hydro1}\dot{x} + D_{hydro2}g_{hydro} + D_{aero1}\dot{x} + D_{aero2}g_{aero} + Kx = F(t,x,\dot{x}) \tag{3.6}$$

The rigid-body equations of motions for spar-type wind turbines are introduced above (Equation 3.6). Usually, the structure is divided into several bodies for an elastic multi-body system. Within each body, the elastic formulation is applied, while the rigid body connections through constraints (i.e., dashpot) are used to link the bodies. This methodology is used in the aero-hydro-servo-elastic codes such as HAWC2 code. Utilising finite element modelling, this equation can be solved for an elastic formulation of a floating wind turbine in the time

domain by time increment approach. In the following, the finite element formulation for the elastic equations of motions for floating wind turbines is discussed.

The dynamic equilibrium of a spatial discretised finite element model of a floating wind turbine can be expressed as the following equation:

$$R^I(r,\ddot{r},t)+R^D(r,\dot{r},t)+R^S(r,t)=R^E(r,\dot{r},t) \tag{3.7}$$

where R^I is the inertia force vector, R^D is the damping force vector, R^S is the internal structural reaction force vector, R^E is external force vector, and $r,\dot{r},\ddot{r}$ are the structural displacement, velocity and acceleration vectors.

This equation is a nonlinear system of differential equations due to the displacement dependencies in the inertia and the damping forces and the coupling between the external load vector and structural displacement and velocity. Also, there is a nonlinear relationship between internal forces and displacements. All force vectors are established by an assembly of element contributions and specified discrete nodal forces.

The external force vector (R^E) accounts for the weight and buoyancy, drag and wave acceleration terms in the Morison formula, mooring system forces, forced displacements (if applicable), specified discrete nodal forces, and aerodynamic loads.

The aerodynamic loads including the drag and lift forces are calculated by considering the instantaneous position of the element and the relative wind velocity. The blade element momentum (BEM) theory is used to present the aerodynamic loads on the tower, nacelle and rotor including the blades and hub. The aerodynamic damping forces can be kept on the right-hand side or moved to the damping force vector on the left-hand side. In the present formulation, the aerodynamic drag and lift forces and hydrodynamic drag forces accounting for the relative velocity are put on the right-hand side in the external force vector.

The inertia force vector (R^I) can be expressed by the following:

$$R^I(r,\ddot{r},t)=[M^S+M^H(r)]\ddot{r} \tag{3.8}$$

where M^S is the structural mass matrix, and $M^H(r)$ is the displacement-dependent hydrodynamic mass matrix accounting for the structural acceleration terms in the Morison formula as added mass contributions in local directions.

The damping force vector (R^D) is expressed as the following:

$$R^D(r,\dot{r},t) = [C^S(r) + C^H(r) + C^D(r)]\dot{r} \tag{3.9}$$

where $C^S(r)$ is the internal structural damping matrix, $C^H(r)$ is the hydrodynamic damping matrix accounting for the radiation effects for floating and partly submerged elements, and $C^D(r)$ is the matrix of specified discrete dashpot dampers, which may be displacement-dependent.

The dynamic equilibrium equations (Equation 3.7) can be solved in the time domain through step-by-step numerical integration based on Newmark-β methods.

3.2 Environmental conditions

To design, install and operate offshore wind turbines in a safe and efficient manner, it is necessary to have realistic metocean (meteorological and oceanographic) data available for the conditions to which the installation may be exposed.

3.2.1 General

The first step in performing rational structural dynamic analysis is setting realistic environmental conditions. The most important for a floating wind turbine are the wind and wave at the wind park site. However, at some offshore locations, other parameters may be important (e.g. air and sea temperature, tidal conditions, current and ice conditions).

The wave and wind are random in nature. This randomness should be represented as accurately as possible to calculate reasonable hydro-aero-dynamic loading. Both the waves and the wind have long-term and short-term variability. The simulation time depends on the natural periods of the system. Wave-induced motions of common floating structures have been carried out considering 3-hour short-term analysis (Naess and Moan, 2005). In wind engineering, the 10-minute response analysis can cover all the physics governing a fixed wind turbine. When it comes to floating wind turbines, the correlation between the wave and wind should be accounted for. For each environmental condition, the joint distribution of the significant wave height, wave peak period, wave direction and mean water level (relevant for shallow water) combined with the mean wind speed, wind direction and turbulence should be considered.

3.2.2 Joint distribution of wave conditions and mean wind

The wave and wind show long-term and short-term variability. The long-term variability of the wind can be defined by the mean wind speed and direction. The short-term variability of

the wind is usually defined by the turbulence. In an offshore site, the ocean waves can be wind-generated and swell. The waves are usually defined by the peak period and significant wave height. The correlation between the waves and wind should be considered for stochastic analysis of floating wind turbines. Site assessments containing metocean data are needed to develop the joint distribution of the waves and wind for the analysis. The joint distribution can include the wave and wind characteristics, such as the mean wind speed, turbulence, direction of the waves and wind, significant wave height, and wave peak period. However, development of the joint distribution requires measurement of simultaneous wave and wind time histories at the offshore sites for several years. Currently, limited site assessments considering the correlated wave and wind time series are available. These data are missing the correlation between the turbulence and wave/mean wind characteristics. The offshore wind turbine is a new technology, and large metrological/oceanological studies for determining the proper joint distribution of wave and wind characteristics are needed.

In the present research, the wind and wave were assumed to have the same direction. The correlation between the mean wind speed, significant wave height, and wave peak period was considered which can be done by fitting the analytical functions to the site assessments by considering a mathematical distribution for the mean wind speed and significant wave height. Johannessen et al. (2001) modelled the significant wave height as a Weibull distribution whose parameters were functions of the mean wind speed. In this thesis, the turbulence was assumed to be correlated to the mean wind speed, and proper values based on currently available offshore wind standards and codes considering operational and survival cases were selected (*Paper 5*).

Figure 3.1 illustrates the Weibull probability density function of the significant wave height (H_S) given the mean wind speed at nacelle (V) for the representative offshore wind park, Statfjord offshore site at 59.7^{o}N and 4.0^{o}E and 70 km distance from the shore (*Paper 2*).

The significant wave height increased with the increase of the wind speed. For higher wind speeds, the Weibull distribution was negatively skewed. For each wind speed, a range of significant wave heights was possible. Smaller wind speeds had a narrower range of significant wave heights. The IEC 61400-3 standard recommends the use of the median significant wave height at each wind speed for dynamic response analysis of offshore wind turbines.

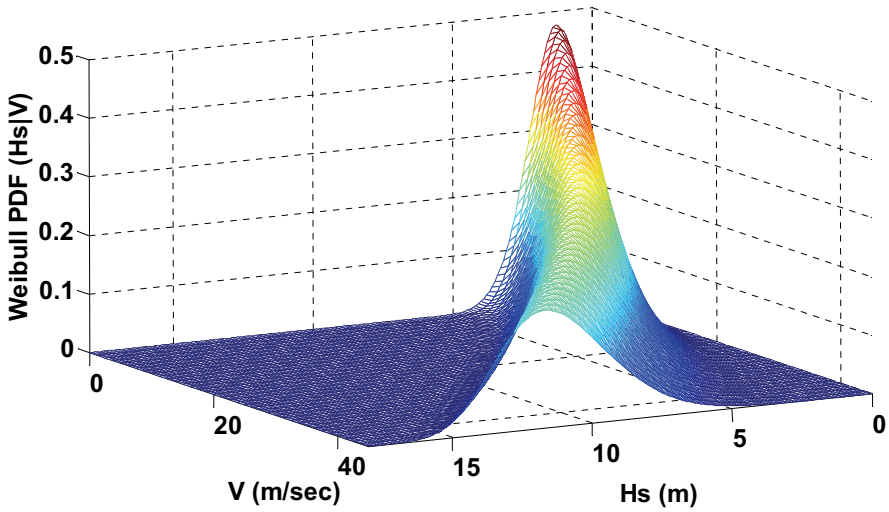

Figure 3.1: The Weibull probability density function of the significant wave height (H_S) given the mean wind speed at nacelle (V) for the Statfjord offshore site at 59.7°N and 4.0°E and 70 km from the shore.

3.3 Hydrodynamics

In this section the regular wave theory, modified regular wave theory and wave loads are described. In Chapter 4, the irregular wave theory and stochastic waves are explained.

3.3.1 Regular wave theory

In the regular wave theory, the wave is assumed to be sinusoidal with constant wave amplitude, wave length and wave period. Thus, the regular propagating wave is defined as $\zeta = \zeta_a \sin(\omega t - kx)$. The linear wave theory, usually called the Airy theory, can be used to represent the wave kinematics. In the Airy theory, the sea water is assumed to be incompressible and inviscid. The fluid motion is irrotational. Then, a velocity potential exists and satisfies the Laplace equations. By applying the kinematic boundary conditions and the dynamic free surface conditions, the velocity potential and the wave kinematics can be found. For more information, refer to Faltinsen (1995). Based on the Airy theory, the horizontal water particle kinematics are described by Equations 3.10 and 3.11 (Faltinsen 1995). The dynamic pressure is presented in Equation 3.12.

$$u = \omega \zeta_a \frac{\cosh k(z+h)}{\sinh kh} \sin(\omega t - kx) \tag{3.10}$$

$$a_X = \omega^2 \varsigma_a \frac{\cosh k(z+h)}{\sinh kh} \cos(\omega t - kx) \tag{3.11}$$

where u and a_X are the water particle velocity and acceleration in the x-direction (wave propagation direction), respectively, ω is the wave frequency, ς_a is the regular wave amplitude, k is the wave number, the z axis is upward, and h is the mean water depth.

$$P_D = \rho g \varsigma_a \frac{\cosh k(z+h)}{\cosh kh} \sin(\omega t - kx) \tag{3.12}$$

In deep water, the water particles move in circles in accordance with the harmonic wave. In deep water, the depth is greater than half of the wave length ($h \geq \lambda / 2$). Thus, the effect of the sea bed cannot disturb the waves. For shallow water the effect of the seabed transforms the circular motion into an elliptic motion.

When the wave amplitude increases, the wave particle no longer forms closed orbital paths. In fact, after the passage of each crest, particles are displaced from their previous positions. This phenomenon is known as the Stokes drift. The Boussinesq equations that combine frequency dispersion and nonlinear effects are applicable for intermediate and shallow water. However, in very shallow water, the shallow water equations may be used.

Linear wave theory represents the first-order approximation in satisfying the free surface conditions. It can be improved by introducing higher-order terms in a consistent manner via the Stokes expansion (Faltinsen 1995). In the present research, the linear wave theory was applied. The wave theory discussed here is just applicable for non-breaking waves. The wave breaks when $H / h \geq 0.78$ in shallow water and when $H / \lambda \geq 0.14$ in deep water (DNV 2007). H is the wave height, and the h is the mean water depth. For extreme waves, when the height increases greatly, the nonlinear features of the wave kinematics cannot be captured through linear wave theory. However, the nonlinear methods are mainly applicable for deterministic waves; they are not suitable for stochastic wave fields. Fortunately, the probability of breaking waves is relatively small. Moreover, most of the waves break close to the coast and not at the offshore wind turbine site. Although not considered further in this document, breaking waves would need to be considered for detailed design.

3.3.2 Modified linear wave theory

The Airy wave theory is only valid up to the mean water level surface and does not describe the kinematics above that level. Different mathematical models, such as constant stretching and Wheeler stretching, have been suggested to describe the wave kinematics above the mean

water level surface. In the constant stretching model, it is assumed that the wave kinematics are constant above the mean water level (MWL). In the Wheeler stretching model, the vertical coordinate z is substituted by the scaled coordinate z' (Equation 3.13). In present research, the Wheeler stretching model was used (*Paper 6*).

$$z' = (z - \zeta)\frac{h}{h + \zeta} \tag{3.13}$$

where ζ is the wave elevation, and $\zeta = \zeta_a \sin(\omega t - kx)$. In Section 4.2, the stretching in the stochastic context is explained.

3.3.3 Wave loads

Considering the size and type of the support structure and turbine, wave loading may be significant and can be the main cause of fatigue and extreme loads that should be investigated in coupled analysis. Hence the selection of a suitable method of determining the hydrodynamic loads can have an important effect on the cost of the system and its ability to withstand environmental and operational loads.

The panel method, Morison formula and pressure integration method or combination of these methods can be used to calculate the hydrodynamic forces. The selection of the method should be concept-dependent. Some of the hydrodynamic aspects for a floating wind turbine that may be considered depending on the concept and site specification are listed below (Faltinsen 1995 and Henderson 2003):

- Appropriate wave kinematics models
- Hydrodynamic models considering the water depth, sea climates and support structures
- Extreme hydrodynamic loading, including breaking waves, using nonlinear wave theories and appropriate corrections
- Stochastic hydrodynamic loading using linear wave theories with empirical corrections
- Consideration of both slender and large-volume structures depending on the support structure of the floating wind turbine

The Morison formula is practical for slender structures where the dimension of the structure is small compared to the wave length, i.e., $D < 0.2\lambda$ (Faltinsen 1995), where D is the characteristic diameter, and λ is the wave length. In other words, it is assumed that the structure does not have significant effect on the waves. The hydrodynamic forces ($F_{Hydrodynamic}$) through the Morison formula include the inertial and quadratic viscous excitation forces. The inertial forces in the Morison formula consist of diffraction and Froude-Krylov forces for a fixed structure. For a floating structure, the added mass forces are included in the Morison

formula through relative acceleration as well and the damping forces appear through the relative velocity.

Equation 3.14 shows the hydrodynamic forces per unit length on the floater based on the Morison formula, which was extended to account for the instantaneous position of the structure for floating wind turbines (Faltinsen 1995).

$$dF = \frac{\rho}{2} C_d D |u_r| u_r + \rho \frac{\pi D^2}{4} C_m \dot{u}_r + \rho \frac{\pi D^2}{4} \dot{u}_W \tag{3.14}$$

$$u_r = u_W - u_B \tag{3.15}$$

where ρ is the mass density of sea water, D is the cylinder diameter, $\dot{u}_r$ and u_r are the horizontal relative acceleration and velocity between the water particle velocity u_W and the velocity of the body u_B (Equation 3.15), respectively, and C_m and C_d are the added mass and quadratic drag coefficients, respectively.

The first term is the quadratic viscous drag force, the second term includes the diffraction and added mass forces, and the third term is the Froude-Krylov force (FK term). A linear drag term $C_l u_r$ can be added to the Morison formula as well, where C_l is the linear drag coefficient. However, for the spar-type platforms such as CMS and TLS, the quadratic viscous drag is dominant, and the linear drag term was not included (*Papers 2 and 6*). The positive force direction is in the wave propagation direction. C_d and C_l have to be empirically determined and are dependent on many parameters as the Reynolds number, Kaulegan-Carpenter number (KC), a relative current number and surface roughness ratio (Faltinsen 1995).

For large-volume structures, the diffraction becomes important. The MacCamy-Fuchs correction for the inertia coefficient in some cases can be applied. Based on the panel method (BEM) the added mass coefficient for a circular cylinder is equal to 1, which corresponds to the diffraction part of the Morison formula. The Froude-Krylov contribution can be found by pressure integration over the circumference; for a cylinder in horizontal direction, is equal to 1. Therefore, the inertia coefficient for a slender circular member is 2.

It is possible to use the pressure integration method to calculate the Froude-Krylov part of the Morison formula and just apply the diffraction part through the Morison formula. The USFOS code uses pressure integration method to calculate the vertical forces and horizontal Froude-Krylov part of the Morison formula. However, the HAWC2 code uses the pressure integration method just for calculating the vertical forces and forces on conical sections.

For a floating wind turbine, the instantaneous position should be accounted for when updating the hydrodynamic forces. Hence, the moving structure Morison formulation should

use the accelerations and velocities at the instantaneous position. The relative velocity will be applied to the quadratic viscous part. The pressure integration method and the Morison formula use the updated wave acceleration at the instantaneous position. The geometrical updating adds some nonlinear hydrodynamic loading that can excite the low natural frequencies of the spar.

Based on second-order wave theory, the mean drift, slowly varying (difference frequency) and sum frequency forces, drift-added mass and damping can be added to the above linear wave theory. The Morison formula combined with the pressure integration method is a practical approach to model the hydrodynamic forces for a spar-type wind turbine. Using the modified linear wave theory accounting for the wave kinematics up to the wave elevation and the pressure integration method in transversal directions (Froude-Krylov), the mean drift forces were considered in the present research. Moreover, the sum frequency forces were considered by using the instantaneous position of the structure to calculate the hydrodynamic forces.

3.4 Aerodynamics

The aerodynamic forces ($F_{Aerodynamic}$) consist of the lift and drag forces. The lift forces, skin friction and pressure viscous drags are the main sources of the aerodynamic forces for the slender parts of a wind turbine. For slender structures the 2D aerodynamic theory is applicable. Through the blade element momentum (BEM) theory, the lift and drag coefficients are used to model the aerodynamic forces. For a parked wind turbine, the aerodynamic forces are calculated directly using the relative wind speed. However, for an operating wind turbine, the induced velocities and wake effects on the velocity seen by the blade element need to be determined.

The wind turbine blades and the tower are long and slender structures. The span-wise velocity component is much lower than the stream-wise component, and in many aerodynamic models, it is therefore assumed that the flow at a given point is two-dimensional and the 2D aerofoil data can be applied (Hansen 2008). Figure 3.2 illustrates a transversal cut of the blade element viewed from beyond the tip of the blade. In this figure, the aerodynamic forces acting on the blade element are also depicted. The blade element moves in the airflow at a relative speed V_{rel}. The lift and drag coefficients are defined as follows:

$$C_L(\alpha) = \frac{f_L}{\frac{1}{2}\rho V_{rel}^2 c}$$
$$C_D(\alpha) = \frac{f_D}{\frac{1}{2}\rho V_{rel}^2 c} \tag{3.16}$$

where f_D and f_L are the drag and lift forces (per length), c is the chord of the airfoil, ρ is the air density, α is the angle of attack, and V_{rel} is the relative velocity.

$$V_{rel} = V\sqrt{(1-a)^2 + (\frac{r\Omega_r}{V}(1+a'))^2} \tag{3.17}$$

$$\alpha = \phi - \beta \tag{3.18}$$

$$\tan(\phi) = \frac{V}{r\Omega_r}\frac{1-a}{1+a'} \tag{3.19}$$

where a and a' are the axial and rotational induction factors, respectively, V is the upstream wind velocity, f_T is the thrust force, r is the distance of the airfoil section from the blade root, and Ω_r is the rotational velocity (rad/sec). a and a' are functions of ϕ, C_L, C_D and the solidity (fraction of the annular area that is covered by the blade element). The aerodynamic theories to calculate the wind loads for operational and parked conditions are very similar. For a parked wind turbine, the rotational speed (Ω_r) is zero as the blades are fixed and cannot rotate. ϕ is 90 degrees, which means the relative wind velocity and the wind velocity are parallel.

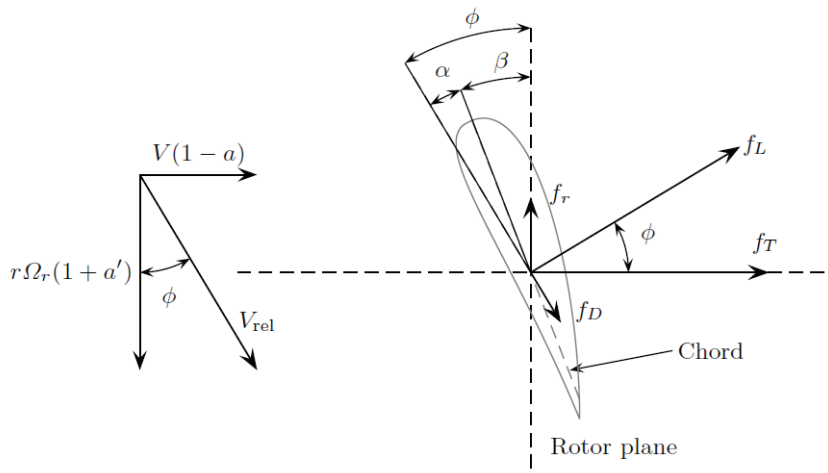

Figure 3.2: Forces on a blade element (Bianchi et al. 2007).

The following features need to be included in the aerodynamic model (Burton et al. 2008):

- Deterministic aerodynamic loads: steady (uniform flow), yawed flow, shaft tilt, wind shear, tower shadow and wake effects
- Stochastic aerodynamic forces due to the temporal and spatial fluctuation/variation of wind velocity (turbulence)
- Rotating blades aerodynamics, including induced flows (i.e., modification of the wind field due to the turbine), three-dimensional flow effects and dynamic stall effects

- Dynamic effects from the blades, drive train, generator and tower, including the modification of aerodynamic forces due to vibration and rigid body motions
- Subsystem dynamic effects (i.e., the yaw system and blade pitch control)
- Control effects during normal operation, start-up and shutdown, including parked conditions

The aerodynamic loads can be divided into different types (Manwell 2006):

- Static loads, such as a steady wind passing a stationary wind turbine
- Steady loads, such as a steady wind passing a rotating wind turbine
- Cyclic loads, such as a rotating blade passing a wind shear
- Transient loads, such as drive train loads due to the application of the brake
- Impulsive loads, i.e., loads with short duration and significant peak magnitude, such as blades passing a wake of tower for a downwind turbine
- Stochastic loads, such as turbulent wind forces
- Resonance-induced loads, i.e., excitation forces close to the natural frequencies

The mean wind induces steady loads while the wind shear, yaw error, yaw motion and gravity induce cyclic loads. Turbulence is linked to stochastic loading. Gusts, starting, stopping, feathering the blades and teetering induce transient loads. Finally, the structure's eigen-frequencies can be the source of resonance-induced loading.

The aerodynamic performance of a wind turbine is mainly a function of the steady state aerodynamics. However, there are several important steady state and dynamic effects that cause increased loads or decreased power production compared to those expected from the basic BEM theory. These effects can especially increase the transient loads. Manwell et al. (2006) listed some of the advanced aerodynamic subjects:

a) Non-ideal steady-state aerodynamic issues
    - Decrease of power due to blade surface roughness (for a damaged blade, up to 40% less power production)
    - Stall effects on the airfoil lift and drag coefficients
    - The rotating condition affects the blade aerodynamic performance. The delayed stall in a rotating blade compared to the same blade in a wind tunnel can decrease the wind turbine life.
b) Turbine wakes
    - Skewed wake in a downwind turbine
    - Near and far wakes. The turbulence and vortices generated at the rotor are diffused in the near wake and the turbulence and velocity profiles in the far wake are more uniformly distributed.
    - Off-axis flows due to yaw error or vertical wind components

c) Unsteady aerodynamic effects
   - Tower shadow (wind speed deficit behind a tower due to tower presence)
   - Dynamic stall i.e., sudden aerodynamic changes that result in or delay the stall
   - Dynamic inflow i.e., changes in rotor operation
   - Rotational sampling. It is possible to have rapid changes in the flow if the blades rotate faster than the turbulent flow rate.

The effect of turbulence on the dynamic responses is investigated for both CMS and TLS wind turbines. The structural responses showed that turbulence has a limited effect on the global responses. The turbulence does not affect the structural responses very much; thus, it is possible to use the constant wind model in fatigue and ultimate limit state analyses with an acceptable accuracy (*Papers 2 and 9*). The turbulence does not affect the mean of the generated power very much. However, the electrical power fluctuations are increased for turbulent wind cases. The rotor configuration effects on the dynamic motion and structural responses for TLS-type wind turbine under different operational and survival cases are studied. The proper tower shadow model for each rotor configuration (downwind and upwind) is applied to represent the tower wake deficit (*Paper 8*).

Aeroelastic instability can occur whenever any modal response creates accompanying periodic aerodynamic forces that feed the resonant response, for instance the negative damping mechanism (Spera 1998). The servo-induced negative damping can present instabilities for resonant motion of TLS wind turbine (*Paper 7*). It is possible to remove the negative damping by modifying the controller gains. The results showed that the tuning can help to reduce the structural responses and increase the power production (*Paper 9*). The cyclic disturbance of the blade's angles of attack can be the prime mechanism of rotor aeroelastic instability. If the controller acts faster than the changes in the wind fields, negative damping can occur. For a floating wind turbine, it is possible to have the controller acting faster than the low natural frequencies. The nacelle/tower instability for the horizontal axis wind turbine is another aeroelastic instability that can occur in the absence of corrective control system actions. Whirl mode instability can occur in which the shaft moves through a conical locus, with the tower deflecting and the hub moving in a nearly circular path. The other instability is the yaw angle oscillation of the turbine shaft, which can occur when the tower axis does not pass through the centre of the nacelle/rotor combination.

3.5 Mooring system, inertial and other forces

The mooring system forces ($F_{Mooring\ System}$) are nonlinear time- and position-dependent restoring forces. Nonlinear spring or finite element modelling is usually applied. Drag forces on the mooring lines can contribute to the damping effect on the spar motions. If inertia and

the damping effects of the mooring system are neglected, it is possible to model the mooring system as a nonlinear spring.

The gravitational forces ($F_{Gravitational}$), deterministic inertial forces ($F_{Inertial}$) including centrifugal loads, gyroscopic forces, breaking loads and other forces, such as sea current and mechanical control forces (i.e., shutdown forces), should be included, if applicable.

Chapter 4

Stochastic Load Modelling and Analysis of Floating Wind Turbines

4.1 General

Accurate analytical methods can be applied to investigate the dynamic response of a floating wind turbine using stochastic wave- and wind-induced response simulations. Knowledge of the joint distribution of the wave and wind is necessary to set realistic environmental conditions. The proper statistical methods are required to investigate the fatigue and ultimate limit states in operational and harsh environmental conditions.

4.2 Irregular wave theory

Wind-generated waves are forced waves that are sustained by receiving energy from the wind. Swell waves are free waves that do not receive wind energy due to absence of wind or movement to a new free-wind location. The practical way to model ocean waves in ocean engineering assumes that the sea surface forms a stochastic wave field that can be assumed to be stationary in a short term period. The stationary assumption of the wave is site-dependent (Naess and Moan, 2005). For most practical offshore engineering purposes this assumption works very well and gives good agreement with full-scale measurements. The wave field is assumed to be Gaussian, which gives a reasonably good approximation of reality in most cases. The stochastic model approved for the waves leads to a normally distributed water surface elevation. The wave crests follow the Rayleigh distribution if the wave elevation is assumed to be Gaussian and narrow-banded. However, some phenomena, such as slamming, do not have a Gaussian distribution.

Based on the Gaussian assumption, the stationary sea (represented by the wave elevation at a point in space) can be modelled by a wave spectrum. The Pierson-Moskowitz (PM) and JONSWAP spectra (Equations 4.1 and 4.2) are examples of mathematical models to represent

the ocean wave spectrum (Sagli 2000). For a fully developed wind sea, the PM spectrum can be used, and for a growing wind sea, the JONSWAP spectrum can be used. Moreover, the Torsethaugen spectrum (two-peaked wave spectrum) is introduced to define a sea comprising wind-generated waves and swells.

$$S_{PM}(f) = \frac{5}{16}\frac{H_S^2}{T_P^4 f^5}\exp(-\frac{5}{4}(f\,T_P)^{-4}) \tag{4.1}$$

where H_S is the significant wave height, T_P is the wave peak period, and f is the frequency in hertz.

$$S_{JS}(f) = F_n\, S_{PM}(f)\,\gamma_{JS}\exp(\frac{-(f-f_P)^2}{2\sigma_{JS}^2 f_P^2}) \tag{4.2}$$

$$\sigma_{JS} = \begin{cases} \sigma_a & for\ f \le f_P\ \ (typically: 0.07) \\ \sigma_b & for\ f > f_P\ \ (typically: 0.09) \end{cases} \tag{4.3}$$

$$F_n = [5(0.065\,\gamma_{JS}^{0.803} + 0.135)]^{-1} \qquad for\ 1 \le \gamma_{JS} \le 10 \tag{4.4}$$

where γ_{JS} is the shape parameter, which is around 3.3 for seas that are not fully developed. For fully developed seas, γ_{JS} is taken to be 1. Therefore, the JONSWAP and PM spectra are the same for $\gamma_{JS} = 1$. $f_P = \frac{1}{T_P}$ is the wave peak frequency in hertz.

In Figure 4.1, the JONSWAP wave spectrum for operational and harsh environmental conditions is illustrated. The extreme sea state has much larger peaks, and it also covers a wider range of frequencies. The peak frequency of a harsh sea state is shifted to lower frequencies as well. This shift means that the probability of resonant motion occurrence is higher in extreme environmental conditions.

For a suitable wave spectrum representing the offshore site, the calculations may begin by converting the spectrum back into individual sinusoids using inverse fast Fourier transformation (IFFT). Each sinusoid has a frequency and amplitude that can be derived from the energy density given by the wave spectrum. The phase angle is assigned randomly to each sinusoid.

In the stochastic context, the Wheeler stretching can be applied as well. For each regular wave, the stretching is applied, and the wave kinematics up to the instantaneous water level is obtained. Then, the wave elevation, and the velocities and acceleration of regular waves are added together to obtain the irregular wave elevation, velocity and acceleration for that particular time.

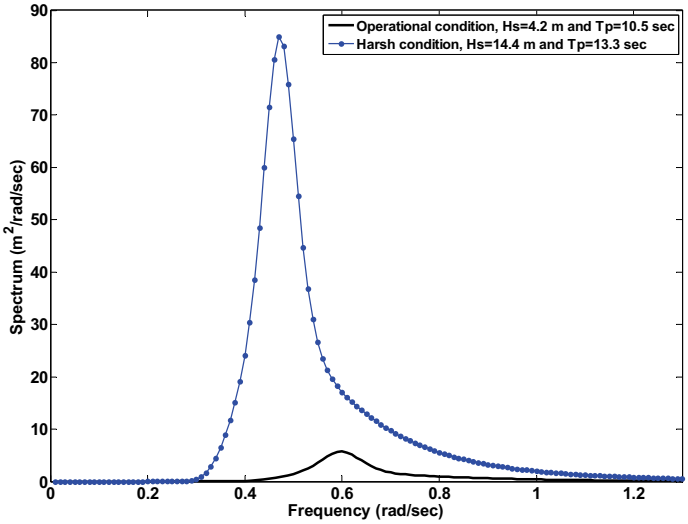

Figure 4.1: The JONSWAP wave spectrum for harsh and operational conditions.

4.3 Turbulent wind theory

The wind varies over space and time. It is important to know these variations to investigate the site energy resources for making electrical power, which is the first concern for a specific location. Spera (1998) mentioned the spatial and temporal variations of the wind:

Spatial variations:

- Trade winds emerging from subtropical, anticyclonic cells in both hemispheres
- Monsoons which are seasonal winds generated by the difference in temperature between land and sea
- Westerlies and sub-polar flows
- Synoptic-scale motions, which are associated with periodic systems such as travelling waves
- Mesoscale wind systems which are caused by differential heating of topological features and called breezes

Time variations:

- Long term variability which are annual variations of wind in a special site
- Seasonal and monthly variability
- Diurnal and semidiurnal variation
- Turbulence (range from seconds to minutes)

The temporal variations are usually represented by the energy spectrum of the wind. In Figure 4.2, the Van der Hoven wind speed spectrum (Hoven 1957) is shown. The yearly wind speed changes, pressure systems and diurnal changes are influencing the left side of the wind speed spectrum. However, the turbulence shows itself in the right side of the spectrum.

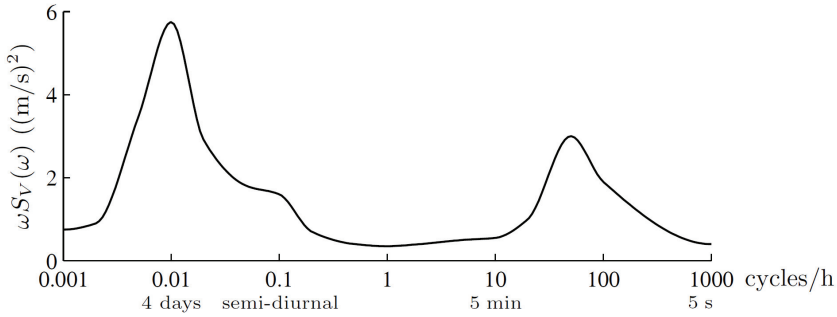

Figure 4.2: Van der Hoven wind speed spectrum (reproduced), Bianchi et al. (2007).

The wind is characterised by its speed and direction. The wind energy is concentrated around two separated time periods (diurnal and 1 min periods), which allows the splitting of the wind speed into two terms: the quasi-steady wind speed (usually called the mean wind speed) and the dynamic part (the turbulent wind). In other words, the time-varying wind speed is considered to be made up of a steady value plus the fluctuations about this steady value. The steady value is assumed to be quasi-static; thus, its time dependency is negligible for the current purpose (the probabilistic dynamic response analysis). The long-term probability distribution of the mean wind speed is predicted by fitting site measurements to the Weibull distribution (Equation 4.5). The Weibull probability density function (f_W) shows that the moderate winds are more frequent than the high-speed winds.

$$f_W(V) = \frac{k_w}{c_w}\left(\frac{V}{c_w}\right)^{k_w-1}\exp\left(-\left(V/c_w\right)^{k_w}\right) \tag{4.5}$$

where V is the wind speed, k_w is the shape parameter describing the variability about the mean, and c_w is a scale parameter related to the annual mean wind speed. In Figure 4.3, the Weibull probability distribution for three different areas, i.e., onshore, coastal and offshore, with typical values of shape and scale parameters are plotted (Twidell and Gaudiosi 2008).

An empirical formula for the annual mean wind speed (V_{Annual}) is given in Equation 4.6 by Lysen (1983).

$$V_{Annual} = c_w(0.568 + 0.433/k_w)^{1/k_w} \tag{4.6}$$

The annual mean wind velocities corresponding to different sites in Figure 4.3 were 6.5, 8 and 11.3 m/sec for the onshore, coastal and offshore sites, respectively. Considering Equation 1.1, the ratio between the offshore and onshore power corresponding to the present example

can be up to 5, which confirms the possibility of generating more electrical power by moving offshore.

The mean wind speed is a function of height, which can be represented by different shear models such as the Prandtl logarithmic and power laws. In these mathematical models, a parameter called the roughness length or exponent, accounts for the effect of the type of surface over which the wind blows (Bianchi et al. 2007).

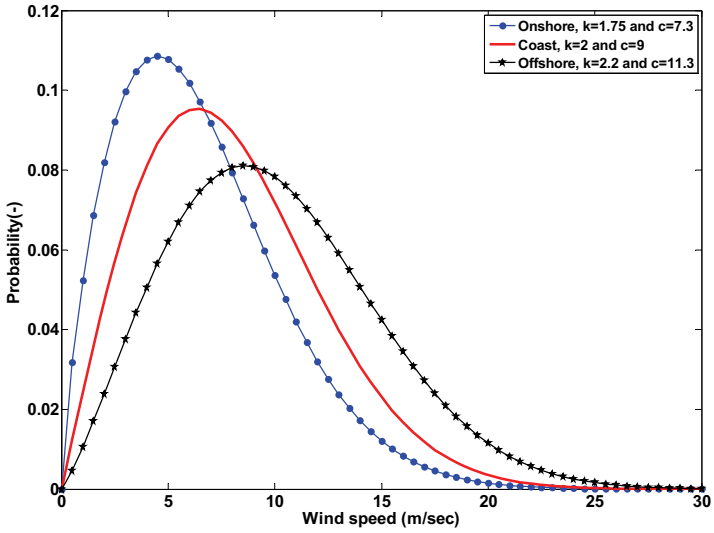

Figure 4.3: Weibull probability distribution of wind velocity for three different sites: onshore, coastal and offshore considering typical values of shape and scale parameters (Twidell and Gaudiosi 2008).

The turbulence in the wind is caused by the dissipation of the wind kinetic energy into thermal energy via the creation and destruction of progressively smaller eddies or gusts. Turbulent wind may have a relatively constant mean over time periods of an hour or more, but over shorter times (minutes or less) it may be quite variable. Turbulent wind consists of longitudinal, lateral and vertical components (Manwell et al. 2006).

The dynamic part of the wind speed, turbulence, includes all wind speed fluctuations with periods below the spectral gap. The spectral gap occurs around 1 hour which separates the slowly changing and turbulent ranges. Therefore, all components in the range from seconds to minutes are included in the turbulence. The captured annual power is not affected by turbulence very much, but the turbulence has a major impact on aero-elastic structural response and electrical power quality. It is common to describe the wind turbulence in a given point in space using the power spectrum. The Kaimal and von Karman spectra are widely used. Both models depend on the mean wind speed and the topography of the terrain. One useful parameter is the turbulence intensity, which is defined as the ratio of the standard

deviation of the wind speed to the mean wind speed. The turbulence intensity decreases with height. The turbulence intensity is higher when there are obstacles in the terrain; hence, the turbulence intensity for an offshore site is less than that for a land site.

The turbulent wind spectrum, such as the Kaimal spectrum (Equation 4.7), is a function of the frequency, turbulence intensity, and mean wind speed (Hansen 2008).

$$S(f) = \frac{I_t^2 V_{10\min} l}{(1+1.5\frac{f\,l}{V_{10\min}})^{5/3}} \tag{4.7}$$

where $I_t = \sigma / V_{10\min}$ is the turbulent intensity, f is the frequency in hertz, $V_{10\min}$ is the 10-minute averaged wind speed, and l is a length scale. $l = 20 h_{agl}$ for $h_{agl} < 30\,m$ or $l = 600\,m$ otherwise, where h_{agl} is the height above ground level.

In Figure 4.4, the Kaimal spectra for onshore and offshore sites are plotted. The harsh and operational environmental conditions with their mean wind speed and turbulent intensity were considered. The spectrum under harsh conditions has much more energy compared to those under operational conditions, especially in the low frequency region. At the offshore site, the wind is steadier, and the turbulence is decreased, but at onshore sites, the obstacles in the terrain influence the boundary layer and make the wind more turbulent.

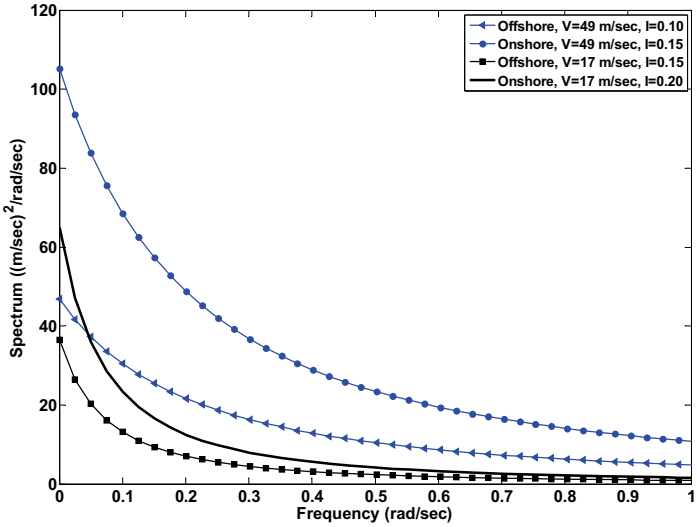

Figure 4.4: Kaimal spectra for onshore and offshore sites under operational and extreme environmental conditions, with the corresponding mean wind velocities and turbulent intensities for those conditions.

4.4 Stochastic response analysis

Frequency-domain, time-domain and hybrid time-frequency domain analyses are widely used for dynamic response analysis of offshore structures. The frequency domain analysis is very fast. However, it is not possible to use the frequency domain methods for a floating wind turbine due to nonlinear wave and wind loading, control, strong coupling of rotor-platform, geometrical updating, and large deformation. Hence, the integrated time domain analysis is necessary for such structures. As the environmental conditions are stochastic, the aerodynamic and hydrodynamic loads, and consequently the responses of offshore wind turbines, are stochastic. We can distinguish mainly generalities from a time domain analysis: maximum, high and low frequency responses, strange peaks and very slow variations. The time series can be transformed into the frequency domain and presented in spectral format to make it easier to follow the nature of the response. IEC recommends 1-hour stochastic time-domain simulations to ensure statistical reliability. The first part of the time-domain stochastic simulation, which is influenced by transient responses, should be eliminated before transforming to the frequency domain.

The fatigue and ultimate limit states are two important factors in the design of ocean structures. The environmental conditions can be harsh and induce extreme responses for a floating structure. For a land-based wind turbine, the fatigue is the key parameter in design, and the extreme responses that occur in operational conditions are connected to the rated wind speed. However, for a floating wind turbine, the extreme responses can occur in survival conditions.

4.4.1 Time domain analysis

The time domain analysis should be applied for solving the equations of motion for nonlinear systems. For a floating wind turbine, because the nonlinearities involved in the loading are dominant, the linearisation of the equations of motion does not accurately represent the dynamic structural responses. Even if linear elastic theory is used to model the structure, the loading is nonlinear. Consequently, the responses are nonlinear as well. The aerodynamic loading is inherently nonlinear and the aerodynamic lift and drag-type forces for a parked or operating wind turbine are fully nonlinear. The hydrodynamic drag forces are similar to aerodynamic forces in nature and add nonlinearities. The instantaneous position of the wind turbine should be accounted for when calculating the hydrodynamic and aerodynamic forces. The geometrical updating introduces nonlinear loading which can excite the resonant motions. The hydrodynamic nonlinearities due to geometrical updating for a catenary moored spar-type wind turbine are investigated in *Paper 2*. It was shown that both the hydrodynamic inertial and drag forces need to be updated considering the instantaneous position of the system. The aerodynamic damping, wave-induced aerodynamic damping, hydrodynamic

damping and wind-induced hydrodynamic damping need to be considered for a floating wind turbine. The coupled time-domain analysis is the reliable approach to account for all these damping phenomena. For an operating wind turbine, the control algorithm controls the output power by controlling the rotational speed of the rotor or the attack angle of the blades by feathering the blades. Time-domain analysis is necessary to implement the control loops. The mooring lines are nonlinear elastic elements; the nonlinear force-displacement or FE modelling can be used.

The above discussion is summarised in the following to introduce the importance of coupled time-domain analysis for a floating wind turbine.

1) Nonlinear hydrodynamic excitation forces:
   - Inertial and drag forces considering the instantaneous position of the system
   - Hydro-elasticity
2) Aerodynamic forces:
   - Lift and drag excitations considering the relative velocity
   - Aero-elasticity
3) Damping:
   - Aerodynamic damping
   - Hydrodynamic damping
   - Wave-induced aerodynamic damping
   - Wind-induced hydrodynamic damping
4) Mooring system:
   - Nonlinear finite elements
5) Control

Figure 4.5 (taken from *Paper 3*) shows the hydrodynamic and aerodynamic damping effects on the dynamic nacelle surge motion of a catenary moored spar-type wind turbine in below-rated operational conditions. In the left part of Figure 4.5, the quadratic viscous hydrodynamic effects are compared for two different drag coefficients. As the structure is inertia-dominated, the increase of the drag coefficient did not affect the wave frequency responses. However, the resonant responses were decreased. In the right part of Figure 4.5, the wave-induced response and wind- and wave-induced response are compared to show the effect of the aerodynamic damping. The aerodynamic damping decreased the resonant responses. However, the wave frequency responses were not affected by the wind loads in this case.

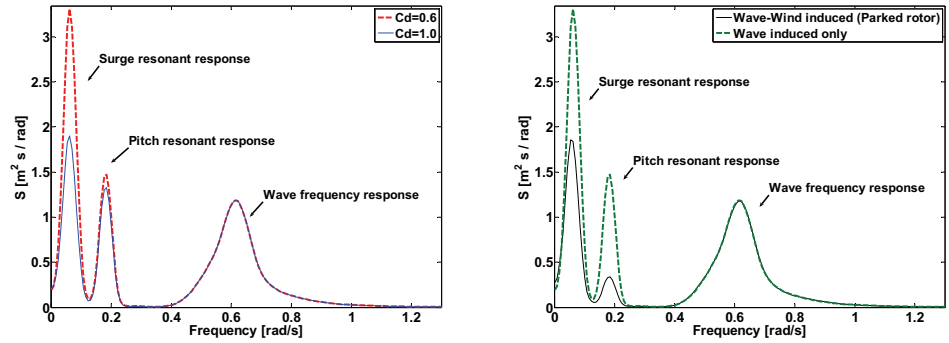

Figure 4.5: Left: Nacelle surge motion spectrum in a wave condition with Hs=3 m and Tp=10 sec, based on a 1-hour time domain simulation in HAWC2 (wave-induced), Right: Nacelle surge motion spectrum (H_S =3 m, T_P =10 sec and V =8 m/sec), based on a 1-hour time domain simulation in HAWC2 (constant wind)

Every time-domain simulation starts with the generation of the wave and wind time series. This step can be done through different strategies based on fast Fourier transforms (FFT) and inverse fast Fourier transform (IFFT) approaches (Moan et al. 2007). If the position is updated due to large motions, e.g., in a floating wind turbine, the FFT algorithm is not directly applicable, and the discrete Fourier transform (DFT) is usually applied. The wave and wind spectrum are used to represent the energy distribution for each frequency. For a specific location, the significant wave height, wave peak period, mean wind speed over a certain level from mean water surface and turbulence intensity are identified. The choice of the wave spectrum depends on the site. For developing wind-generated waves, the JONSWAP spectrum is suitable for the North Sea. Based on the significant wave height and the peak wave period, the distribution of energy for each frequency is defined for the chosen characteristics. The amplitude of each regular wave (ζ_a) is related to the wave spectrum. After introducing the regular waves for each frequency, the regular waves are added together to make the ocean surface (Equation 4.8). Random phases (ϕ_n) are used for the stochastic realisation. ω_n and k_n are the wave frequency and the wave number of the nth regular wave, respectively. N is the number of regular wave frequencies. To avoid repetition of the irregular wave, 1000 regular wave frequencies were chosen in the present study for each 1-hour analysis.

$$\zeta = \sum_{n=1}^{N} \zeta_{a,n} \sin(\omega_n t - k_n x + \phi_n) \tag{4.8}$$

If the turbulence intensity and the mean wind speed are defined for a site, the inverse DFT approach can be used to develop the turbulent wind. The Fourier transform that satisfies the wind spectrum may be in the form of Equation 4.9 (Hansen 2008).

$$V(t) = \bar{V} + \sum_{n=1}^{N/2} \sqrt{\frac{2S(\omega_n)}{T}} \cos(\omega_n t - \varphi_n) \qquad (4.9)$$
$$t = i \times \Delta t \quad for\ i = 1, ..., N$$

where T is the total time, and the phase angle φ_n is not reflected in the wind spectrum and can be modelled using a random number generator yielding a value between 0 and 2π. Mathematically, by performing a DFT of the wind spectrum, all frequencies between 0 and ∞ are involved. However, frequencies between $1/T$ and $N/2T$ are sufficient for generating the proper wind time series.

For a 3D wind simulation not only the frequency but also the distance between different points is important. In other words the time series for different points are not independent. This is introduced by the coherence function. If the distance between the points increases, then the correlation of their energy will be less.

The generated wave and wind time series should not contain repetition. There is a limitation of the turbulence box for most of the 3D turbulent wind generators. For instance, for an over-rated wind speed case, if a 1-hour simulation is needed then the simulation should be split to 2-4 shorter simulation periods with different seeds to ensure accurate stochastic representation. The responses of these shorter periods are combined together to make the 1-hour response. For the wave time series, the number of the frequencies and cut-in and cut-out frequencies of the spectrum are connected to repetition of the waves in a defined time-domain analysis. A wider frequency range and fewer frequencies lead to repetition even in a short simulation.

After generating the wave and wind time series, the motion equations should be set up, taking into account the coupling. At each time step, the position-dependent aerodynamic and hydrodynamic forces can be calculated based on aerodynamic and hydrodynamic theories. Integration methods are used to calculate the responses step by step. After finding the responses including the position of the structure in the new time step, all the terms in equations of motions can be updated considering the new geometrical and environmental conditions.

The time-domain analysis for a floating wind turbine is very time-consuming. Sufficient simulation time is needed to capture accurate dynamic responses. To capture accurate responses, the lowest natural frequency of the system is important. For example, if the surge natural frequency is around 0.07 (rad/sec) then each 1-hour simulation contains only 40 surge cycles. The other important factor in time-domain simulations is the selection of the time step. Less accuracy can be achieved with a larger time step. The maximum time step should be less than a certain value to capture at least 20 cycles of the lowest natural period involved in the

system. For example, for a catenary moored spar wind turbine, the largest eigen-frequencies are the blade eigen-frequencies, which are around 3 rad/sec. Twenty cycles can be achieved by choosing 0.1 sec for the time step in this example.

Figure 4.6 (taken from *Paper 2*) shows the nacelle surge time history (turbulent wind case) and nacelle surge spectrum (constant and turbulent wind cases) for harsh environmental conditions. All of the smoothed spectra in the present study were obtained based on time-domain simulations by applying a Fourier transformation. The nacelle surge motion in a survival condition is dominated by the pitch-resonant response. The comparisons between the turbulent and constant wind cases show that the turbulent wind excites the rigid body pitch and surge natural frequencies. The resonant response is dominant in both pitch motion and nacelle surge motion. Resonance should not be confused with instability. A resonant motion requires external excitation and initially grows linearly and not exponentially as in the case of instability.

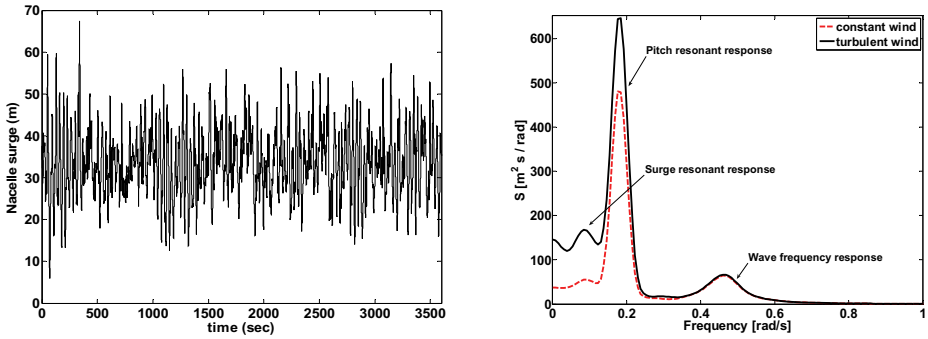

Figure 4.6: left: nacelle surge time history (turbulent wind case), right: nacelle surge spectrum for turbulent and constant wind cases. H_S *=14.4 m,* T_P *=13.3 sec,* V *=49 m/sec and* I_t *=0.1 (Paper 2).*

In Figure 4.7 (taken from Paper 2) the bending moments at the tower/spar interface for different mean wind speeds are plotted. The statistical characteristics are based on five 1-hour samples. The maximum responses correspond to the up-crossing rate of 0.0001 and are obtained by extrapolation.

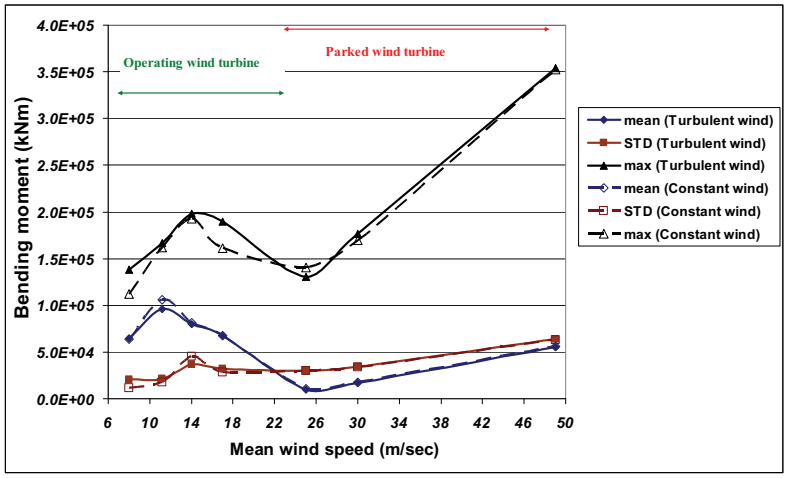

Figure 4.7: Bending moment at the tower-spar interface (wave- and wind-induced) for constant and turbulent wind cases. The statistical characteristics are based on five 1-hour samples. The maximum responses correspond to the up-crossing rate of 0.0001 and are obtained by extrapolation (Paper 2).

4.4.2 Response characteristics

In this section the characteristic features of the response are briefly outlined. The response of floating wind turbines may consist of three kinds of responses: quasi-static, resonant and inertia dominated responses. When the frequency of the excitation is much less than the natural frequencies, the response is quasi-static; the dynamic response is close to the response due to static loading. For example, the mean wind speed can create quasi-static surge responses. The resonant responses can occur if the excitation frequencies are close to the natural frequencies of the system. The nonlinear hydrodynamic and aerodynamic forces can excite the natural frequencies and create the resonant responses. The inertia-dominated response happens when the loading frequencies are much higher than the natural frequencies. The rigid body motions can be inertia-dominated as the wave frequencies are greater than the platform natural frequencies.

The idea is to minimise the wave- and wind-induced responses to therefore increase the power output with less fluctuation. The aerodynamic damping due to operation of the wind turbine can reduce the resonant responses. However, this aerodynamic damping is not significant for a parked or idling wind turbine (when the turbine does not generate power). The controller in variable-speed wind turbines can be tuned to skip rotational frequencies around the natural frequencies. Thus, the top displacement and fatigue damage are reduced. Moreover, adjustment of the blade pitch can provide damping, but it increases the rotor loads. This extra damping may help to produce more electrical power.

By reducing the projected area of the support structure against the waves in splash zone (where the hydrodynamic loads are maximal), it is possible to reduce wave-induced responses. Therefore, the main part of the platform should be below the splash zone. In deep spars (i.e., CMS or TLS), a large portion of the spar is below the splash zone.

The resonant motions (rigid-body natural frequencies) can be avoided by adjusting the low rigid-body natural periods away from the wind and wave spectral peaks. Usually, the pitch and surge natural frequencies are put below the wave frequencies.

The other option is to increase the inertia of the structure. This option is an effective but costly approach. However, the hydrodynamic damping may be increased by the following means (Henderson 2008):

- Damping plates
- Vortex-suppression strakes
- Buoyancy cans at the water line

When applying the above damping features, it is necessary to always keep in mind the possibility of increasing the excitation forces. Moreover, some of these features change the added mass and consequently change the natural periods of the system. Proper dynamic response analysis and experiments are needed to investigate the effects.

Figure 4.8 (taken from *Paper 4*) shows the bending moment spectrum for a CMS wind turbine subjected to wave and wind loads. The first elastic mode of the system connected to the tower's flexible bending mode was clear at 2.4 rad/sec. The flexible mode response was comparable to the wave frequency and pitch resonant responses. Hence, elastic modelling of floating wind turbines is necessary to present the structural responses correctly.

The tension spectrum (based on 1-hour time domain analysis) for a TLS wind turbine is presented in Figure 4.9 (taken from *Paper 6*). The tension response below 1 rad/sec was formed by several complex combinations of the three characteristic frequencies: wave, surge and pitch natural frequencies. These frequencies are mixing through the nonlinear relationship of the tension leg stiffness. More precisely, the square and square-root functions in the tension relationship generated the sum and difference of frequencies. For the higher frequencies, the lowest bending mode of the tower had a frequency of 2.4 rad/sec (*Paper 5*), and the heave natural frequency was 3.7 rad/sec. The heave resonant part of the tension is as important as the low frequency parts. The other high frequencies seen in the USFOS result were connected to the tower's eigen-frequencies. However, the HAWC2 code did not capture some of the high frequencies which may be related to the linear beam theory of the HAWC2 code.

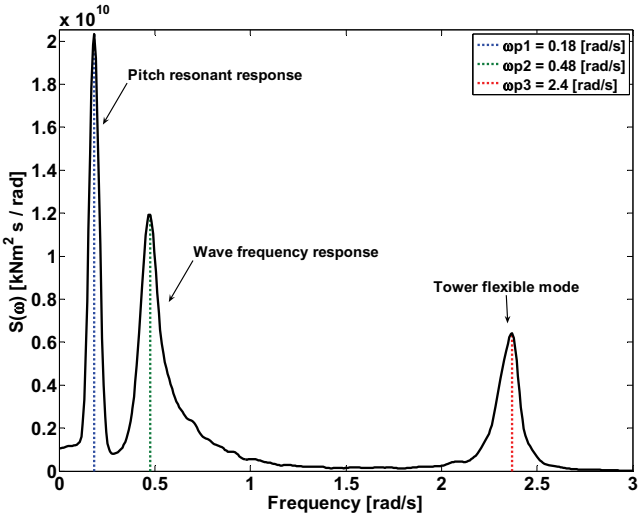

Figure 4.8: Bending moment spectrum at z= -20 m (20 m below MWL) based on a 1-hour time-domain simulation considering wave- and wind-induced loads. H_S =14.4 m, T_P =13.3 sec, V =49 m/sec and I_t =0.1 (Paper 4).

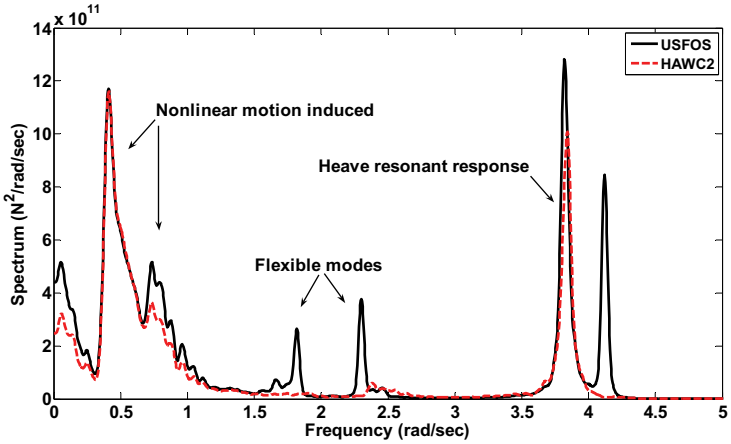

Figure 4.9: Tension spectra, smoothed spectra are based on a 1-hour time-domain simulations. Significant wave height: 15 m and wave peak period: 16 sec (Paper 6).

Figure 4.10 (*Paper 7*) shows the comparison between the nacelle surge motion with the untuned and tuned controller to avoid negative damping in the over-rated constant wind condition (V =17 m/sec, H_S =4.2 m and T_P =10.5) for a downwind TLS. The tuned controller has much lower pitch resonant response. In the over-rated wind speed range and due to the negative damping effect of the controller, the pitch resonant was dominant. After tuning the controller gains, the pitch resonant response is positively damped out.

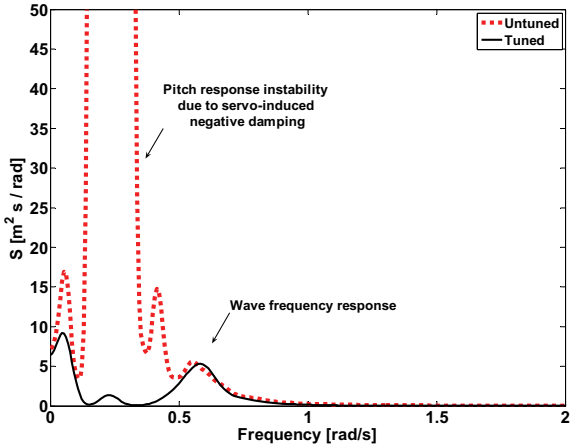

Figure 4.10: Nacelle surge spectra, with an untuned and tuned controller in the over-rated constant wind condition (V =17 m/sec, H_S =4.2 m and T_P =10.5).The motion response instabilities are due to servo-induced negative damping (Paper 7).

4.5 Extreme response

4.5.1 General

For offshore wind turbines, limited research has been performed, especially in terms of the extreme value analysis of these structures. However, for land-based wind turbines, various techniques for the estimation of extreme loads/responses have been used. Peak over threshold methods using Weibull models (Moriarty et al. 2004 and Sorensen et al. 2007) and block maxima techniques (Fogle et al. 2008 and Agarwal et al. 2008) comprise some of the recent attempts to model the extreme value statistics of fixed wind turbines by determining the extreme value distribution. In most of these works, comprehensive effort was needed to determine the type of the extreme value distribution and its parameters, which can be uncertain.

While analytical models are used for determining the linear response, the distribution of the nonlinear response generally needs to be treated in a semi-empirical manner by modelling the distribution of the response peaks or up-crossing rates. Several methods have been introduced to estimate extreme values such as Monte Carlo methods, the Weibull tail, the Gumbel method, the Winterstein method and the peaks-over-threshold method (POT). Alternatively, extreme value statistics for a 1-hour or 3-hour period are obtained by taking into account the regularity of the tail region of the mean up-crossing rate.

Extreme values have a low probability of occurrence. Therefore, even with the present computational power, the prediction of low exceedance probabilities requires a large sample size, which results in a time-consuming calculation. Moreover, simulations of complicated dynamic structural systems subjected to stochastic wave and wind loading are computationally intensive. This computational cost is even worse when dealing with a floating wind turbine, as the total simulation time is higher than that for a fixed wind turbine. Therefore, extrapolation methods are used to accurately estimate the extreme values. The extrapolation methods were applied to investigate the extreme value response of a catenary moored spar-type wind turbine (*Paper 5*).

One of the most reliable and robust approaches to estimate the extreme value is based on the mean up-crossing rate. The up-crossing rate is the frequency of passing a specified response level. For a higher response level, the up-crossing rate is lower. As the occurrence of extreme values is rare, it is therefore possible to assume the Poisson distribution for extreme values. The Poisson distribution can be defined based on the up-crossing rate. For a floating wind turbine, the response is nonlinear and non-Gaussian. Therefore, the semi-empirical approach based on the up-crossing rate is more robust and accurate. The time histories are used to count the number of up-crossings for each response level. Long time-domain simulations are needed to obtain low up-crossing rates. For instance, a 1-hour or 2-hours simulation cannot provide any information about an up-crossing rate of 0.0001; this rate roughly corresponds to a 50% fractile in a 100-year extreme value distribution. Extrapolation methods can be applied to extrapolate raw data and provide information for higher response levels (Naess et al. 2008).

To predict long-term extreme response of offshore structures, different approaches can be applied based on the environmental conditions and the structure characteristics. In the following, alternative approaches are mentioned (Haver et al. 2004):

- Complete long term response analysis
  a) All sea state approach (for extratropical areas like the North Sea)
  b) Random storm approach (for hurricane prone area)
- Selected sea states
- Reliability methods used for long-term response prediction
- Contour surface method, a short-term approach for prediction long-term extremes
  a) Neglecting the short-term response variability
  b) Accounting for the short-term response variability

Full long-term analysis for some structures is very time-consuming when each short term analysis is carried out in the time domain. The all sea state approach is the most general method. An alternative is to consider the responses in connection with storms exceeding a certain severity. This approach is convenient in areas where the weather is almost calm most of the time with rare storms happening randomly in time (Haver et al. 2004). The reliability

methods utilising the first-order-reliability-method (FORM) can be applied for long-term response analysis to find the extreme values. For complicated response structures, such as floating wind turbines, performing the full long term analysis is not practical. In these cases the contour line approach can be applied to investigate the extreme responses.

4.5.2 Contour line (surface) method

As mentioned earlier, full long-term analysis of floating wind turbines to estimate the extreme value responses is not practical. For wave-induced responses, it is found that the extreme values are governed by a few sea states. One way to select the wave conditions is the so-called contour line method (Sagli 2000). The contour surface method can give the load and response extremes corresponding to a prescribed return period, or equivalently, a prescribed annual probability of exceedance (Naess and Moan, 2005) by use of the joint model of the probability density function (PDF) of the mean wind speed, the significant wave height and the wave peak period parameters for the relevant site.

To find a contour line corresponding to a constant annual exceedance probability, the joint model should be transformed to a space consisting of independent and standard Gaussian variables. All combinations of environmental parameters (the mean wind speed, the significant wave height and the wave peak period) corresponding to a special annual exceedance are located on a sphere in the standard Gaussian space (Johannessen et al. 2001). The radius of this sphere is related to the desired annual exceedance. By applying the inverse first-order reliability method (IFORM), the desired contour line (surface) can then be obtained after transforming back from the Gaussian space (Winterstein et al. 1993).

The contour surface (line) method is an approximate method for estimating the extremes corresponding to a given annual probability. In this approach, the inherent randomness of the short-term extreme value is excluded from the given contours. It is therefore necessary to introduce this missing randomness by alternative approaches. Haver et al. (2004) suggested the utilisation of one of the following methods:

- Artificially inflating the 100-year variability artificially;
- Introducing a correction factor to the predicted median response; and
- Selecting a higher fractile as the short-term characteristic instead of selecting the median response.

The benefit of the contour surface method is that in the time-domain simulations, only a limited set of environmental cases needs to be analysed. The 100-year extreme response can be taken as the fractile of the distribution of the 3-hour extreme response value obtained from the contour surface approach (Sagli 2000). For the wave-induced responses of ocean structures, the 10% fractile seems reasonable to capture the 100-years extreme value response

(Naess and Moan, 2005). However, for wave- and wind-induced responses of floating wind turbines the contour surface method is not proven yet and further research is needed to accomplish this task.

To find the fractile level needed in the contour method for a special problem, the following steps need to be carried out (Baarholm et al. 2010):

- Performing a full long-term analysis with a sufficient number of 3-hour time-domain simulations for a sufficient number of different environmental conditions.
- Finding the worst environmental condition by a screening analysis performed along the required contour surface (e.g., 100-year return period contour line).
- Setting up the 3-hour extreme value distribution for the worst environmental condition.
- The fractile level is then obtained by the fractile that gives the same result as the long term simulation.

However, this method is not proven for wind turbines subjected to wave and wind loads. For wind turbines, different operational and nonoperational conditions including fault machine status should be considered. In this thesis "design" wave and wind conditions corresponding to Statfjord site are selected (Table 4, *Paper 2*) and the focus herein has been on the short term analysis.

Figure 4.11 (taken from *Paper 5*) shows the up-crossing rate for 20 different 2-hour simulations and the average up-crossing rate for all samples (40 hours). The results of 20 1-hour, 20 3-hour and 20 5-hour simulations had the same trend. Therefore, we just plotted the results of the up-crossing rate for the 20 2-hour simulations to illustrate the trend.

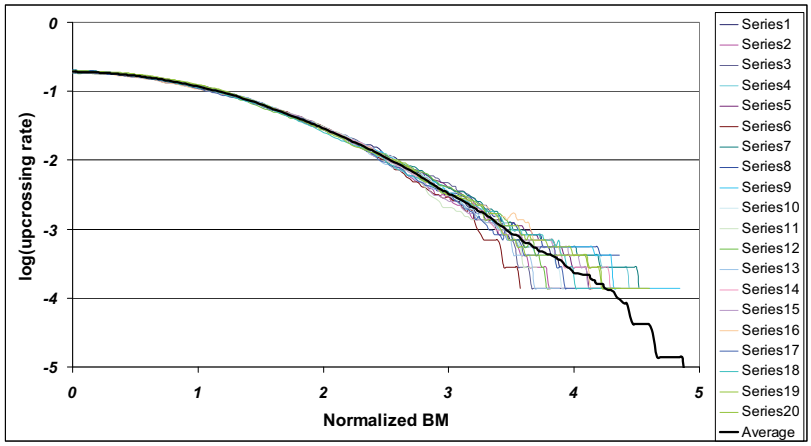

Figure 4.11: Up-crossing rate for 20 2-hour simulations and the average up-crossing rate over 40 hours (Paper 5).

In Figure 4.12 (taken from *Paper 5*), the coefficient of variation (σ/μ) of the bending moment for an up-crossing rate of 10^{-3} is plotted as a function of the simulation time (20 1-hour, 20 2-hour, 20 3-hour and 20 5-hour simulations). The original up-crossing rate was obtained from the analysis of the raw time series. The Naess and Winterstein methods for extrapolating to lower up-crossing rates were used. The comparison of the different simulation periods shows that the 20 1-hour simulations were sufficient for predicting the 3-hour extreme bending moment if the up-crossing rate was based on a reasonable extrapolation.

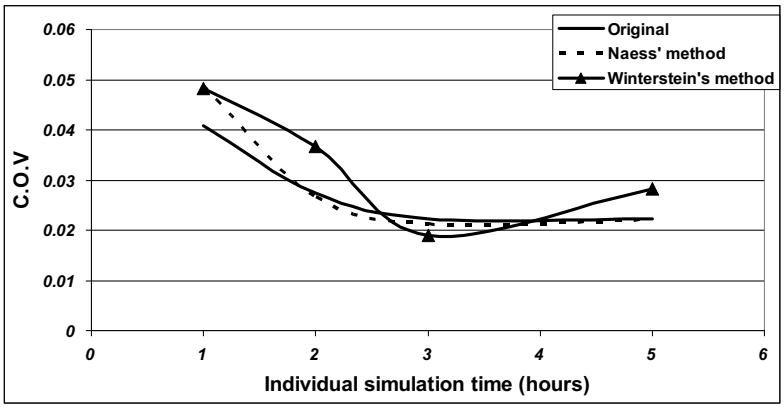

Figure 4.12: Coefficient of variation (σ/μ) *of the bending moment for an up-crossing rate of* 10^{-3} *versus simulation time (Paper 5).*

The extreme value response can be roughly estimated by: $\mu + k\sigma$, where μ is the mean value, σ is the standard deviation (STD) and k is the normalized maximum response and varies between 2 and 6 which is concept, environmental condition and offshore site dependent. Figure 4.13 shows the normalized maximum responses for the TLS-type wind turbine (*Paper 9*). The normalized maximum responses in Figure 4.13 correspond to up-crossing rate of 0.0001 and they are close to the 3-hours most probable maximum for the present case study. In Figure 4.13, STD is the standard deviation.

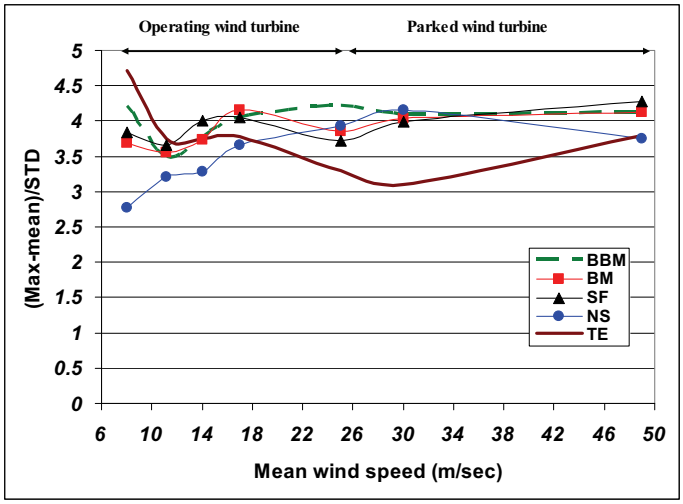

Figure 4.13: Normalized maximum of the bending moment (BBM) at the blade root, the bending moment (BM) at the tower-spar interface, the shear force (SF) at the tower-spar interface, the nacelle surge (NS) and the tension (TE). Statistical characteristics are based on five 1-hour samples. The maximum responses correspond to an up-crossing rate of 0.0001 and are obtained by extrapolation (Paper 9).

Chapter 5

Conclusions and Recommendations for Future Research

5.1 Conclusions

The objective of the research conducted in this thesis was to study the power production and structural integrity of spar-type wind turbines with catenary and tension leg mooring systems. Stochastic dynamic motion and structural response analysis was the key issue in the present thesis as documented in a collection of articles. The main conclusions obtained are presented here.

A comparison of hydrodynamic and hydro-elastic computer codes for a spar with catenary mooring and a spar with tension leg mooring systems (CMS and TLS) based on codes such as HAWC2, DeepC (Simo/ Riflex) and USFOS/vpOne was performed (*Papers 2 and 6*). This comparison showed that predictions of motion and tension responses in the programs to a reasonable extent agreed for both concepts. However, some differences were found in the resonant responses. Accounting for the instantaneous position of the platform when calculating the forces, introduced hydrodynamic nonlinearity (*Paper 2*).

For the TLS, all the motions were highly connected through the tension leg. The governing mode was the pitch response for both the TLS and CMS concepts. In the TLS concept, all the other responses were affected by the pitch motion through the tension leg. The nonlinear action of the line introduced the sum and difference of pitch, surge and wave frequencies for the heave and tension responses. It was necessary to ensure that the pitch natural frequency is outside the wave spectrum. However, the nonlinear hydrodynamic loading could excite the natural frequencies. The effect of the stochastic waves on the response of each code was studied as well. The response was different for different wave time histories. More precisely, the stochastic low-frequency responses (surge and pitch resonance) were affected. Ten 1-hour simulations in the HAWC2 and USFOS codes were used, and the averages of the simulations

showed a better agreement (*Paper 6*). However, there were still some differences in the resonant responses.

Different methods for calculating the hydrodynamic forces were investigated. The panel method, Morison formula, displaced volume method and pressure integration methods were used in this thesis (*Papers 2 and 6*). The hydrodynamic comparison was performed based on different codes for both TLS and CMS. It was found that for spar-type wind turbines, the combination of the Morison formula and pressure integration methods can introduce a robust numerical tool.

Two parked rotor configurations for CMS, the blades parallel to the wind and blades perpendicular to the wind, were discussed (*Paper 1*). The wave-wind-induced motion responses in harsh environmental conditions were studied. The results showed that when blades are parallel to the wind due to a decrease of aerodynamic loading, the nacelle surge motion can be 2 times less than that in the fault condition.

The rigid body and elastic modelling of the CMS showed that the effect of elasticity on motions can be neglected, but the structural responses can be affected by the elastic structural response (*Paper 1*). The first elastic bending mode can be affected by the wind- and wave-induced responses. For extreme environmental conditions, the elastic response is comparable with the rigid body wave frequency responses (*Paper 4*). The comparison of models with rigid body and elastic modelling of the spar and the tower showed that the structural damping of the elastic body slightly affects the rigid body motions. For the TLS, the structural damping has a clear influence on the modes associated with the high eigen-frequencies (*Paper 6*).

Different strategies for modelling the mooring system were considered in the present thesis. The comparison of the DLL and real line model (in the TLS concept) showed that the spring effect of the tension leg is governing the overall motion of the spar (*Paper 6*). However, the heave resonance in the tension is sensitive to the damping. For the CMS concept, the full finite element model of the mooring system including clump masses and delta lines was applied in Simo/ Riflex (*Paper 1*). Based on a quasi-static analysis of the mooring system, the force-displacement relation for different modes of motions was calculated and applied through a dynamic link library (DLL) to the HAWC2 code. This feature significantly decreases the simulation time. The accuracy of this DLL approach was investigated through the analysis of the TLS concept.

The structural response for both concepts was to limited extent affected by turbulence (*Papers 2 and 9*). Hence, this suggests that it is possible to use the constant wind model in fatigue and ultimate limit state analyses with an acceptable accuracy. However, this needs to

be systematically verified in the further analyses. The turbulence does not affect the mean of the generated power very much. However, the electrical power fluctuations are increased for turbulent wind cases. For the over-rated wind speeds, the mean values and standard deviations of electrical power produced are almost the same for the constant and turbulent wind cases. However, for the below-rated wind speeds, the differences are notable. These differences are due the calm sea state that corresponds to low wind speeds. For CMS, the mean of electrical power generated at the rated wind speed in the turbulent wind case was 4.1 MW, compared to 5 MW for the original land-based wind turbine (*Paper 2*). This aspect may be considered in the design of new wind turbines for offshore applications.

To obtain a good quality for the generated power (steady electrical power), the wave frequency responses and resonant responses (surge and pitch resonances) should be decreased. The fluctuations of the generated electrical power are dominated by the wave frequency responses, and the motion responses are governed by the pitch resonant responses (*Paper 3*). It was found that the higher frequencies in motion response have a greater effect on the quality of the electrical power than the low resonant frequencies.

Coupled wave- and wind-induced motion response analyses were performed in the operational conditions in order to investigate the ability of a floating wind turbine to produce power. Wind- and wave-induced motions directly affect the nacelle motion and its velocity, which can influence the relative velocity. The magnitude and frequency of the platform's rigid motions influence the power production and quality (*Paper 3*).

The motion responses and power production of CMS wind turbines in operational environmental conditions were considered as well. The coupled time-domain analysis was performed for over-rated, rated and below-rated wind speeds in different sea states. Comparisons were made for wave-induced and wave-wind-induced responses of parked and operating floating wind turbines. The effect of aerodynamic and hydrodynamic damping in different frequency ranges on the dynamic motion responses and electrical power production was investigated (*Paper 3*). The coupling is inevitable in such structures, as the aerodynamic and hydrodynamic damping and excitation forces are highly affected by each other through the relative motions.

A comparison of the rotating rotor wind-wave-induced response, parked rotor wave-wind-induced response and parked rotor wave-induced response showed that (*Paper 3*) the aerodynamic damping of the rotating rotor reduces the wave-induced responses through the control of the blades/rotational speed of shaft and also reduces the pitch resonant response through the relative motion of the platform.

The aerodynamic and hydrodynamic damping are active in resonant responses. It is not possible to damp all of the resonances because of the wind excitation forces and nonlinear hydrodynamic loads arising from the quadratic drag terms and consideration of instantaneous positions for calculating loads (*Paper 3*). The relative wind velocity contains the motion response frequencies that can excite the rigid body resonant motions. For below-rated wind speed, the aerodynamic damping is sufficient for reducing the resonant responses, but for over-rated wind speed, the aerodynamic excitation forces are higher, and the damping is not sufficient. By introducing more hydrodynamic damping (through the addition of passive hydrodynamic features such as pin/strake), the resonance can be damped out.

The blade pitch control of an operating turbine can introduce negative damping in a floating wind turbine. It is necessary to avoid the servo-induced negative damping to get an adequate fatigue life. In *Paper 7*, the controller gains are modified to reduce the instabilities caused by the servo negative damping. When the tuned controller was applied, the pitch resonant motion was reduced and the power production was improved compared with when the untuned controller was used. For TLS, the ratio between the standard deviation of the electrical power generated when the untuned and tuned controller is applied for an over-rated wind speed case is 8.1. The similarly defined ratio for the nacelle surge motion, the bending moment at the tower-spar interface and the bending moment at the blade root is 14.5, 4.4 and 2.7, respectively. These results show that negative damping adversely affects the performance and structural integrity of a floating wind turbine (*Papers 7 and 9*).

The effect of upwind vs. downwind rotor on the performance and responses of tension leg spar-type wind turbine was studied. The results show that the global responses of downwind and upwind turbines are close. However, some small differences are clear which can be due to the small difference applied to the upwind turbine to make a downwind turbine (*Paper 8*). The wave-induced and wind-wave-induced responses are compared for TLS with downwind and upwind rotors. The results show that the wave frequency part of the responses is less affected by the aerodynamic or controller actions in integrated analysis. The pitch resonant response is damped for below-rated wind case due to aerodynamic damping. The surge resonant response is excited by aerodynamic excitation forces for the rated wind speed case. For operational below- and over-rated wind speed cases the responses are governed by wave-induced responses when a tuned controller is applied (*Papers 7 and 8*). Under survival environmental conditions the aerodynamic damping helps reducing the pitch motion resonance. In storm and hurricane conditions the wave loading is dominant compared to wind loads (*Paper 8*).

The effect of the turbulence and tower shadow effect on the different structural and motion responses were discussed for TLS with downwind rotor. The results showed that the global responses were less affected by the tower shadow. However, the dynamic part of the blade

root bending moment the dynamic part of the responses was more affected. The relative magnitude of the turbulence effects was larger than the tower shadow effects. The ratio of standard deviation of the blade root's bending moment, nacelle surge motion and tension response considering turbulent and constant wind speed cases were found to be 8.5, 2.3 and 1.4, respectively (*Paper 9*). The results showed that the turbulence effect on the mean value of electrical power and tower structural response was negligible. The ratio of the responses to a 100-year environmental condition and to the load case associated with the rated wind speed was found to be as high as 2.6, 3.2, 1.3 and 1.2 for the bending moment (BM), shear force (SF), nacelle surge (NS) and tension (TE) responses. This finding showed that for the present tension leg spar-type floating wind turbines, the extreme value of responses can occur under survival conditions. However, land-based wind turbine extreme values are linked to the rated wind speed and occur under operational conditions (*Paper 9*).

The structural responses of a catenary moored spar wind turbine in both survival and operational conditions were compared to show the importance of analysing the structural response in survival conditions to obtain the lifetime maxima (*Papers 4 and 5*). The critical structural sections due to the bending moment and shear forces were found, and the responses at those sections were determined. The bending moment and shear forces in the tower and spar are dominated by the platform pitch resonant response. The analysis showed that for a floating wind turbine the extreme responses can occur in harsh environmental conditions, while for a fixed wind turbine, the extreme value responses are connected to the rated wind speed in operational conditions. The maximum of the structural response for the survival case was found to be almost two times greater than its value for operational conditions.

To limit the computational efforts required to determine the 100-year extreme response value, a contour surface method was applied based on a joint distribution of the wind speed, significant wave height and wave period. The 100-year return period environmental condition was set in order to obtain the 100-year response of the floating wind turbine under harsh environmental condition (*Paper 4*).

Extreme values for severe environmental conditions were obtained based on 20 1-hour, 20 2-hour, 20 3-hour and 20 5-hour simulations (*Paper 5*). Because the response is governed by resonance, the response is close to Gaussian. However, the process is wide-banded. The minimum total simulation time (number of simulations multiplied by simulation period) to obtain accurate results depends on the needed up-crossing rate. The 1-hour and 2-hour original values cannot provide any information for 0.0001 up-crossing rates. The extrapolation of the 1-hour period was used to capture the up-crossing rate of 0.0001.

If up-crossing of the high response level is needed, the total simulation time should be increased. The extrapolation of the up-crossing rate based on the Naess and Winterstein

approaches was used to predict the high response level crossing. The most probable maxima obtained by these approaches are close. The most probable maximum of the bending moment is very close to the bending moment for an up-crossing rate of 0.0001 in the present study. A comparison of different simulation periods showed that the 20 1-hour simulations are sufficient to predict the 3-hours extreme bending moment if the up-crossing rate is based on a reasonable extrapolation (*Paper 5*).

Generally, normalized responses are greater for survival conditions than for operational conditions. For CMS under survival conditions, the normalized maximum corresponding to an up-crossing rate of 0.0001 varies between 4 and 6. Under operational conditions, the normalized maximum responses of CMS-type wind turbine vary between 2 and 4. The turbulence has limited effect on structural responses, while nacelle surge motion is more affected by turbulence (*Paper 2 and 9*). The normalized responses of TLS-type wind turbine under both operational and survival conditions corresponding to an up-crossing rate of 0.0001 vary between 3 and 5 (*Paper 9*).

The original scientific contributions of this thesis are summarised as follows:

- The comparison of computer codes for dynamic analysis of TLS and CMS, using HAWC2, USFOS/vpOne and Simo/Riflex (DeepC)
- Comparison of alternative hydrodynamic models for CMS and TLS
    - Panel method (boundary element method) and Morison formula for the CMS concept
    - Panel method, Morison formula and pressure integration methods for the TLS concept
    - Investigating the geometrical updating (instantaneous position) when calculating the hydrodynamic loads and its effect on the wave-induced responses
    - Nonlinear hydrodynamic loads based on linear wave theory, mean drift forces and Wheeler stretching
- Sensitivity study of the hydrodynamic model with respect to stochastic wave generation
- Integrated dynamic response analysis
    - Time-domain analysis of offshore spar-type floating wind turbines with catenary and tension leg mooring systems
    - Wave- and wind-induced response analysis
    - Comparison of wave-induced and wind-wave-induced responses
    - Effect of turbulence in wind loads, power production, structural and motion responses
    - Effect of elastic and rigid body modelling
- Investigation of the servo-induced negative damping of the TLS

  - Modifying the controller gains to remove negative damping
  - Comparison of responses obtained with application of tuned and untuned controller to study the effect of tuning in different load cases
- Study the effect of rotor configuration on the performance of the wind turbine
  - Analyzing both the upwind and downwind turbine for TLS
  - Effect of tower shadow on the power production and dynamic responses
- Extreme value estimation for spar-type wind turbines for short-term responses
  - Study of the effect of simulation periods in extreme value analysis
  - Alternative extrapolation methods

5.2 Recommendations for future research

Further research on spar-type floating wind turbines is needed. For the catenary moored spar the modelling of the mooring lines was limited in present research. In the present model, the inertia and damping of the mooring lines were neglected in the dynamic analysis. In the future, the quasi-static model can be replaced by a more complex coupled model.

This study is primarily concerned with response analysis for ULS design. Moreover, in the present study, the contour line method was assumed to be valid. The contour surface method needs to be validated for floating wind turbines. The fatigue limit state of the present and other concepts also needs to be investigated.

Accidental limit state analysis was not addressed in this study. Consideration of fault conditions for floating wind turbines, and especially the transient response during shutdown and control actions for these conditions should be studied in future research. Another aspect is to validate current analysis by comparison with experiments for scaled models as well as field measurements.

In the present study, the focus was on the spar-type floating wind turbines. Other concepts such as semisubmersibles, disk buoys and TLPs may also be relevant especially for intermediate water depths. A conceptual study based on the analysis of wave- and wind-induced responses should be performed.

A modified linear wave theory was applied in this study. Appropriate wave theory for shallow water is needed to represent the waves correctly. For large-volume structures such as semisubmersibles and ship-shaped structures, the second-order wave excitation and damping forces should be calculated. The spar is a slender structure compared to wave length, and the free surface memory of the waves can be neglected. For large structures, the convolution integrals through using retardation functions should be set in the equations of motion to represent the dynamic responses correctly.

The conventional wind turbine control algorithms tuned for offshore applications were used in the present research. More advanced control algorithm proper for floating wind turbines could be developed.

One of the important aspects of offshore wind technology is the cost of generated electricity. The present thesis did not deal with cost assessment neither for the capital cost of the design nor the cost of operating the wind farm. This is a topic for future research.

The response and generated power of a wind turbine in a farm can be different compared to that of a single wind turbine. Due to wake of the surrounding wind turbines and different boundary layers, the aeroelastic response may be different. Floating wind turbine farms and their wake generation, the turbine park effect on the wind velocity, and other similar aspects is a subject for future research.

References

Agarwal, A. K. and Jain, A. K. (2003) Nonlinear coupled dynamic response of offshore Spar platforms under regular sea waves. Ocean Engineering; Vol. 30, pp. 517-551.

Agarwal, P. and Manuel, L. (2008) Extreme loads for an offshore wind turbine using statistical extrapolation from limited field data. Wind Energy; Vol. 11, Issue 6, pp. 673-684.

Agarwal, P. and Manuel, L. (2009) Modelling Nonlinear Irregular Waves in Reliability Studies for Offshore Wind Turbines. Paper No. OMAE2009-80149, Proceedings of the 28th International Conference on Offshore Mechanics and Arctic Engineering, Hawaii, USA.

Ahlstrom, A. (2005) Influence of wind turbine flexibility on loads and power production. Wind Energy Journal; Vol. 9, Issue 3, pp. 237-249.

Archer, C. Z. and Jacobson, M. L. (2005) Evaluation of global wind power. Journal of geophysical research; Vol. 110.

Argyriadis, K. and Klose, M. (2006) Integration of Load Analysis and Structural Design of Offshore Wind Turbines. Paper No. OMAE2006-92081, Proceedings of the 25th International Conference on Offshore Mechanics and Arctic Engineering, Hamburg, Germany.

Baarholm, S. G., Haver, S., and Økland, O. D. (2010) Combining contours of significant wave height and peak period with platform response distributions for predicting design response. Marine Structures; Vol. 23, Issue 2, pp. 147-163.

Bianchi, D. F., Battista, H. D. and Mantz, R. J. (2007) Wind Turbine Control Systems. Springer, Germany.

Bir, G. and Jonkman, J. (2007) Aeroelastic Instabilities of Large Offshore and Onshore Wind Turbines. EAWE 2007, Torque from Wind Conference, DTU, Denmark.

Burton, T., Sharpe, D., Jenkins, N. and Bossanyi, E. (2008) Wind Energy Handbook. John Wiley and Sons Ltd, England.

Butterfield, S., Musial, W., Jonkman, J., and Sclavounos, P. (2005) Engineering Challenges for Floating Offshore Wind Turbines. Copenhagen Offshore Wind Conference, Denmark.

DNV (2007) Design of Offshore Wind Turbine Structures. DNV-OS-J101, Det Norske Veritas, Oslo, Norway.

DNV (2008) DeepC theory manual, Det Norske Veritas, Oslo, Norway.

Falnes, J. (2005) Ocean Waves and Oscillating Systems. Cambridge University Press, USA.

Faltinsen, O. M. (1995) Sea Loads on Ships and Offshore Structures. Cambridge University Press, UK.

Fogle, J., Agarwal, P. and Manuel, L. (2008) Towards an improved understanding of statistical extrapolation for wind turbine extreme loads. Wind Energy; Vol. 11, Issue 6, pp. 613-635.

Hansen, M. O. L., Sorensen, J. N., Voutsinas, S., Sorensen, N. and Madsen, H. Aa. (2006) State of the art in wind turbine aerodynamics and aeroelasticity. Progress in Aerospace Sciences Journal; Vol. 42, pp. 285-330.

Hansen, M. O. L. (2008) Aerodynamics of Wind Turbines. Second Edition, Erathscan, UK.

Haslum, H, A and Faltinsen, O. M. (1999) Alternative shape of Spar Platform for Use in Hostile Areas. Paper No. 10953, Offshore Technology conference (OTC), Houston, Texas, USA.

Haver, S. and Kleiven, G. (2004) Environmental contour Lines for Design Purposes- Why and When?. Paper No. OMAE2004-51157, 23th International Conference on Ocean, Offshore and Arctic Engineering, Vancouver, BC, Canada.

Henderson, A. R., Leutz, R. and Fujii, T. (2002) Potential for Floating Offshore Wind Energy in Japanese Waters. ISOPE Conference, ISBN 1-880653-58-3, Kitakyushu, Japan.

Henderson, A. R. (2003) Hydrodynamic Loading on Offshore Wind Turbines. OWTES Task 4.2, TUDelft, the Netherlands.

Hoven, I van der (1957) Power spectrum of horizontal wind speed in the frequency range of 0.0007 to 900 cycles per hour. Journal of Metrology; Vol. 14, Issue 2, pp. 160-164.

IEA (2008) Renewable Energy Essentials: Wind. http://www.iea.org/

IEC (2009) International Standard 61400-3, Wind turbines, Part 3: Design requirements for offshore wind turbines.

ISSC (2006) Specialist Committee V.4, Ocean Wind and Wave Energy Utilization. 16th International Ship and Offshore Structures Congress, Southampton, UK.

ISSC (2009) Specialist Committee V.4, Ocean Wind and Wave Energy Utilization. 17th International Ship and Offshore Structures Congress, Seoul, Korea.

Johannessen, K., Meling, T. S. and Haver, S. (2001) Joint distribution for wind and waves in the Northern North Sea. Paper No. 2001-SH-06, ISOPE Conference, Stavanger, Norway.

Jonkman, J., Marshall, L. and Buhl, Jr. (2005) FAST User's Guide, Technical Report NREL/EL-500-38230, Golden, Colorado, USA.

Jonkman, J. (2007) Dynamics Modelling and Loads Analysis of an Offshore Floating Wind Turbine. NREL, Technical Report, NREL/TP-500-41958, Golden, Colorado, USA.

Jonkman, J. (2008) Influence of Control on the Pitch Damping of a Floating Wind Turbine. ASME Wind Energy Symposium, Reno, Nevada, USA.

Jonkman, J. (2009) Dynamics of offshore floating wind turbines-model development and verification. Wind Energy; Vol. 12, Issue 5, pp. 459-492.

Jonkman, J. et al. (2010) Offshore Code Comparison Collaboration within IEA Wind Task 23: Phase IV Results Regarding Floating Wind Turbine Modelling. European Wind Energy Conference, EWEC 2010, Warsaw, Poland.

Kallesøe, B. S. (2007) Aero servo elasticity of Wind Turbines. PhD thesis, Department of Mechanical Engineering, Technical University of Denmark, Lyngby, Denmark.

Karimirad, M. and Moan, T. (2009a) Wave and Wind Induced Motion Response of Catenary Moored Spar Wind Turbine. Computational Methods in Marine Engineering Conference, Trondheim, Norway. Published by International Center for Numerical Methods in Engineering (CIMNE), Barcelona, Spain.

Karimirad, M., Gao, Z. and Moan, T. (2009b) Dynamic Motion Analysis of Catenary Moored Spar Wind Turbine In Extreme Environmental Condition. Offshore Wind Conference 2009, Stockholm, Sweden.

Karimirad, M. and Moan, T. (2010a) Effect of Aerodynamic and Hydrodynamic Damping on Dynamic Response of a Spar Type Floating Wind Turbine. European Wind Energy Conference EWEC 2010, Warsaw, Poland.

Karimirad, M. and Moan, T. (2010b) Extreme Structural Dynamic Response of a Spar Type Wind Turbine. Paper No. OMAE2010-20044, 29th International Conference on Ocean, Offshore and Arctic Engineering, China.

Karimirad, M. and Moan, T. (2011a) Wave and Wind Induced Dynamic Response of Catenary Moored Spar Wind Turbine. Journal of Waterway, Port, Coastal, and Ocean Engineering; ASCE.

Karimirad, M. and Moan, T. (2011b) Extreme Dynamic Structural Response Analysis of Catenary Moored Spar Wind Turbine in Harsh Environmental Conditions. Journal of Offshore Mechanics and Arctic Engineering, ASME.

Karimirad, M. and Moan, T. (2011c) Ameliorating the Negative Damping in the Dynamic Responses of a Tension Leg Spar-Type Support Structure with a Downwind Turbine. European Wind Energy Conference EWEC 2011, Brussels, Belgium.

Karimirad, M. and Moan, T. (2011d) Tension Leg Spar-Type Offshore Wind Turbine with Upwind or Downwind Rotor Configuration. AWEA-WINDPOWER2011, Anaheim, CA, USA.

Karimirad, M. and Moan, T. (2011e) Stochastic Dynamic Response Analysis of a Tension Leg Spar-Type Offshore Wind Turbine. Submitted for publication.

Koo, B. J., Kim, M. H. and Randall, R. E. (2004) Mathieu instability of a spar platform with mooring and risers. Ocean Engineering Journal; Vol. 31, Issues 17-18, pp. 2175-2208.

Larsen, T. J. and Hanson, T. D. (2007) A method to avoid negative damped low frequent tower vibrations for a floating, pitch controlled wind turbine. Journal of Physics; The Science of Making Torque from Wind, IOP Publishing, Conference Series 75 (2007) 012073.

Lysen, E. H. (1983) Introduction to wind energy. SWD Publications, SWD 82-1, the Netherlands.

Madsen, P. H., Pierce, K. and Buhl, M. (1999) Predicting Ultimate Loads for Wind Turbine Design. Paper No. AIAA-99-0069, AIAA/ASME Wind Energy Symposium, Reno, Nevada, USA.

Manwell, J. F., McGowan, J. G. and Rogers, A. L. (2006) Wind Energy Explained, Theory, Design and Application. John Wiley and Sons Ltd, Chichester, England.

MARINTEK (2008) Riflex theory manual, Trondheim, Norway.

Meissonnier, Q., Karimirad, M., Gao, Z. and Moan, T. (2010) Hydro-elastic Code-to-Code Comparison for a Tension Leg Spar Type Floating Wind Turbine. Journal of Marine Structures.

Moan, T., Zheng, X. Y. and Quek, S. T. (2007) Frequency-domain analysis of non-linear wave effects on offshore platform responses. International Journal of Non-Linear Mechanics; Vol. 42, Issue 3, pp. 555-565.

Moriarty, P., Holley, W. and Butterfield, S. (2004) Extrapolation of Extreme and Fatigue Loads using Probabilistic Methods. Technical Report: NREL/TP-500-34421, National Renewable Energy Laboratory, Golden, Colorado, USA.

Naess, A. and Moan, T. (2005) Probabilistic Design of Offshore Structures. Chakrabarti, S. (Ed.), Chapter 5, Handbook of Offshore Engineering. Elsevier Ltd, UK.

Naess, A., Gaidai, O. and Teigen, P. S. (2008) Extreme response prediction for nonlinear floating offshore structures by Monte Carlo simulation. Applied Ocean Research; Vol. 29, Issue 4, pp. 221-230.

Nielsen, F. G., Hanson, T. D. and Skaara, B. (2006) Integrated Dynamic Analysis of Floating Offshore wind Turbine. Paper No. OMAE2006-92291, Proceedings of the 25th International Conference on Offshore Mechanics and Arctic Engineering, Hamburg, Germany.

Roddier, D., Cermelli, C. and Weinstein, A. (2009) WINDFLOAT: A Floating Foundation for Offshore Wind Turbine Part I: Design Basis and Qualification Process. Paper No. OMAE2009-79229, Proceedings of the 28th International Conference on Offshore Mechanics and Arctic Engineering, Hawaii, USA.

Sagli, G. (2000) Model uncertainty and simplified estimates of long term extremes of hull girder loads in ships. Doctoral thesis, Department of Marine Technology, NTNU, Trondheim, Norway.

Sclavounos, P., Tracy, C. and Lee, S. (2007) Floating Offshore Wind Turbines: Responses in a Seastate Pareto Optimal Designs and Economic Assessment. Department of Mechanical Engineering, MIT, Cambridge, Massachusetts, USA.

Sclavounos, P. D., Lee, S., and DiPietro, J., Potenza, G., Caramuscio, P., and DeMichele, G. (2010) Floating Offshore Wind Turbines: Tension Leg Platform and Taught Leg Buoy Concept Supporting 3-5 MW Wind Turbines. European Wind Energy Conference (EWEC), Warsaw, Poland.

Sorensen, J. D. and Nielsen, S. R. K. (2007) Extreme wind turbine response during operation. Journal of Physics; The Science of Making Torque from Wind, IOP Publishing, Conference Series 75 (2007) 012074.

Spera, D. A. (1998) Wind Turbine Technology Fundamental Concepts of Wind Turbine Engineering. ASME press, New York, USA.

Tempel, J. V. D. (2006) Design of Support Structures for Offshore Wind Turbines. Doctoral Thesis, Delft University of Technology, Delft, Netherland.

Twidell, J. and Gaudiosi, G. (2008) Offshore Wind Power. Multi-Science Publishing Co Ltd, UK.

Utsunomiya, T., Sato, T., Matsukuma, H. and Yago, K. (2009) Experimental Validation for Motion of a Spar-Type Floating Offshore Wind Turbine Using 1/22.5 Scale Model. Paper No. OMAE2009-79695, Proceedings of the 28th International Conference on Offshore Mechanics and Arctic Engineering, Hawaii, USA.

Wayman, E. N., Sclavounos, P. D., Butterfield, S., Jonkman, J. and Musial, W. (2006) Coupled Dynamic Modelling of Floating Wind Turbine Systems. Paper No. 18287, Ocean Technology Conference (OTC), Houston, Texas, USA.

Winterstcin, S., Udc, T., Cornell, C. A., Bjeragcr, P. and Haver, S. (1993) Environmental parameters for extreme response: Inverse FORM with omission factors. Proceedings of International Conference on Structural Safety and Reliability (ICOSSAR-93), Innsbruck, Austria.

Withee, J. E. (2004) Fully Coupled Dynamic analysis of a floating wind turbine system. Doctoral Thesis, Department of Mechanical Engineering, Cambridge, Massachusetts, MIT, USA.

Appendix

Paper 1

Dynamic Motion Analysis of Catenary Moored Spar Wind Turbine in Extreme Environmental Condition

Madjid Karimirad, Zhen Gao and Torgeir Moan

Published in the proceeding of the European Offshore Wind Conference, EOW2009, September 2009, Stockholm, Sweden

Is not included due to copyright

Paper 2

Wave and Wind Induced Dynamic Response of Catenary Moored Spar-Type Wind Turbine

Madjid Karimirad and Torgeir Moan

Accepted for publication at
Journal of Waterway, Port, Coastal, and Ocean Engineering, ASCE

Is not included due to copyright

Paper 3

Effect of Aerodynamic and Hydrodynamic Damping on Dynamic Response of Spar Type Floating Wind Turbine

Madjid Karimirad and Torgeir Moan

Published in the proceeding of the European Wind Energy Conference (EWEC2010), April 2010, Warsaw, Poland

Is not included due to copyright

Paper 4

Extreme Structural Dynamic Response of a Spar Type Wind Turbine

Madjid Karimirad and Torgeir Moan

Published in the proceedings of the 29th International Conference of Offshore Mechanics and Arctic Engineering (OMAE2010), June 2010, Shanghai, China

Is not included due to copyright

Paper 5

Extreme Dynamic Structural Response Analysis of Catenary Moored Spar Wind Turbine in Harsh Environmental Conditions

Madjid Karimirad and Torgeir Moan

Accepted for publication at
Journal of Offshore Mechanics and Arctic Engineering (JOMAE), ASME

Is not included due to copyright

Paper 6

Hydro-elastic Code-to-Code Comparison for a Tension Leg Spar Type Floating Wind Turbine

Quentin Meissonnier, Madjid Karimirad, Zhen Gao and Torgeir Moan

Submitted to the Journal of Marine Structures
(a revised-version of this paper will be published in the journal and as agreed among the authors, ***Madjid Karimirad*** will be the first-author in the final-paper)

HYDROELASTIC CODE-TO-CODE COMPARISON FOR A TENSION LEG SPAR-TYPE FLOATING WIND TURBINE

Quentin Meissonnier Madjid Karimirad* Zhen Gao Torgeir Moan

Centre for Ships and Ocean Structures
Norwegian University of Science and Technology
Trondheim, Norway, N-7491

ABSTRACT

The development of robust design tools for offshore wind turbines requires knowledge of both wave and wind load models. Existing numerical codes are typically extended to account for both aerodynamic and hydrodynamic effects on a structure. Therefore, verification of the extended codes is required by the use of experiments and code-to-code comparisons. This paper presents a hydroelastic code-to-code comparison between the HAWC2 and USFOS/vpOne codes for a floating platform that is suitable for offshore wind turbines. The HAWC2 code, which is an aero-servo-elastic code that was developed by Risø/DTU for the dynamic response analysis of land-based wind turbines, was extended to account for hydrodynamic loads. The USFOS/vpOne code, which is a hydroelastic code that was developed by USFOS Ltd. for the dynamic response analysis of offshore structures, was extended to include the aerodynamic effects on offshore wind turbines. This study compares the two codes for a tension leg spar (TLS) with a single tether, which is a hybrid concept that combines the TLP and Spar concepts. The comparison is performed using coupled hydroelastic time domain simulations under wave loads. Additionally, the methods that are required to perform a time-domain analysis for this concept are presented based on systematic studies of several aspects such as damping, wave simulation, and hydrodynamic and structural modelling. Wave-induced motion of a support platform affects the power generation of a wind turbine. Furthermore, overload of the tension leg should be avoided. The tension leg introduces nonlinear effects on the spar motion. The difference and sum frequency responses are created by nonlinear wave loads. Therefore, the motion and tether tension are compared. Yaw motion is constrained in this study. The spectral analysis and statistical characteristics of the results are presented. A combination of the Morison formula and the pressure integration method provides accurate results for the structure. A comparison indicates that the motion responses and the tension obtained in the two codes are in good agreement. However, some differences were found in the resonant responses.

Keywords: Tension Leg Spar (TLS), Coupled Hydroelastic Dynamic Analysis, Floating Wind Turbine

NOMENCLATURE

FK: Froude-Krylov force
KC: Kaulegan-Carpenter number
MWL: Mean water level
NREL: National renewable energy laboratory
TLP: Tension leg platform
TLS: Tension leg spar

C_d : Quadratic hydrodynamic drag coefficient
C_M : Mass coefficient
C_m : Added mass coefficient
d : Draft
D : Diameter of the spar
E : Elastic modulus of the tension leg
h : Mean water depth
H : Wave height (regular wave)
H_S : Significant wave height
L : Length of the tension leg
T : Wave period (regular wave)
T_P : Peak wave period

λ : Wave length
ω : Wave frequency (rad/sec)

* *Corresponding Author, Madjid Karimirad*
Email: madjid.karimirad@ntnu.no
Otto Nielsens v 10, N-7491, Trondheim, Norway

1. INTRODUCTION

Wind turbines on land have been widely used in the past two decades to generate green energy. In recent years, the wind energy industry has transitioned from land-based wind power to offshore fields.

Numerous concepts have been proposed for floating wind turbines with different floaters such as TLP, semi-submersibles and spars [1]. Each concept requires specific methods to handle the relevant dynamic behaviour of the turbine. In this paper, a hybrid concept combining a TLP and spar is chosen: the tension leg spar (TLS) with a single tether for deep-water wind farms. The current TLS type floating wind turbine is similar to SWAY [2]. The spar exhibits a very good heave motion characteristic because of the deep draft; on the other hand, the multiple legs TLP exhibits less angular motion but a higher cost for the tension legs. This new concept requires specific numerical tools.

Numerous studies have been performed for catenary moored spar type floating wind turbines [3, 4, 5, and 6]. This paper introduces a hydrodynamic code-to-code comparison between the HAWC2 and USFOS/vpOne codes for a spar with a single tension leg. The HAWC2 code [7], which is an aero-servo-elastic code that was developed by Risø for the dynamic response of wind turbines, was extended to account for hydrodynamic effects. The USFOS/vpOne code [8], which is a hydroelastic code that was developed by USFOS Ltd. for the dynamic response of offshore structures, was extended to include aerodynamic effects on offshore wind turbines. A time domain code-to-code hydroelastic comparison was performed in this study. This study is limited to wave induced responses; no wind or aerodynamic effects were included. Aerodynamic effects will be considered in a subsequent paper. First, the theoretical basis of the relevant parameters is discussed, and the model of the single leg spar is described. Based on systematic studies of several aspects (wave generation, hydrodynamic modelling, damping and the like), a global stochastic analysis is presented.

Wave-induced motion of the nacelle affects power generation in the wind turbine, and the tension can be a limiting parameter for TLP concepts because of tether slack or buckling. Therefore, the motion and tether tension were chosen as relevant response variables. The results are presented in terms of time histories, spectral density functions and statistical characteristics.

2. TENSION LEG SPAR WIND TURBINE

The NREL 5 MW wind turbine [9] was chosen as a reference. The turbine was mounted on a 120-m spar platform with a displacement of 8,126 m^3. Figure 1 shows a schematic layout of the TLS concept. The primary system properties are shown in Table 1.

In the single leg TLS concept, a pre-tensioned vertical tension leg connects the bottom of the spar to the seabed. The torsion stiffness provided by one leg is not very high; consequently, for the TLS, an upwind turbine is much less convenient in yaw compared to a downwind configuration. The downwind turbine has a rotor on the back side of the turbine, and the nacelle is typically designed to follow the wind (Figure 1). In this study, yaw motion is constrained to avoid instabilities because of the lack of controller yaw stiffness. The total mass is directly related to pretension.

Table 1: System properties (single leg TLS)

Draft	120 m
Diameter Above Taper	6.5 m
Diameter Below Taper	9.4 m
Centre of Buoyancy	$z = -60\ m,\ x = y = 0$
Displacement	8126 m^3
Total Mass	7.682E+06 kg
Centre of Gravity (CG)	$z = -80\ m,\ x = y = 0$
Pitch/Roll Inertia About CG	2.18E+10 $kg.m^2$
Yaw Inertia About Centreline	1.215E+08 $kg.m^2$
Pretension	7.624 MN

The linearised stiffness of the line (at the initial position of the spar) is used to calculate the surge, heave and pitch natural frequencies.

$$K_{Surge} = \frac{T_0}{L} \tag{1}$$

$$\omega_{Surge} = \sqrt{\frac{K_{Surge}}{M + A_{11}}} = \sqrt{\frac{T_0}{L(M + A_{11})}} \tag{2}$$

Equation 2 presents the surge natural frequency, where K_{Surge} is the surge stiffness, T_0 is the pretension, L is the leg length, M is the total mass and A_{11} is the surge added mass.

$$K_{Heave} = K_{H_{Hydro}} + K_{H_{Leg}} \quad (3)$$

$$K_{H_{Leg}} = \frac{EA}{L} \quad (4)$$

$$\omega_{Heave} = \sqrt{\frac{K_{Heave}}{M + A_{33}}} = \sqrt{\frac{EA}{L(M + A_{33})}} \quad (5)$$

Equation 5 presents the heave natural frequency, where K_{Heave} is the heave stiffness, $K_{H_{Hydro}}$ is the hydrostatic heave stiffness, $K_{H_{Leg}}$ is the tension leg stiffness, E is the modulus of elasticity, A is the leg section area and A_{33} is the heave added mass. The hydrostatic heave stiffness is negligible compared to the tension leg stiffness.

$$K_{Pitch} = K_{P_{Hydro}} + K_{P_{Leg}} \quad (6)$$

$$K_{P_{Hydro}} = \rho \nabla GM \quad (7)$$

$$GM = (KB - KG + \frac{I}{\nabla}) \quad (8)$$

$$K_{P_{Leg}} = \frac{T_0}{L}(KG + L)KG \quad (9)$$

$$\omega_{Pitch} = \sqrt{\frac{K_{Pitch}}{I_P + I_{55}}} = \sqrt{\frac{T_0(KG + L)KG + \rho \nabla GM}{L(I_P + I_{55})}} \quad (10)$$

Equation 10 presents the pitch natural frequency, where K_{Pitch} is the pitch stiffness, $K_{P_{Hydro}}$ is the hydrostatic pitch stiffness, $K_{P_{Leg}}$ is the tension leg stiffness, ρ is the water density, ∇ is the submerged volume, GM is the metacentric height, KG is the distance of the centre of gravity (CG) from the bottom of the spar, KB is the distance of the centre of buoyancy (CB) from the bottom of the spar, I is the area moment of inertia, I_P is the pitch inertia and I_{55} is the added pitch inertia.

In Table 2, the natural frequencies of the first (rigid body) modes that were obtained based on the above equations are summarised (Equations 1-10).

Table 2: System natural frequencies obtained from the analytical formulas ($rad/\sec$).

Surge/Sway	0.05
Heave	3.69
Pitch/Roll	0.20

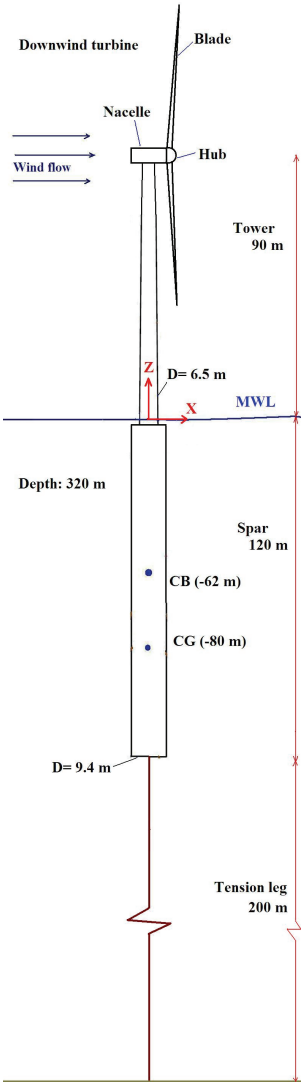

Figure 1: Tension leg spar wind turbine.

3. THEORETICAL BACKGROUND

This section contains the theories that were used to model the system, including the wave, hydrodynamic and structural models. The stochastic theory that was used to treat the responses is also discussed. To be consistent, the same theories for both the HAWC2 and USFOS/vpOne codes were applied as

much as possible. Any differences in the modelling of the codes are explicitly mentioned.

3.1. Environmental conditions

A correlation of the waves and wind is considered to determine realistic environmental conditions. The Statfjord site was chosen as a representative site for a floating wind turbine park. Statfjord is an oil and gas field in the Norwegian sector of the North Sea that is operated by StatoilHydro. The site is located at 59.7°N and 4.0°E at a distance of 70 km from the shore. Simultaneous wind and wave data from the northern part of the North Sea were smoothed and fitted to analytical functions. For the representative site, environmental conditions of H_S =15 m and T_P = 16 sec were chosen [10, 11].

3.2. Wave theory and wave history sampling

Linear wave theory (often called Airy theory, Eq. 11) with Wheeler stretching was used [12]. By stretching the Airy theory, the kinematics calculated at the MWL were applied to the true wave elevation [8]. The stretching was performed by substituting the vertical coordinate z with the scaled coordinate z' (Eq. 12).

$$\zeta = \zeta_a \sin(\omega t - kx) \tag{11}$$

$$z' = (z - \zeta)\frac{h}{h + \zeta} \tag{12}$$

The Joint North Sea Wave Project (JONSWAP) spectrum was used to represent long-crested irregular waves. Three parameters (H_S, T_P, γ) from the JONSWAP spectrum were used to model the wave. The peakedness parameter γ, which is the ratio of the maximum spectral energy to the Pierson-Moskowitz spectrum [13], was chosen with a default value of 3.3. The significant wave height and wave peak period are given in Section 3.1.

The time domain simulation was based on random waves that were obtained using random numbers for phase angles at discretised frequencies. A constant $\Delta\omega$ was applied in both of the codes. To avoid repetition of the wave sample with a sampling time of 1 hour, 1800 frequencies were used to generate a sample time series of the waves. The cut-in and cut-out wave periods were selected as 1.5 and 40 seconds, respectively.

3.3. Hydrodynamic forces

For this structure, both viscous and potential flow may be important depending upon the wave height. Figure 2 [14] can be used to judge the relevant effects of inertial and drag forces.

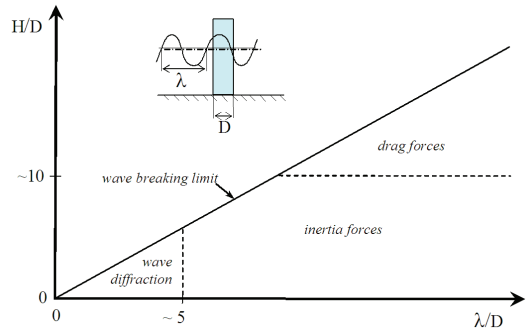

Figure 2: Relative importance of the inertial, drag and diffraction wave forces [14].

In Figure 2, H/D is the ratio of the wave height to the structure diameter, and λ/D is the ratio of the wave length to the structure diameter. For the TLS case, in extreme wave conditions, the ratios are $H/D = 2.5$ and $\lambda/D = 26$.

Inertial force is the governing force, and wave diffraction can be neglected. Furthermore, the motion is large; thus, the linear theory from the Panel method (sometimes referred to as the boundary element method (BEM), which computes the wave loads at the mean position of the spar) is not applicable. The instantaneous position of the platform must be accounted for at each time step. Then, the Morison formula should be used. The Morison formula combined with a pressure integration method was used to model hydrodynamic loads on the structure.

3.3.1. Morison formula

The hydrodynamic force per unit length on the floater of the wind turbine (strip of a cylinder) is partially determined according to Morison's equation [12]. The Morison formula was originally developed for fixed bottom mounted offshore structures, but it can be extended to a floating structure (Eq. 13).

$$dF = \frac{\rho}{2} C_d D |u_r| u_r + \rho \frac{\pi D^2}{4} C_m \dot{u}_r + \rho \frac{\pi D^2}{4} \dot{u}_W \tag{13}$$

$$u_r = u_W - u_B \tag{14}$$

where ρ is the mass density of sea water, D is the diameter of the cylinder and $\dot{u}_r$ and u_r are the horizontal relative acceleration and velocity between the water particle velocity u_W and the velocity of the body u_B (Eq. 14), respectively. C_m and C_d are the added mass and quadratic drag coefficients, respectively.

The first term is the quadratic viscous drag force, the second term includes the diffraction and added mass forces and the third term is the Froude-Krylov force (FK term). A linear drag term $C_l u_r$ can also be added to the Morison equation (Eq. 13). C_l is the linear drag coefficient. However, for a spar type of platform such as the TLS, the quadratic viscous drag is dominant, and the linear drag term is not included. The positive force is along the wave propagation direction. C_d and C_l must be empirically determined and are dependent on many parameters like Reynolds number, Kaulegan-Carpenter number (KC), relative current number and surface roughness ratio [12]. The mass and drag coefficients were chosen based on the KC number using Table 3 [15]. In Table 3, C_M is the inertia coefficient.

Table 3: Drag and inertia coefficients for an isolated, large scale vertical circular cylinder in a wave with no currents.

	Smooth		Rough	
KC	C_d	C_M	C_d	C_M
5	0.60	2.00	1.30	1.90
15	0.70	1.75	1.40	1.60
30	0.70	1.60	1.40	1.45
50	0.70	1.55	1.20	1.20
70	0.70	1.55	1.20	1.10
100	0.70	1.55	1.20	1.00

For the TLS, the KC number is about 5, and the structure is assumed to be smooth. Therefore, the following values were used: $C_d = 0.60$ and $C_m = C_M - 1 = 1.00$. Furthermore, WAMIT and WADAM analyses indicated that the frequency dependency of surge/sway added mass is low for this case [3, 4]. Because the structure is dominated by inertia, the hydrodynamic drag does not significantly influence the wave frequency portion. However, an increase in the drag coefficient decreases the resonant response. Therefore, the selected drag coefficient is conservative [5].

The heave forces (excitation and damping) and heave added mass are not included in the original Morison formula. In the HAWC2 code, there is a feature to include heave damping, but this feature is not available in the USFOS/vpOne code; therefore, the model does not include any heave damping. The heave FK force was included in both of the codes in the dynamic pressure integration (Section 3.3.2).

3.3.2. Buoyancy and wave excitation forces

The Morison formula does not provide any excitation force in heave and does not account for buoyancy. By using these two codes, different approaches were used to calculate these forces. Two features are available in the USFOS/vpOne code, and one feature is available in the HAWC2 code.

The first feature in the USFOS/vpOne code is a pressure integration method. This method consists of integrating the static and dynamic pressures (Eq. 15) over the wetted surface of the body. The static pressure corresponds to the buoyancy (Eq. 16), and the dynamic pressure of the waves corresponds to the wave FK excitation forces (Eq. 17). The transversal component of the dynamic pressure integration corresponds to the FK term in the Morison formula. Therefore, if the pressure integration method is applied, then the FK term should be removed from the Morison formula.

$$P = P_S + P_D \tag{15}$$

$$P_S = -\rho g z \tag{16}$$

$$P_D = \rho g \zeta_a \frac{\cosh k(z+h)}{\cosh kh} \sin(\omega t - kx) \tag{17}$$

where P is the total pressure; P_S and P_D are the static and dynamic pressures for regular waves, respectively; ρ is the water density; g is the gravitational acceleration; ζ_a is the wave amplitude; k is the wave number; h is the mean water depth; ω is the wave frequency; t is time; x is the wave propagation direction and z is the vertical distance to the MWL.

The second feature in the USFOS/vpOne code is a calculation of the displaced volume up to the wave elevation at each time step. In the displaced volume approach, the force is calculated using Equation 18.

$$F_B = \rho g \Delta \quad (18)$$

where F_B is the buoyancy force and Δ is the displaced volume up to the wave elevation. The displaced volume method is an approximation of the pressure integration method. If z is small compared to h in Equation 17, then the $\frac{\cosh k(h-z)}{\cosh kh}$ term is close to one, which results in a simpler expression of the total pressure P' (Eq. 19).

$$P' = \rho g(\zeta - z) \quad (19)$$

Integrating this new pressure P' over the body results in Equation 18. The displaced volume method only provides a vertical force; thus, the FK term must remain in the Morison formula. For a deep draft structure, this method is not appropriate. However, for small draft structures, this method is often applied in industry. In this paper, both of these methods are compared for the TLS.

The hydrodynamic feature in the HAWC2 code is also a simplification of the pressure integration method. The buoyancy is determined from the displaced volume up to the MWL, which corresponds to the static pressure integration (Eq. 16). Transversal excitation forces are included in the FK term in the Morison formula, which corresponds to dynamic pressure integration in the transversal direction. The dynamic pressure is then integrated over the bottom and conical sections of the structure to compute the vertical forces on the spar.

3.3.3. Nonlinear hydrodynamic loads

This study is based on linear wave theory; however, because of geometrical updating and Wheeler stretching, some hydrodynamic nonlinearity was included. The instantaneous position of the structure was used to calculate the hydrodynamic loads. This geometrical updating adds some nonlinearity, which primarily affects the resonant responses [2, 3, 4 and 5]. The quadratic hydrodynamic viscous drag term also introduces nonlinear excitation and damping forces. The wave kinematics are correctly accounted for up to the wave elevation. Therefore, the mean drift force is considered by pressure integration in the transversal direction (FK term).

3.4. Structural theory

The structure was modelled using beam elements in both of the computer codes. In both of the codes, the rotor and nacelle were modelled as point masses at the top of the wind turbine tower. The corresponding mass and inertia matrices of these parts were applied in the analysis. Two structural theory approaches were used (linear and nonlinear), as described below. The structural damping was modelled using Rayleigh damping in both of the codes.

3.4.1. Beam theory

The structural theory of the HAWC2 code is based on a multi-body formulation. In this formulation, the primary structure portion is subdivided into a number of bodies. Each body is an assembly of Timoshenko beam elements. The Timoshenko beam model takes into account shear deformation and rotational inertia effects. Inside of the body, the formulation is linear and assumes small deflections and rotations. The leg modelled as a single body does not include the same nonlinear geometric effects related to large deflections as a leg that is divided into several bodies [6, 15]. Therefore, large rotations and translations of the body motion are accounted for.

The structural theory of the USFOS/vpOne code is based on nonlinear beam theory. In this formulation, the primary structure is subdivided into a limited number of elements in which the effects of large displacements and a coupling between lateral deflection and axial strain are included by using nonlinear strain relations (Green strain). In this study, linear material properties were used. The beam model in the USFOS/vpOne code ensures that the beam element properly models the behaviour of a beam with axial forces.

3.4.2. Structural damping

Mass and stiffness proportional damping (Rayleigh damping) was used in both of the HAWC2 and USFOS/vpOne codes to model structural damping at the frequencies at which flexible modes of the structure occur.

$$C = \alpha_1 M + \alpha_2 K \quad (20)$$

$$\alpha_1 = \frac{2\omega_1\omega_2}{\omega_2^2 - \omega_1^2}(\lambda_1\omega_2 - \lambda_2\omega_1) \quad (21)$$

$$\alpha_2 = \frac{2(\lambda_2\omega_2 - \lambda_1\omega_1)}{\omega_2^2 - \omega_1^2} \quad (22)$$

where C is the structural damping coefficient; K is the tension leg stiffness (Eq. 20); M is the total mass of the system; α_1 and α_2 are the mass and stiffness damping

coefficients, respectively; and λ_1 and λ_2 are the damping ratios at ω_1 and ω_2, respectively.

For horizontal motion, structural damping is negligible compared to hydrodynamic damping. However, for vertical motion, the hydrodynamic damping is small, and the structural damping in the tension leg is more active. Therefore, the Rayleigh damping parameters were based on the heave resonance frequency: $\omega_1 = \omega_{heave} = 4.5\ rad/\sec$, and the damping ratio was chosen as $\lambda_1 = 1\%$. Because ω_1 exhibits a relatively high frequency, the Rayleigh damping can be considered to be stiffness proportional damping, i.e., $\alpha_1 = 0$. Furthermore, ω_2 is considered to be 10% of ω_1. Consequently, λ_2 and α_2 were determined from Equations 21 and 22 as $\lambda_2 = 0.1\%$ and $\alpha_2 = 0.004$.

3.4.3. Tension leg model

The tension leg was modelled in both codes using beam element theory. The tension leg is a 200-m-long pipe and is linked with pin joints to the spar and the bottom of the sea. The cross-sectional area of the tension leg was chosen based on the pretension.

In the HAWC2 code, the leg effect can also be modelled as an external force depending on the motion of the top end of the tension leg, which was implemented in a dynamic link library (DLL) routine. This model will be used to demonstrate the dominant spring effect of the line. The model will also be used to introduce the importance of structural damping on the tension at the heave resonance frequency.

In this DLL, the line was modelled with a straight spring acting between the bottom of the spar and a fixed point at the sea bed (anchor). The spring stiffness was defined using Hooke's law applied to the leg (Eq. 23). Then, the stiffness was applied to a time- and position-dependent strain and unit vector to determine the tension (Eq. 24). The strain and unit vector are nonlinear functions of the position of the spar (Eqs. 25 and 26). In these equations, K is the line stiffness, A is the cross-sectional area of the line, $\vec{T}$ is the line force vector, ΔL is the strain of the line, $\vec{e}$ is the unit vector between the bottom of the spar and the anchor and (x, y, z) is the position of the bottom of the spar.

$$K = \frac{EA}{L} \tag{23}$$

$$\vec{T} = K\,\Delta L\,\vec{e} \tag{24}$$

$$\Delta L = \sqrt{x^2 + y^2 + (h+z)^2} - L \tag{25}$$

$$\vec{e} = \frac{1}{\sqrt{x^2 + y^2 + (h+z)^2}} \begin{vmatrix} x \\ y \\ h+z \end{vmatrix} \tag{26}$$

The total tension ($\vec{T}$) includes both the static (pretension) and dynamic tension. The pretension is represented as an elongation of the line (vertical motion of the spar) because of the difference between the weight and buoyancy forces. The DLL model in this study does not include structural damping.

3.5. Stochastic theory

To generate irregular waves, various discretisation methods of the wave spectrum can be used. The USFOS/vpOne code provides options with a constant $\Delta\omega$ and constant area ($S(\omega)\Delta\omega$). The HAWC2 code uses only a constant $\Delta\omega$. Therefore, in this study, a constant $\Delta\omega$ was used in both of the codes. In this method, the wave spectrum is discretised at constant intervals depending on the number of frequencies, cut-in and cut-out frequencies. The mid-frequency in each interval is the representative frequency that defines the corresponding regular wave. The irregular wave time history can be determined from a superposition of the regular waves (Eq. 27). The amplitude of each regular wave (ζ_a) is related to the wave spectrum. Random phases (ϕ_n) were used to make the stochastic realisation. ω_n and k_n are the wave frequency and the wave number of the nth regular wave, respectively. N is the number of regular wave frequencies. In this study, to avoid repetition of the irregular wave, 1,000 regular wave frequencies were chosen.

$$\zeta = \sum_{n=1}^{N} \zeta_{a,n} \sin(\omega_n t - k_n x + \phi_n) \tag{27}$$

The Wave Analysis for Fatigue and Oceanography (WAFO) [16] toolbox in MATLAB was used for spectral and statistical analyses of the response time series. As previously mentioned, a one-hour time domain analysis was performed to study the hydroelastic dynamic response. The time domain results were transformed to the frequency domain by applying an inverse Fourier transformation using WAFO. Several

realisations of the process are required to accurately estimate the spectrum of a Gaussian process. However, in many cases, based on the smoothing of one realisation, it is possible to estimate the results and capture the primary phenomena. In this paper, the spectra were smoothed by using a kernel smoother. The maximum lag size of the Parzen window controls the smoothing. In this study, for all of the plotted spectra, the corresponding value of the smoothing parameter in WAFO was chosen as 2,000 [16].

3.6. Time domain simulation methods

Step-by-step integration methods were used to calculate the response by using an iterative routine. The Newmark-β method, which is available in both codes, was used with the following parameters: $\beta = 0.25$ and $\gamma = 0.5$.

In the time domain simulation, the duration and the time step must be carefully determined. The time step must be small enough to capture the highest frequency of the load/response phenomena, and the duration must be sufficiently long to capture the lowest frequency phenomena.

The highest frequency in the system is the heave natural frequency (Table 2). Furthermore, to capture one cycle of phenomena in the time domain, about 15 time steps are required. Therefore, the time step should be smaller than the heave natural period divided by 15. The time step was chosen as $0.1 \text{ sec} \le T_{heave}/15$.

The lowest frequency in the system is the surge natural frequency (Table 2); therefore, a one-hour sample includes 30 cycles. Furthermore, the calculation of irregular wave kinematics without repetition is very time consuming and is a direct function of the sampling time. The choice of different seeds to generate the sample affects the low frequency response; this effect will be discussed in Section 4.1.2.

During the first few seconds of the dynamic simulation, the loads must be applied smoothly to avoid spurious transient effects; thus, the loads were applied with a ramp function. The duration of the ramp is based on the highest natural frequency. The initial results indicated that a duration of three times the smallest period is required. Therefore, the first 200 seconds of the results were removed to ensure the damping of transient effects and initial numerical uncertainties.

4. HYDROELASTIC DYNAMIC ANALYSIS

The hydroelastic analysis includes several aspects. The primary purpose of this study is to perform a code-to-code comparison. However, because none of the codes were custom-made for this analysis, alternative models for the tension leg model, buoyancy and large motion analysis were addressed.

Before presenting the hydrodynamic comparison, the effect of the time step on the convergence of the simulation will be discussed. For this purpose, five simulations with different time steps and the same wave time series were compared. The surge motion results from the USFOS/vpOne analysis are shown in Figures 3 and 4. The results indicate that a time step of 0.5 is too large to capture the behaviour. The simulations converge for smaller time steps. However, small time steps are time consuming. In this analysis, a time step of 0.1 was chosen and is used in the remainder of the paper. The effect of wave elevation sampling on the stochastic dynamic response and the total simulation time using an average of the responses will be discussed in Section 4.1.2.

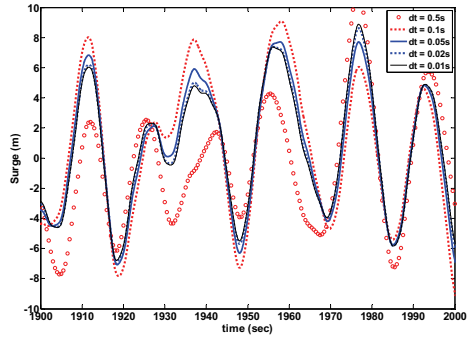

Figure 3: Surge time history at MWL for five different time steps (H_S =15 m and T_P =16 sec).

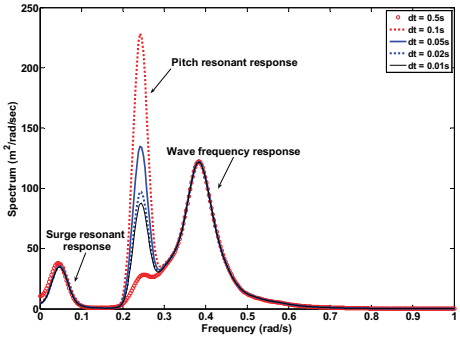

Figure 4: Surge spectra at the MWL, smoothed spectra based on one-hour time domain simulations for five different time steps (H_S =15 m and T_P =16 sec).

4.1. Code-to-code hydrodynamic comparison

In the following section, the hydrodynamic codes are compared for the sea state with H_S =15 m and T_P =16 sec. The effects of the different seeds on the response of each code are discussed.

4.1.1 Identical wave input

The code-to-code comparison was performed with the same wave time series in both of the codes (Figure 5). The motion and tension time series as well as the corresponding spectra are presented in the following figures. For clarity, only the time series samples for 500 seconds of the one-hour simulation are shown. For the tension, a duration of only 100 seconds is shown to demonstrate the high frequency response variation.

In Figures 6 and 7, the surge response time history and spectra at the mean water level (MWL) are shown. The surge and pitch natural frequencies as well as the wave-induced frequencies are clearly shown in the response. The surge motion at the mean water level is dominated by pitch motion because of its distance from the centre of gravity. The effect of pitch motion on the nacelle surge motion is even greater.

Regarding the surge motion at the bottom of the spar (not shown), similar to the surge at the MWL, the surge and pitch natural frequencies appear. The primary difference is the wave frequency portion, which is larger at the MWL and smaller at the bottom of the spar. Because of the nonlinearity, the low natural surge frequency combines with the pitch natural frequency to create motion with the same frequency as the wave (sum frequency effects).

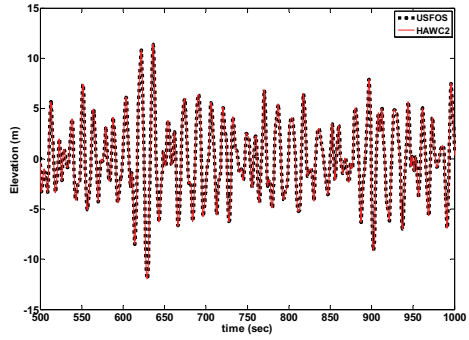

Figure 5: Wave elevation time history (H_S =15 m and T_P =16 sec, identical wave elevation).

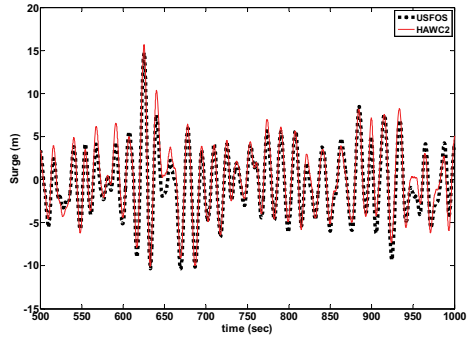

Figure 6: Surge time history at MWL (H_S =15 m and T_P =16 sec, identical wave elevation).

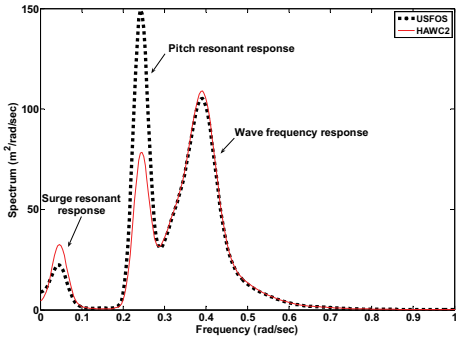

Figure 7: The surge spectrum at the MWL, smoothed spectrum based on a one-hour time domain simulation (H_S =15 m and T_P =16 sec, identical wave elevation).

Figures 8 and 9 show the pitch motion time history and spectrum, respectively. The pitch natural frequency was chosen as far as possible from the peak wave frequency; however, for harsh conditions, the pitch natural frequency is excited by the wave. For a poor system design in which the pitch natural frequency matches the wave peak frequency, the pitch resonance causes problems for the code-to-code comparison. The differences in this resonance spread throughout all of the other responses because of the highly nonlinear contribution of the line. These nonlinearities are more obvious in the heave and tension spectra.

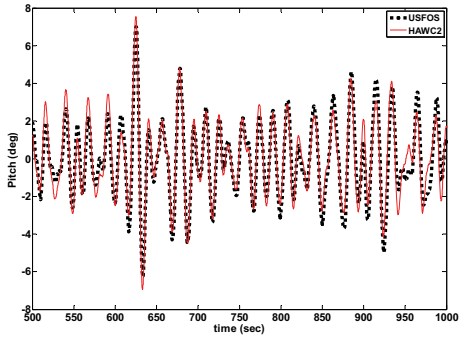

Figure 8: Pitch time history (H_S =15 m and T_P =16 sec, identical wave elevation).

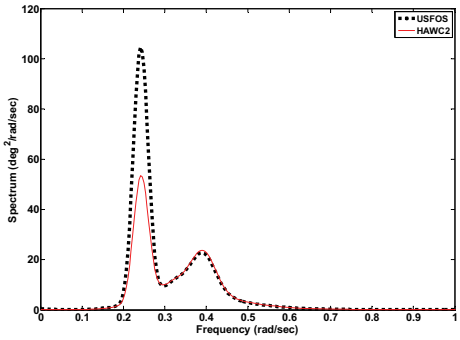

Figure 9: The pitch spectrum, smoothed spectrum based on a one-hour time domain simulation (H_S =15 m and T_P =16 sec, identical wave elevation).

Figures 10 and 11 show the heave motion response at the mean water level. The low frequency portion may be surge induced. The higher frequencies are related to the pitch motion. Because the strain of the tension leg is small, it is assumed that the bottom of the spar moves along the surface of a sphere. Therefore, one cycle of the pitch motion or the surge motion induces two cycles of the heave motion. Therefore, the heave spectrum exhibits a peak at twice the surge natural frequency and a peak at twice the pitch natural frequency. The peak at 0.65 rad/sec may be wave induced. The heave motion at the bottom of the spar is similar to that at the MWL. However, the other peaks appear due to a combination of various characteristic frequencies from nonlinear effects. The heave at the bottom of the spar is strongly related to the tension (spring relation, Section 3.4.3). A more detailed discussion is given below.

The tension time history and spectrum are presented in Figures 12 and 13. The tension response below 1 rad/sec formed because of several complex combinations of three characteristic frequencies: wave, surge and pitch natural frequencies. From Eq. 24, because of the nonlinear relation of the tension leg stiffness, these frequencies are mixing. More precisely, the square and square-root functions generate the sum and the difference of the frequencies. For higher frequencies, the lowest bending mode of the tower has a frequency of 2.4 rad/sec [5], and the heave natural frequency (Table 2) is 3.7 rad/sec. The heave resonant portion of the

tension is as important as the low frequency portion. The other high frequencies shown in the USFOS/vpOne result are related to the tower eigenfrequencies. However, the HAWC2 code does not capture some of the high frequencies. This may be related to the linear beam theory in the HAWC2 code (Section 3.4.1).

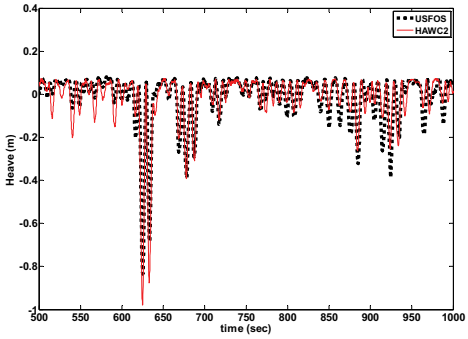

Figure 10: Heave time history at the MWL (H_S =15 m and T_P =16 sec, identical wave elevation).

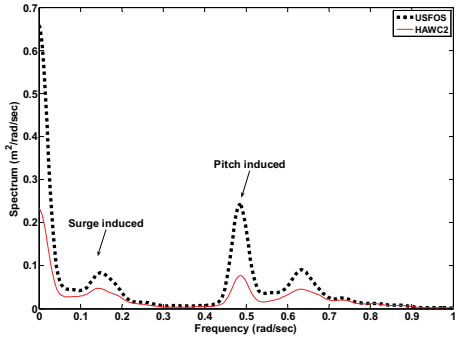

Figure 11: Heave spectrum at the MWL, smoothed spectrum based on a one-hour time domain simulation (H_S =15 m and T_P =16 sec, identical wave elevation).

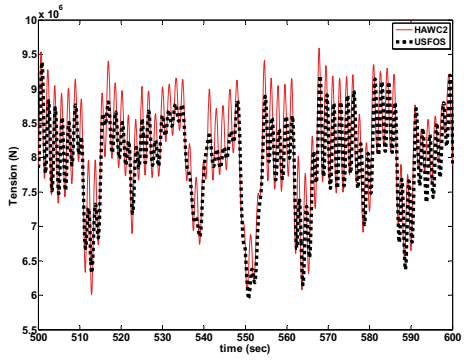

Figure 12: Tension time history (H_S =15 m and T_P =16 sec, identical wave elevation), pretension is 7.6 MN (Table 1).

In Table 4, the mean and standard deviation (STD) of the responses are compared for each of the codes. The mean and STD of the surge and the pitch are in good agreement. The means are very small compared to the respective dynamic amplitudes (Figures 6 and 8). The means of the tension in both of the codes are in good agreement with the pretension (Table 1).

In Table 5, the skewness and kurtosis of the responses are compared. The comparison of skewness and kurtosis indicates that the results obtained from the codes are in good agreement. The surge motions at the MWL and pitch responses are close to Gaussian. However, the heave at the MWL and tension responses exhibit some non-Gaussian behaviour.

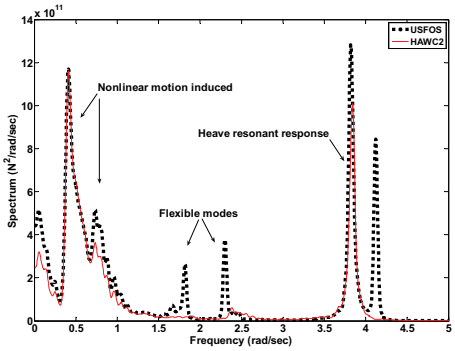

Figure 13: Tension spectrum, smoothed spectrum based on a one-hour time domain simulation (H_S =15 m and T_P =16 sec, identical wave elevation).

Table 4: Mean and standard deviation of the responses.

Response	Mean		Standard deviation	
	USFOS/ vpOne	HAWC2	USFOS/ vpOne	HAWC2
Surge at the MWL (m)	-0.46	0.31	4.62	4.37
Pitch (deg)	-0.11	0.03	2.80	2.40
Heave at the MWL (m)	-0.08	-0.05	0.23	0.16
Tension (N)	7.77e+6	7.95e+6	8.12e+5	7.05e+5

Table 5: Skewness and kurtosis of the responses.

Response	Skewness		Kurtosis	
	USFOS/ vpOne	HAWC2	USFOS/ vpOne	HAWC2
Surge at the MWL (m)	0.27	0.29	3.14	2.94
Pitch (deg)	0.17	0.19	3.33	3.10
Heave at the MWL (m)	-2.73	-2.83	12.30	13.64
Tension (N)	0.54	0.52	3.71	3.17

4.1.2 Effect of wave elevation sampling on the stochastic dynamic response

The time domain simulation was based on a realisation of random waves that were obtained using random numbers for phase angles at discrete frequencies. Because the simulation period is limited, the number of cycles for the low frequency responses is less than that of the wave frequency portion. Therefore, the low frequency response will be sensitive to the wave elevation sample size. In Figures 14 and 15, the effect of sampling is shown for the HAWC2 and USFOS/vpOne codes, respectively. For each code, 10 different seeds were chosen, and the spectra of surge motion at the MWL are plotted for all of the samples and their averages. The average spectra, which are shown in Figure 16, represent a ten-hour simulation (ten, one-hour simulations). However, there are some differences in the resonant responses. In Figure 16, trends similar to the response behaviour in Figure 7 are shown with different magnitudes. By performing very long simulations, the agreement for low frequency responses can be obtained, but it requires extensive time domain simulation effort.

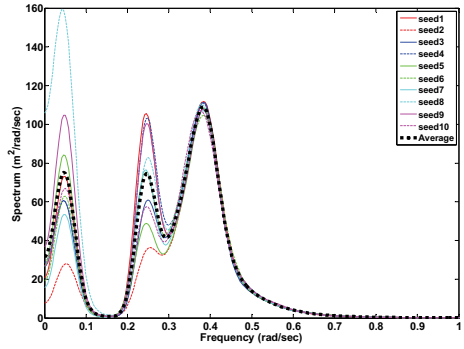

Figure 14: Surge motion spectra and their averages at the MWL for different seed numbers. Each smoothed spectra is based on one-hour simulations using the HAWC2 code (H_S =15 m and T_P =16 sec).

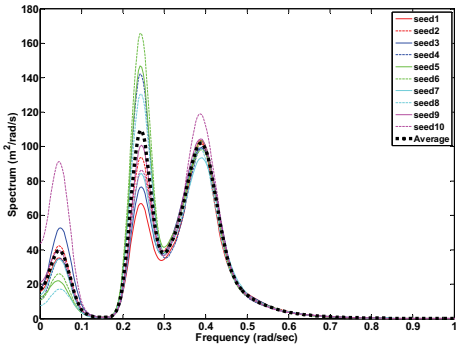

Figure 15: Surge motion spectra and their averages at the MWL for different seed numbers. Each smoothed spectra is based on one-hour simulations using the USFOS/vpOne code (H_S =15 m and T_P =16 sec).

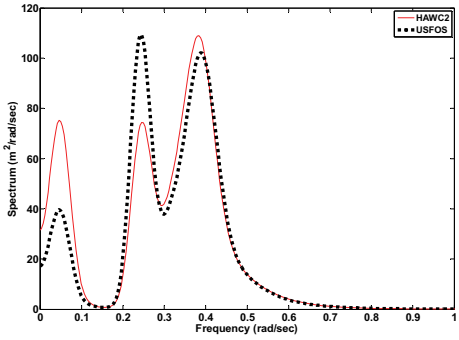

Figure 16: Surge motion spectra comparison between the HAWC2 and USFOS/vpOne codes at the MWL. The smoothed average spectra are based on ten different one-hour simulations using each code (H_S =15 m and T_P =16 sec).

4.2. The displaced volume method versus the pressure integration method

Two methods were introduced to calculate the FK wave excitation forces; the primary difference between them is the vertical excitation force (Section 3.3.2). The pressure integration method is the correct approach but is very time consuming compared to the inaccurate and quick displaced volume method. In fact, the computational time of the former is about 10 to 15 times longer than that of the latter method.

Figure 17 compares surge motion spectra at MWLs that were obtained from the two methods, and the agreement is reasonable. However, the tension spectra introduced in Figure 18 are very different, and the result from the displaced volume method (Archimedes) is not acceptable. As mentioned in Section 3.3.2, there is a large difference in the heave excitation forces. Additionally, the displaced volume method produces inaccurate vertical excitation forces, but the horizontal forces are the same.

For a general motion analysis (e.g., nacelle surge motion) of the concept, the computational time can be significantly reduced by using the displaced volume method. This method is much more efficient than the pressure integration method. However, for the mooring system analysis, the pressure integration method must be used.

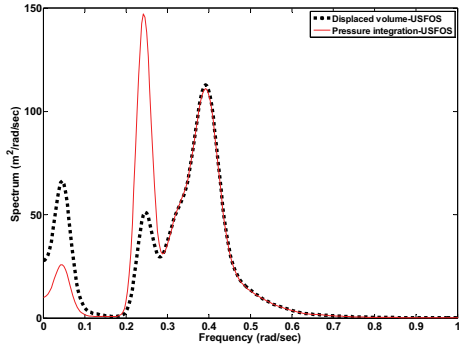

Figure 17: Surge motion spectra comparison for the Archimedes and pressure integration methods at the MWL. The smoothed spectrum is based on one-hour simulations using the USFOS/vpOne code (H_S =15 m and T_P =16 sec, identical wave elevation).

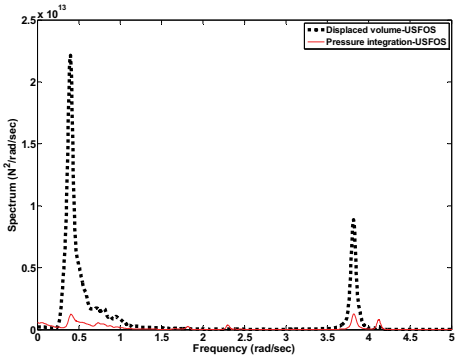

Figure 18: Tension spectra comparison for the Archimedes and pressure integration methods. The smoothed spectrum is based on one-hour simulations using the USFOS/vpOne code (H_S =15 m and T_P =16 sec, identical wave elevation).

As previously mentioned, Figure 18 shows the tension, which is a nonlinear function of the surge and heave motions (Figures 7 and 11). The appearance of various sum and difference frequencies of the characteristic frequencies (surge, heave, pitch and wave frequencies) in tension is due to this nonlinear formulation.

A comparison of Figures 7 and 17 indicates that the surge response of the HAWC2 code is similar to the surge response that was obtained from the displaced volume method in the USFOS/vpOne analysis. As previously mentioned, the HAWC2 code uses the displaced volume method to calculate buoyancy forces (Section 3.3.2).

4.3. Tension leg spring and damping effects

This section presents a comparison between a physical model (a beam with structural damping) and the DLL model of the tension leg (only the spring effect was included). Both of these features are only available in the HAWC2 code. The purpose of this comparison is to demonstrate the predominance of the spring effect of the tension leg and the importance of the structural damping in the tension leg (Figures 19 and 20).

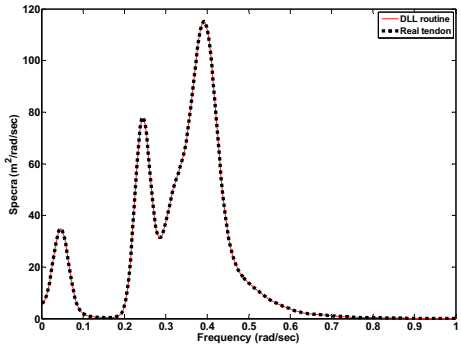

Figure 19: Surge motion spectra comparison between the simple DLL routine and the beam model of the tension leg using the HAWC2 code. The smoothed spectra is based on one-hour simulations (H_S =15 m and T_P =16 sec, identical wave elevation).

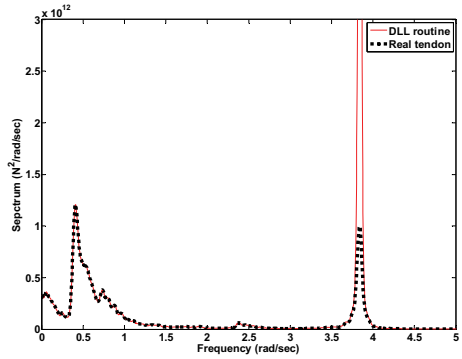

Figure 20: Tension spectra comparison between the simple DLL routine and the actual model of the tension leg using the HAWC2 code. The smoothed spectra is based on one-hour simulations (H_S =15 m and T_P =16 sec, identical wave elevation).

In Figures 19 and 20, the low frequency responses at less than 2 rad/sec match perfectly between the two models. Therefore, a simple spring (Section 3.4.3) is sufficient to model the global motion of the concept and the low frequency portion of the tension. In Figure 20, the high frequency portion that was obtained by the DLL and the physical model of the tension leg are different. The heave viscous damping is not included in

this study (Section 3.3.1); thus, the structural damping is the only source of damping. However, the DLL routine does not include this feature (Section 3.4.3). Consequently, the DLL model exhibits a much higher response around the heave natural frequency.

4.4. Rigid versus elastic modelling

This section presents a comparison between the rigid and elastic models of the spar and the tower. The spar is a stiff structure in bending. However, the tower is more flexible, and, because of the elastic deflection, it can induce some structural damping.

Figure 21 shows that the surge spectra for the rigid and elastic models are slightly different. The elastic case is more damped than the rigid case because of structural damping in the spar and the tower. However, the tension spectrum (Figure 22) is not significantly affected. For low frequencies (less than 2 rad/sec), Section 4.3 demonstrated that this portion of the spectrum is dominated by the spring formulation of the tension leg. The eigenfrequencies, which appear at 1.9 and 2.4 rad/sec in the flexible model, disappear in the rigid body model. The response at the heave resonance is only slightly affected.

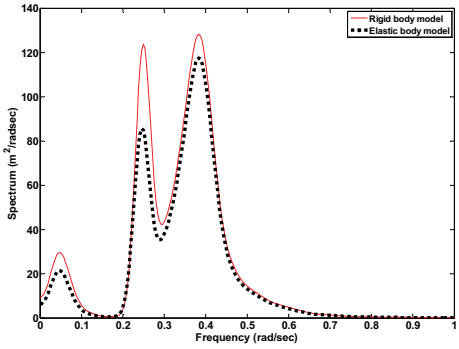

Figure 21: Surge motion spectra comparison between the rigid and elastic models of the spar and the tower using the HAWC2 code. The smoothed spectra is based on one-hour simulations (H_S =15 m and T_P =16 sec, identical wave elevation).

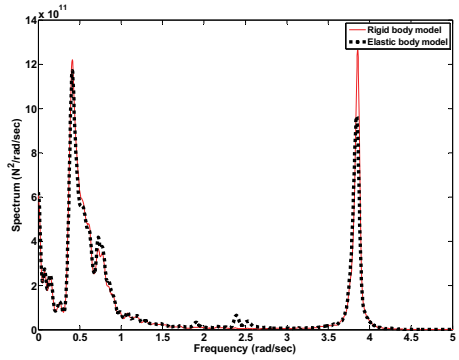

Figure 22: Tension spectra comparison between the rigid and elastic models of the spar and the tower using the HAWC2 code. The smoothed spectra is based on one-hour simulations (H_S =15 m and T_P =16 sec, identical wave elevation).

5. CONCLUSIONS

This paper deals with a code-to-code hydrodynamic comparison of the USFOS/vpOne and HAWC2 codes for a tension leg spar wind turbine. The analyses were limited to wave-induced responses. The purpose of this paper is to contribute to the validation of commercial codes used for this purpose and to demonstrate some essential features in the modelling process of this type of structure. A coupled hydroelastic stochastic time domain analysis was performed to estimate the dynamic behaviour of a tension leg spar (TLS) wind turbine. The hydrodynamic and structural models were described.

The comparisons indicated that the surge as well as the pitch motion and tension responses is in reasonably good agreement. However, some differences were identified in the resonant responses, especially in heave motion and tension responses. By accounting for the instantaneous position of the platform in the calculation of the forces, some hydrodynamic nonlinearity was implicitly introduced because of nonlinear hydrodynamic excitation. All of the motions are highly connected through the tension leg. The governing behaviour mode is the pitch response that affects all of the other responses through the tension leg. The nonlinear effect of the tension leg introduces the sum and difference of the pitch, surge and wave frequencies for the heave and tension responses. The system should be designed such that the pitch natural frequency is

outside of the wave spectrum. However, nonlinear hydrodynamic loading can excite the natural frequencies, which can be even worse for wind-induced motion because turbulent wind has significant energy around these frequencies.

The effect of wave elevation sampling on the response of each code was examined as well. The results for the low frequency responses (surge and pitch) are significant because the number of cycles in each sample is small. Ten, one-hour simulations of each of the codes were conducted, and the averages of them exhibited better agreement. However, there were also some differences in the resonant responses. By performing very long simulations, the agreement for low frequency responses can be improved, but a significant time domain simulation effort would then be required.

Two methods were introduced to calculate wave excitation forces: the pressure integration method and the displaced volume method. The computational time differed by an order of magnitude between these two methods. For a full hydrodynamic study of a tension leg, the pressure integration method should be used. However, for studies that do not focus on the tension leg response, the displaced volume method can be used to save computational time.

A comparison of the DLL and actual line models indicated that the spring effect of the tension leg governs the overall motion of the spar. However, the heave resonance in tension is sensitive to damping. A feature for hydrodynamic heave damping can be added to the model to reduce this high frequency.

A comparison of the use of a rigid and elastic formulation of the spar and the tower indicated that structural damping of the elastic body only slightly affects the general surge and pitch motion. However, the tension is not affected by this feature, except for the resonant responses.

6. ACKNOWLEDGEMENTS

We would like to thank Prof. Jørgen Amdahl from NTNU and Dr. Tore Holmas from Virtual Prototyping for discussions regarding the USFOS/vpOne code. The authors would like to acknowledge financial support from the Norwegian Research Council that was granted to the Centre for Ships and Ocean Structures (CeSOS).

REFERENCES

[1] Roddier D., Cermelli C and Weinstein A., “Windfloat: a Floating Foundation for Offshore wind Turbines Part I: Design Basis and Qualification Process’’, OMAE2009-79229, Hawaii, USA, 2009

[2] Holmas T. and Amdahl J., “Design of Floating Wind Turbines’’, Computational Methods in Marine Engineering III, Trondheim, Norway, 2009

[3] Karimirad M., Gao Z. and Moan T., “Dynamic Motion Analysis of Catenary Moored Spar Wind Turbine in Extreme Environmental Condition”, Proceeding of the European Offshore Wind Conference, EOW2009, September 2009, Stockholm, Sweden

[4] Karimirad M. and Moan T., “Wave and Wind Induced Dynamic Response of Catenary Moored Spar Wind Turbine’’, Submitted to the Journal of Waterway, Port, Coastal, and Ocean Engineering, ASCE

[5] Karimirad M. and Moan T., “Effect of Aerodynamic and Hydrodynamic Damping on Dynamic Response of a Spar Type Floating Wind Turbine ”, European Wind Energy Conference EWEC 2010, Warsaw, Poland, 2010

[6] Karimirad M. and Moan T., “Extreme Structural Dynamic Response of a Spar Type wind Turbine’’, ASME 2010 29th International Conference on Ocean, Offshore and Arctic Engineering, OMAE 2010-20044, Shanghai, China, 2010

[7] Larsen T. J., “HAWC2, the User’s Manual’’, version 3-8, Risø National Laboratory, DTU, Denmark, 2009

[8] Holmas T., “USFOS User’s Manual’’, version 8-1, Norway, 2004

[9] Jonkman J., Butterfield S., Musial W., and Scott G., “Definition of a 5-MW Reference Wind Turbine for Offshore System Development’’, NREL/TP-500-38060. NREL, Golden, Colorado, USA, 2009

[10] DNV, “Position Mooring’’, DNV-OS-E301, Norway, 2004

[11] Johannessen K., Meling T. S. and Haver S., “Joint distribution for wind and wave in the Northern North Sea’’, ISOPE, Stavanger, Norway, 2001

[12] Faltinsen O. M., “Sea Loads on Ships and Offshore Structures’’, Cambridge, UK, 1995

[13] DNV, “DeepC User Manual’’, Norway, 2008

[14] DNV, “Design of offshore wind turbine structures’’, DNV-OS-J101, Norway, 2004

[15] Chaplin J. R. and Ikeda Y., “Viscous Forces on Offshore Structures and Their Effects on the Motion of Floating Bodies’’, Proceedings of the ninth International Offshore and Polar Engineering Conference, Brest, France, 1999

[16] Larsen T. J. and Hanson T. D., “A method to avoid negative damped low frequent tower vibrations for a floating, pitch controlled wind turbine’’, Journal of Physics, The Science of Making Torque from Wind, IOP Publishing, Conference Series 75 (2007) 012073, 2007

[17] WAFO, “Theory manual’’, Centre for Mathematical Sciences, Lund University, Sweden, 2000

Paper 7

Ameliorating the Negative Damping in the Dynamic Responses of a Tension Leg Spar-Type Support Structure with a Downwind Turbine

Madjid Karimirad and Torgeir Moan

Accepted for publication at the proceeding of the European Wind Energy Conference (EWEC2011), March 2011, Brussels, Belgium

Is not included due to copyright

Paper 8

Tension Leg Spar-Type Offshore Wind Turbine with Upwind or Downwind Rotor Configuration

Madjid Karimirad and Torgeir Moan

Accepted for an oral presentation and publication at
AWEA-WINDPOWER2011 Conference, May 2011, Anaheim, CA, USA

Is not included due to copyright

Paper 9

Stochastic Dynamic Response Analysis of a Tension Leg Spar-Type Offshore Wind Turbine

Madjid Karimirad and Torgeir Moan

Submitted for publication

Stochastic Dynamic Response Analysis of a Tension Leg Spar-Type Offshore Wind Turbine

Madjid Karimirad* CeSOS, NTNU, Norway

Torgeir Moan CeSOS, NTNU, Norway

ABSTRACT

This paper deals with stochastic dynamic response analysis of a tension leg spar-type wind turbine subjected to wind and wave actions. The model is implemented in HAWC2 code. The controller gains are tuned to avoid negative damping at over-rated wind speeds. Amelioration of the negative damping can reduce the structural dynamic responses, which is very important for the fatigue life. The responses induced by wave and wind actions at the wave frequencies are not affected very much by the aerodynamic excitation or damping forces. Near the rated wind speed, the surge resonant response governs the responses and is excited by the aerodynamic forces and controller actions. Because of the nonlinear effects of the tension leg, all the motion responses are strongly coupled. The global responses of the upwind and downwind turbines are found to be close because the tower shadow has limited effect on the global responses. However, the blade structural dynamic responses are more affected by the tower shadow. The results show that the mean values of the responses are less affected by the turbulence. However, the ratio of the standard deviation for turbulent and constant wind speeds are 8.5 and 2.3 for the blade root's bending moment and nacelle surge motion. Extrapolation methods are applied to estimate the maximum responses. The maximum response is found to occur in the survival cases as a result of the wave actions. The results show that the normalised maximum responses corresponding to the up-crossing rate of 0.0001 vary between 3 and 5.

Keywords: Wind-wave-induced, Stochastic dynamic response, Tension Leg Spar, Offshore Floating Wind Turbine

NOMENCLATURE

BEM: Blade element momentum
BM: Bending moment
DLL: Dynamic link library
MWL: Mean water level
NREL: National renewable energy laboratory
PDF: Probability density function
STD: Standard deviation
TLS: Tension leg spar
VS: Versus
H_S : Significant wave height (m)
I : Turbulence intensity
T_P : Wave peak period (sec)
V : Mean wind speed (m/sec)
α : Shape parameter
β : Scale parameter

INTRODUCTION

Offshore floating wind turbines are one of the most challenging ocean structures, which demand coupled time domain analysis to consider the aerodynamic, hydrodynamic, structural dynamics and control algorithms [1]. These structures are subjected to stochastic wave and wind loads described by a joint distribution.

In this paper, a tension leg spar (TLS) similar to SWAY [2] is considered as a base structure for a floating wind turbine. The 5-MW NREL upwind wind turbine is modified to be a downwind turbine. An integrated dynamic response analysis is performed for both the upwind and downwind turbines.

The hydro-elastic response of the TLS wind turbine under the stochastic wave loading has been studied and the hydrodynamic modelling has been documented [3] through the code-to-code comparison.

In the present analysis, the yaw bearing is at the top of the tower, though in SWAY [2], it is at the bottom of the support structure. Moreover, the yaw motion of the platform is constrained to avoid the instabilities due to the lack of yaw stiffness. The deployment of the collective pitch controller for the downwind turbine is not the best option for such a rotor configuration. However, the results are relevant for the present research.

* Corresponding author, Madjid Karimirad
Centre for Ships and Ocean Structures (CeSOS),
Norwegian University of Science and Technology (NTNU), Norway
Email: madjid.karimirad@ntnu.no Phone: +47 94484785

The results are presented in the format of the time domain, frequency domain (spectral analysis based on the time domain results) and statistical characteristics of the responses. This study considers both constant and turbulent wind. The objectives of the present study are

1) Ameliorating the negative damping in the dynamic responses of a TLS wind turbine,
2) Comparison of upwind and downwind rotor configurations for TLS,
3) Studying the dynamic responses due to wave-only and wave and wind loads,
4) Studying the tower shadow effects,
5) Comparison of the dynamic responses for turbulent and constant wind load cases,
6) Normalised responses to draw more generalised conclusions.

THEORY

The irregular long crested waves are generated using the JONSWAP spectrum [4]. The cut-in, cut-out and the number of frequencies are precisely set to avoid any repetition of the waves [3]. The hydrodynamic loads are expressed by the Morison formula [4] considering the instantaneous position of the structure. Thus, geometrical updating is applied [5]. In addition, the heave excitation forces are expressed by the pressure integration method [3]. The linear (Airy) wave theory with Wheeler stretching to take into account the wave kinematics up to the wave elevation is used [3, 4]. Thus, the mean drift forces are included approximately.

The aeroelastic model in the HAWC2 code is based on a finite element formulation of the structural dynamics and an advanced blade element momentum theory for the aerodynamics [6]. The structural modelling is based on the multi-body formulation. The floating wind turbine is divided into several beams, each beam is a Timoshenko beam, and the beams are connected to each other by constraints. The dashpot, stiffness, ball joint and bearing are some of the modelling features in the HAWC2 code [7].

The HAWC2 code is based on an advanced blade element momentum theory (BEM). The power law for the mean wind shear with an exponent of 0.1 is used. A normal BEM dynamic induction, Prandtl tip loss model and the MHH (M. H. Hansen)-Beddoes method for the dynamic stall are applied [7]. Leishman-Beddoes model for unsteady blade aerodynamics is used [8]. The aerodynamic drag of the nacelle and tower and the drag and lift forces on the blades are considered [9]. The Mann turbulence model is used to generate three-dimensional turbulent winds [6].

The effect of the presence of the turbine tower on the flow field is modelled by the tower shadow. The potential flow and jet wake models for tower shadow effects on the upwind and downwind rotors in the HAWC2 code [7] are chosen. The tower shadows used in this study allow the shadow source to move and rotate in space as the tower coordinate system moves and rotates, which is suitable for floating wind turbines [7].

The potential flow model is appropriate for upwind rotors. The modified flow velocity component in the axial direction (u) based on the potential flow model is [10]

$$u = V_0 (1 + (D/2)^2 \frac{x^2 - y^2}{x^2 + y^2}) \tag{1}$$

where D is the tower diameter, x and y are the lateral and axial Cartesian coordinates in tower cross section with respect to the tower centre (y : from the hub toward the nacelle for the upwind rotor) and V_0 is the ambient undisturbed flow velocity.

In the case of a downwind rotor, the flow separation and generation of eddies are less amenable to analysis, so empirical methods are used [11]. The HAWC2 code uses the jet wake model for tower shadow of downwind rotors. In this model, the modified axial velocity component (u) is defined as [10, 11]

$$u = \frac{\sqrt{3}}{2} \sqrt{\frac{J_M \sigma}{\rho y'}} (1 - \tanh^2(\sigma \frac{x'}{y'})) \tag{2}$$

where σ is an empirical constant equal to 7.67 and x' and y' are lateral and axial non-dimensional (with respect to the tower diameter) Cartesian coordinates in the tower cross section. y' is toward the hub from the nacelle for the downwind rotor, and ρ is the air density.

Using the correlation between the initial tower wake deficit and the drag coefficient of the tower (C_D), the momentum deficit behind the tower (J_M) is defined by

$$J_M = \frac{V_0^2 D}{2} \frac{\rho}{\pi} [\frac{1}{8} + \frac{16}{3\pi}] C_D^2 \tag{3}$$

For below cut-in wind speed, the turbine is shutdown because the production of electricity is not cost effective. Between the cut-in and the cut-out wind speed, the wind turbine produces electricity, and the control is active. The wind

turbine is parked in storm conditions with blades parallel to the wind.

The Bladed-style DLL (dynamic link library) controller is used to implement a variable-speed generator-torque controller and PI collective blade pitch controller for the NREL Offshore 5-MW baseline wind turbine. The routine was written by Dr. Jonkman of NREL/NWTC for use in the IEA Annex XXIII OC3 studies [12]. The collective pitch controller is not the best option for the TLS type floating wind turbines. However, the results of this research can give an insight to this concept.

The variable-speed generator-torque controller and PI collective blade pitch controller (constant power) act based on the relative wind velocity. For below-rated wind speeds, the control is active by changing the rotational speed of the shaft (no feathering of the blades in the below-rated region). For over-rated wind speeds, the control is active by feathering the blades (the shaft rotational speed is constant). For a floating wind turbine in a rated wind speed, depending on the relative wind velocity, the controller acts similar to the below- or over-rated wind speed cases.

The blade pitch control of a turbine during operation can introduce some negative damping on a floating wind turbine. As an example, assume that the relative wind speed experienced by the blades is increased because of the rigid body motion of the system. Then, the conventional controller, if used, feathers the blades to maintain the rated electrical power. Thus, the thrust force decreases, which introduces some negative damping for over-rated wind speed cases. However, it is not the case for fixed wind turbines because the frequency of the blade pitch controller is normally less than the frequencies associated with the relative wind speed induced by structural responses [13].

The target of the controller is modified from a constant power to constant torque to reduce the aerodynamic loads. To eliminate the negative damping of the controller, the controller gains should be tuned such that the controller action frequencies are lower than the natural frequencies of the system [13, 14]. Based on Newton's second law and performing some mathematics, the controller gains can be linked to the system characteristics as following

$$\omega_0 = \frac{\omega_d}{\sqrt{1-\zeta^2}} \qquad K_I = \frac{\Omega_0 I \omega_0^2}{\frac{\partial P}{\partial \theta}} \qquad K_P = \frac{2\zeta K_I}{\omega_0} \tag{4}$$

where the ω_0, ω_d and ζ are the controller natural frequency, controller damped natural frequency and controller relative damping, respectively. I is related to the second moments of inertia of the rotor and generator, Ω_0 is the reference shaft rotational speed, P is the power, θ is the blade pitch angle and K_P and K_I are the proportional and integral gains of the controller. To avoid negative damping, the controller frequency should be less than the natural frequency of the floating wind turbine (for, i.e., pitch natural frequency), which requires that $\omega_d \le \omega_{pitch}$. In this paper, the controller relative damping is chosen to be 0.7 [14].

All the smoothed spectra in this study are obtained based on time domain simulations by performing Fourier transformations. In this study, the maximum lag size of the Parzen window function controls the smoothing [15].

The size of the turbulent box is limited, and, over long simulation periods, the wind starts to repeat itself. To avoid the repetition of the wind in turbulent wind cases, each 1-hour simulation is divided into four 15-min simulations with different seed numbers. After running each 15-min simulation, the obtained results are used to make a 1-hour simulation.

TENSION LEG SPAR WIND TURBINE

The NREL 5-MW Wind Turbine [12] is chosen as a reference. It is a 3-bladed upwind wind turbine. Changes are applied to this turbine to make it a downwind turbine. The simplest way to make a downwind turbine from an upwind one is to hang the rotor behind the tower, which ensures that the aerodynamic properties of the blades and airfoils are applied correctly. An upwind turbine has a shaft tilt and hub cone angle to prevent the blades from hitting the tower due to large aeroelastic deflections. In a downwind turbine, these values can be set to zero because the rotor is behind the tower. The changes applied to the upwind turbine to make it a downwind turbine are presented in Table 1. The turbine is mounted on a 120-m spar platform with displacement of $8126\,\mathrm{m}^3$. Figure 1 illustrates the schematic of the TLS concept.

The main system properties are listed in Table 2. In the single leg TLS concept, a pretensioned leg connects the bottom of the spar to the seabed. The torsional stiffness provided by one leg is not very high. Thus, a proper yaw mechanism and the application of an individual blade pitch controller are needed. In this study, the yaw motion is constrained to avoid

the instabilities due to the lack of the yaw stiffness. The collective blade pitch controller is applied. In Table 3, the natural frequencies (first modes) are summarised. The analytical formulas are used to calculate the natural frequencies using the linearised stiffness of the tension leg.

Table 1: Changes applied to the 5-MW NREL wind turbine.

Parameter	Upwind	Downwind
Rotor position	Front of tower	Behind the tower
Shaft upward tilt	5.0 (deg)	0.0 (deg)
Hub upwind cone	2.5 (deg)	0.0 (deg)

Table 2: System properties (single leg TLS wind turbine).

Wind turbine	5 *MW*
No. blades	3 bladed
Blade length	61.5 *m*
Hub height	90 *m*
Controller	Collective blade pitch
Rated wind speed	11.2 *m*/sec
Draft	120 *m*
Diameter above taper	6.5 *m*
Diameter below taper	9.4 *m*
Centre of buoyancy	-62 *m*
Displacement	8126 m^3
Total mass	7,682E+03 *kg*
Centre of gravity (CG)	-80 *m*
Pitch/Roll inertia about (CG)	2.18E+10 $kg.m^2$
Yaw inertia about centreline	1.215E+08 $kg.m^2$
Leg length	Up to 200 *m*
Leg diameter	1.0 *m*
Leg thickness	0.036 *m*
Pretension	7.624 *MN*

Table 3: System natural frequencies (*rad* / sec).

Surge/Sway	0.05
Heave	3.69
Pitch/Roll	0.20

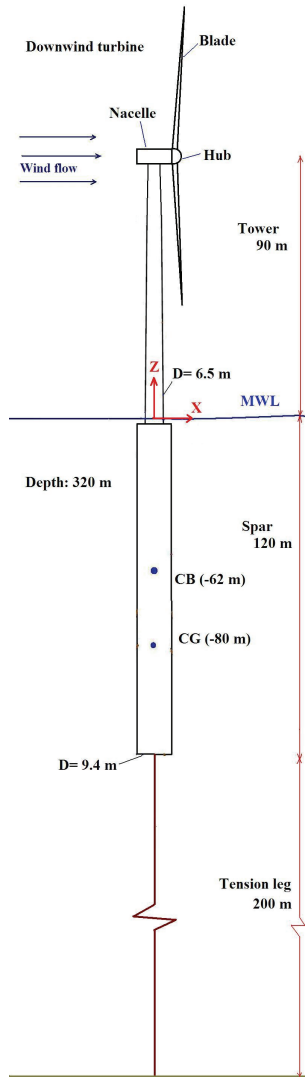

Figure 1: Schematic layout of the tension leg spar wind turbine.

METOCEAN CONDITIONS

To design, install and operate offshore wind turbines in a safe and efficient manner, it is necessary to have a realistic metocean (meteorological and oceanographic) data available for the conditions to which the installation may be exposed. The most important data for a floating wind turbine are the wind and wave conditions. However, at some offshore

locations, other parameters may be important (e.g., tidal current and ice conditions).

In this study, the Statfjord site has been chosen as a representative site for the floating wind turbine. Statfjord is an oil and gas field in the Norwegian sector of the North Sea operated by Statoil. The site location is 59.7°N and 4.0°E with a 70-km distance from the shore. Simultaneous wind and wave measurements covering the years 1973-1999 from the Northern North Sea are used as a database. The data have been smoothed and fitted to analytical functions [16].

The probability density function (PDF) of the 1-hour mean wind speed at 10 m above the MWL can be described by a 2-parameter Weibull distribution:

$$f(V) = \frac{\alpha}{\beta}(V/\beta)^{\alpha-1}\exp(-(V/\beta)^{\alpha}) \quad (5)$$

The shape and scale parameters recommended for the representative site are $\alpha = 1.708$ and $\beta = 8.426$.

For the wind turbine the wind velocity at the top of the tower (nacelle) is more relevant to the study. Figure 2 illustrates the Weibull PDF of the wind speed at the nacelle (90 m above the MWL) and the reference (10 m above the MWL).

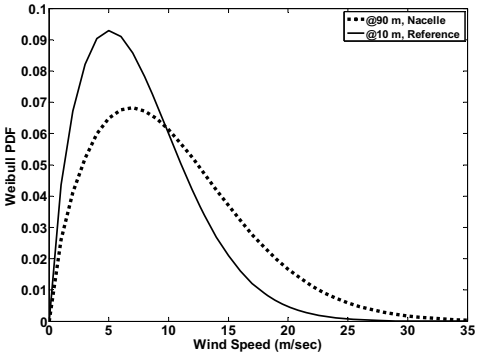

Figure 2: Weibull probability density function of the wind speed at the nacelle (90 m above the MWL) and the reference (10 m above the MWL) for the representative offshore site.

The probability of the wind speed at the nacelle for three ranges is listed in Table 4. When the wind speed at the nacelle is less than 3 m/sec, the wind turbine does not work because the wind speed is too low to make cost effective electricity. Between the cut-in and cut-out wind speeds (3-25 m/sec), the wind turbine operates and produces electrical power. After passing the cut-out wind speed, the wind turbine is shut down to prevent the damage and failure of the wind turbine parts, especially the blades. In this region, the wind turbine is parked with blades parallel to the wind, and the controller is inactive. The probability of the occurrence of high wind speeds (hurricanes and storms) is low. According to Table 4, only 2.3% of winds are more than 25 m/sec. However, for a floating turbine, due to combined wave- and wind-induced loading, extreme responses can occur in harsh environmental conditions [5, 6].

Table 4: Probability of wind speed at the nacelle.

Wind speed (m/sec)	Probability
Less than 3	0.096
3-25	0.881
More than 25	0.023

The significant wave height is often described by a Weibull distribution.

$$f(H_S) = \frac{\alpha_{H_S}}{\beta_{H_S}}(H_S/\beta_{H_S})^{\alpha_{H_S}-1}\exp(-(H_S/\beta_{H_S})^{\alpha_{H_S}}) \quad (6)$$

The proposed parameters for the shape and scale parameters are $\alpha_{H_S} = 2 + 0.135V$ and $\beta_{H_S} = 1.8 + 0.1V^{1.322}$ [16]. In Figure 3, the Weibull distribution for the significant wave height given the wind speed (top of tower) for the representative offshore site is shown for three different wind speeds. The significant wave height increases with the increase of the mean wind speed. Moreover, for higher wind speeds, the Weibull distribution of the significant wave height is negatively skewed. For each wind speed, a range of significant wave heights are possible. Smaller wind speeds have a narrower range of significant wave heights.

In Table 5, the load cases based on the relevant metocean data are listed [5]. V is the 10-min averaged wind speed at the nacelle.

For design purposes, metocean conditions that may occur once in a hundred years are required. Estimating extreme values associated with return periods of 100 years and beyond is an area of active research [6]. For the present offshore site, the 100-year environmental conditions are assumed to be V =49 m/sec, H_S =14.4 m and T_P =13.3 sec [6].

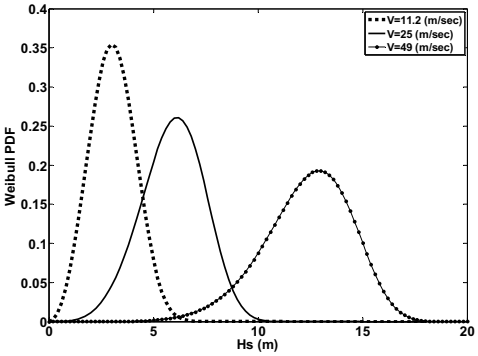

Figure 3: Weibull probability density function for the significant wave height given the wind speed for the representative offshore site for three different wind speeds (at the nacelle).

Table 5: Load cases for operational and survival conditions.

V (m/sec)	H_S (m)	T_P (sec)	Turbulence intensity (I)	Turbine status
49	14.4	13.3	0.10	Parked
30	7.1	11.9	0.11	Parked
25	5.9	11.3	0.12	Parked
17	4.2	10.5	0.15	Operating
14	3.6	10.2	0.15	Operating
11.2	3	10	0.15	Operating
8	2.5	9.8	0.18	Operating

AMELIORATING NEGATIVE DAMPING BY TUNING THE CONTROLLER GAINS

The comparison of wave-induced versus wind-wave-induced responses for operating and shutdown of the wind turbines in the previous studies showed that [13]

- In the below-rated wind speed case, no negative damping is present because the controller does not feather the blades
- In the rated wind speed case, some negative damping is caused by the controller action in the surge resonant response
- In the over-rated wind speed case, some negative damping is caused by the controller action for the pitch resonant response

As discussed in the theory part of this paper, the controller can introduce some negative damping if the controller natural frequency is greater than the resonant response frequencies. The tuning procedure is explained in the theory part of this paper (for more information refer to [13]). The surge resonant response is very slow, and its effect on the power production and fatigue damage is limited, so, in the present study, the controller gains are tuned to set the frequency of the controller action to less than the pitch resonant frequency. Thus, if the relative wind speed and, consequently, the power change due to the pitch resonant motion, then the controller action to modify the blade angle of attack occurs with a frequency less than the pitch natural frequency. The pitch natural frequency of the system is 0.2 rad/sec (Table 3), which means that the damped natural frequency of the controller (ω_d) must be less than 0.2 rad/sec. Using Equation 4, the proportional and integral gains of the controller are found to be $K_P = 0.86$ and $K_I = 0.13$. These gains are used in the input files of the HAWC2 code for the following tuned cases.

The nacelle surge motions for the operating downwind TLS turbine with tuned and untuned controllers subjected to the wave and wind loads are compared. Then, the statistical characteristics of different responses are compared for the tuned and untuned controllers.

Figure 4 shows the comparison of the nacelle surge motion with untuned and tuned controllers to avoid negative damping in the over-rated constant wind condition (V =17 m/sec, H_S =4.2 m and T_P =10.5). The tuned controller has decreased the instabilities. In the over-rated wind speed range, due to the negative damping effects of the controller, the pitch resonant response was dominant. After tuning the controller gains, the pitch resonant response is positively damped out.

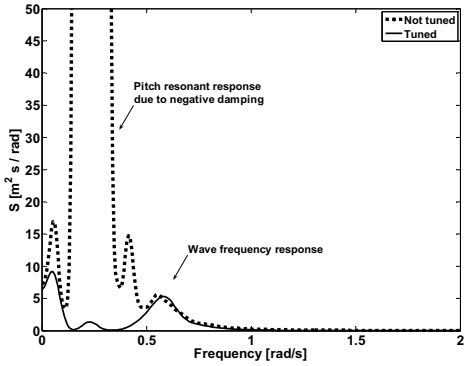

Figure 4: Nacelle surge spectra with untuned and tuned controllers in the over-rated constant wind condition (V =17 m/sec, H_S =4.2 m and T_P =10.5).

In Table 6, the mean value and standard deviation of the different responses are compared for the tuned and untuned controllers to highlight the positive effects of the tuning. The ratio between the standard deviation of the power and nacelle surge motion with the untuned and tuned controller are 8.1 and 14.5, respectively. Reducing the standard deviation of the responses can help to increase the fatigue life of the system. For the bending moment at the tower-spar interface and at the blade root, the ratios of the standard deviation with the untuned and tuned controller are 4.4 and 2.7, respectively. The spectra of the shaft rotational speed have a trend similar to the nacelle surge spectra presented in Figure 4. The ratio of the standard deviation for the shaft speed for the untuned and tuned controllers is 5. Hence, tuning can reduce the fatigue damage of the drive train. The shaft rotational speed for the original land-based wind turbine is 1.26 (rad/sec). The negative damping increased the mean of the shaft rotational speed to 1.29 (rad/sec). By tuning the controller, the rotational speed is close to its original value.

The tuning of the controller does not affect the rated and below-rated wind speed cases very much. As previously mentioned, the blade pitch control is not active for the below-rated wind speed cases. The rated wind speed case is also dominated by the surge resonant responses. In this study, the controller gains are tuned to remove the negative damping caused by the pitch resonant response. Thus, if the relative wind speed and, consequently, the power change due to surge resonant motion, then the controller action to modify the blades angle of attack can occur with a frequency close to the surge natural frequency. Hence, some negative damping can be seen for the surge resonant motion, which can be important for the fatigue life of the mooring system.

Table 6: The mean value and standard deviation of the wave-wind-induced responses for untuned and tuned controller (V =17 m/sec, H_S =4.2 m and T_P =10.5).

Response	Not Tuned		Tuned	
	Mean	STD	Mean	STD
Nacelle surge (m)	22.8	20.4	20.7	1.4
BM at blade root (kNm)	5.1 E+3	4.2E+3	4.3 E+3	1.5E+3
BM at tower-spar interface (kNm)	8.2E+4	1.3 E+5	7.5 E+4	2.9E+4
Shaft speed (rad/sec)	1.29	0.15	1.26	0.03
Tension (kN)	8.8	0.5	8.5	0.3
Power (MW)	4.80	1.05	5.00	0.13

DOWNWIND VERSUS UPWIND ROTOR

The wind-wave-induced responses of the downwind and upwind rotor configurations are compared with the wave-induced response of a shutdown turbine. The purpose of this section is

a) Comparison of the wave-induced and wind-wave-induced responses to show the dominant effects,
b) Comparison of upwind and downwind rotor configurations to illustrate the aerodynamic features of the downwind floating wind turbine.

For the wave only case, the rotor configuration obviously does not affect the wave-induced responses. A shutdown upwind rotor subjected to only wave loads is used for this load case. As mentioned above, a constant torque is chosen for the control algorithm to minimise the aerodynamic forces on the structure. The controller is tuned to avoid the pitch response instabilities due to the servo negative damping. However, some

negative damping is present for the surge resonance. Because the rated wind speed load case is governed by the surge resonant motion, the rated wind speed load case is considered to address the effects of the rotor configuration on the dynamic responses.

Rated wind speed case

For the rated wind speed case, the environmental conditions are chosen to be V =11.2 m/sec, H_S =3 m and T_P =10 sec. The wind-wave-induced responses of TLS with upwind and downwind rotor configurations are compared with the wave-induced responses (without wind action) to illustrate the aerodynamic effects.

Figure 5 shows the nacelle surge time history for floating TLS with a downwind rotor configuration subjected to simultaneous wave and wind action for the rated wind speed case. The slowly varying surge motion governs the response. The relative wind velocity and, consequently, the aerodynamic excitation forces change due to the rigid body motions. In other words, for a floating wind turbine, the resonant responses can be self-excited. A previous study [13] showed that the servo negative damping is present for the surge natural frequency.

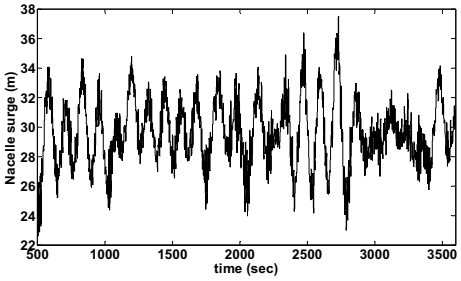

Figure 5: Nacelle surge time history of an operating downwind TLS subjected to wave and wind loading for a rated constant wind (V =11.2 m/sec, H_S =3 m and T_P =10 sec).

Figure 6 illustrates the nacelle surge spectra obtained based on a 1-hour time domain simulations for downwind and upwind rotor configurations subjected to simultaneous wind and wave actions and wave only action. The wave frequency parts of the responses are almost the same for wind-wave and wave only cases. Thus, the wind does not affect the wave frequency part. The controller is tuned to remove the pitch motion instabilities. The wave-induced and wave-wind-induced responses are very close at the pitch natural frequency. The surge resonant response is greater for the wave-wind cases than the wave only case due to the extra aero-servo excitation forces, and some negative damping for this frequency might be present due to the servo actions (refer to the paragraph above).

Figure 7 shows the tension spectra obtained based on a 1-hour time domain simulation for downwind and upwind rotor configurations subjected to simultaneous wind and wave actions and wave action for the rated constant wind case. The tension response below 2 rad/sec is formed by several complex combinations of the three characteristic frequencies: wave, surge and pitch natural frequencies. Through the nonlinear relation between tension and motions, these frequencies are mixed. More precisely, the square and square-root functions of the tension relation generated sum and difference of frequencies [3]. For the higher frequencies, the heave natural frequency (Table 3) is 3.7 rad/sec. The heave resonant part of the tension is as important as the low frequency parts. Due to the wind action the responses below 1 rad/sec are increased compared to those from wave only case (linked with the surge resonant response). The high frequency part of the tension spectrum is almost the same for both operating upwind and downwind rotors as well as the wave only case. Hence, this part of the tension response is mainly wave-induced.

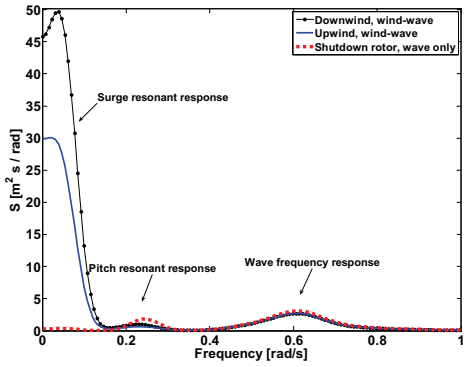

Figure 6: Nacelle surge spectra for wave-induced (shutdown) and wave-wind-induced responses for operating downwind and upwind rotor configurations of TLS in rated constant wind conditions (V =11.2 m/sec, H_S =3 m and T_P =10 sec).

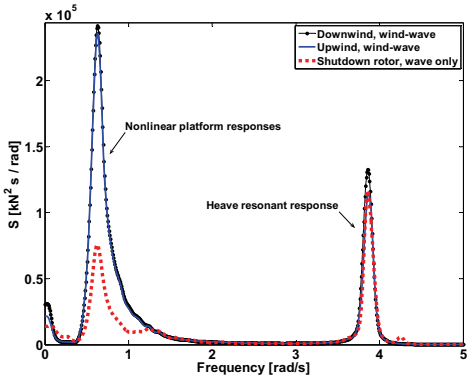

Figure 7: Tension spectra for wave-induced (shutdown) and wave-wind-induced responses for operating downwind and upwind rotor configurations of TLS in rated constant wind conditions (V =11.2 m/sec, H_S =3 m and T_P =10 sec).

The comparison of the upwind versus downwind rotors for the other load cases showed the same trends with the exception that the nacelle surge motions of the upwind and downwind rotors are found to be closer for the other load cases than what is presented here for the rated wind speed case. For the rated wind speed case, the surge resonant response of the downwind rotor is greater than the response for the upwind rotor. The tower shadow effect is the difference in the aeroelastic modelling of the upwind and downwind turbines. In the next section, the tower shadow effects on the responses are presented.

TOWER SHADOW AND TURBULENCE EFFECTS

The tower shadow and turbulence effects on the responses are discussed in this section. The dynamic response of the downwind TLS subjected to simultaneous wave and wind actions are compared for constant and turbulent wind with and without the tower shadow. The jet model tower shadow, as explained in the theory part of this paper, is used for the downwind turbine. The mean value and standard deviation of the blade root bending moment, nacelle surge, tension response, electrical generated power and bending moment at the tower-spar interface for the tension leg spar are compared for different load cases and environmental conditions while considering the tower shadow and turbulence.

Blade root bending moment

The tower shadow is a modification of the velocity pattern seen by the blades. It is not necessary that the blades be located behind the tower or exactly in front of the tower to feel this velocity modification. However, when the blades are close to the tower region or when they pass the tower, an impulse can be seen in the local responses (such as the blade deflections). The effects of the tower deficit on the blade response are presented here.

Figure 8 shows the blade root bending moment time history for a downwind TLS subjected to stochastic wave and wind actions for the below-rated wind speed case (V =8 m/sec, I =0.18, H_S =2.5 m and T_P =9.8 sec). The tower shadow has limited effects on the mean of the response. However, the dynamic response is more affected. The comparison shows that the effect of turbulence on the dynamic response is relatively greater than the tower shadow effect.

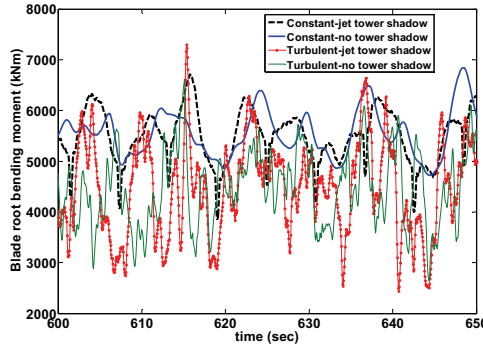

Figure 8: Blade root bending moment time history for the below-rated wind speed case (V =8 m/sec, I =0.18, H_S =2.5 m and T_P =9.8 sec), tower shadow and turbulence effects on the wave-wind-induced dynamic response of a downwind TLS.

Figure 9 shows the blade root bending moment spectrum for the downwind TLS subjected to stochastic wave and wind actions for the below-rated wind speed case. The turbulent wind has energy in the low frequency range and can excite the low resonant responses. The surge resonant response appears due to the turbulence effects. However, in the constant wind cases, the resonant responses do not affect the structural responses of blade. The tower shadow and turbulence do not affect the wave frequency part of the responses. The first,

second and third rotor harmonics are obviously affected by the tower shadow and turbulence. The effect of the turbulence is greater than the tower shadow.

Figure 10 and 11 show the mean value and standard deviation of the blade root bending moment (BM) for different environmental conditions, respectively. Significant wave heights refer to the load cases in Table 5 and the corresponding wind speed. The tower shadow and turbulence effects on the wave-wind-induced dynamic response of a downwind TLS are studied. The wind turbine is shut down for wind speeds higher than 25 m/sec. The results show that the mean values of the blade structural responses are not affected very much by the turbulence and tower shadow. The maximum of the mean response in the 1-hour analysis is linked to the rated wind speed. However, the maximum of the standard deviation for constant and turbulent wind occurs in the over-rated wind (operational) and storm wind (survival), respectively. The results show that the ratio of the standard deviation of the blade root bending moment for turbulent and constant wind is up to 8.5 times in the survival conditions.

It is necessary to note that the simplified tower shadow models are applied in the present research. In future, more advanced methods such as computational fluid dynamic (CFD) can be used to study more precisely the tower shadow effects for floating wind turbines. Generally, the influence from tower shadow is much less significant with turbulent wind loading compared to constant wind loading. The maximum velocity deficit will be much smaller for a floating wind turbine than a more stationary tower because the shadow and thus also the velocity deficit in time is being spread over a much larger area than the tower diameter due to the tower motion. For a bottom fixed turbine and a floating wind turbine the absolute contribution from the tower deficit is almost the same. But, for a fixed turbine, the tower shadow has a relatively higher contribution to the total response standard deviation because the other contribution to the standard deviation is only from the turbulence. However, for a floating wind turbine wave-induced motions have a significant contribution to the standard deviation of the responses.

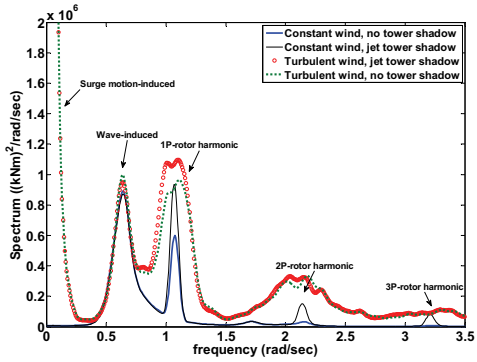

Figure 9: Blade root bending moment spectrum for the below-rated wind speed case (V =8 m/sec, I =0.18, H_S =2.5 m and T_P =9.8 sec), tower shadow and turbulence effects on the wave-wind-induced dynamic response of a downwind TLS.

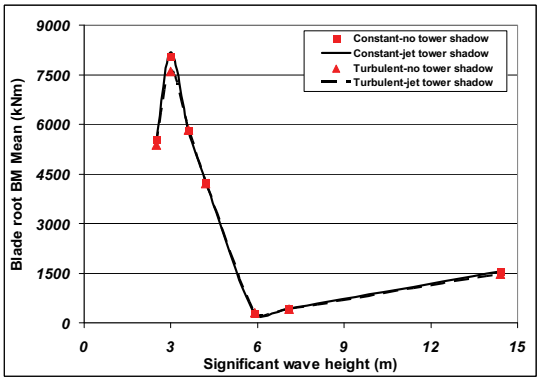

Figure 10: The mean value of the blade root bending moment (BM), tower shadow and turbulence effects on the wave-wind-induced dynamic response of a downwind TLS. The wind turbine is shut down for wind speeds higher than 25 m/sec. Significant wave heights refer to the load cases in Table 5 and the corresponding wind speeds.

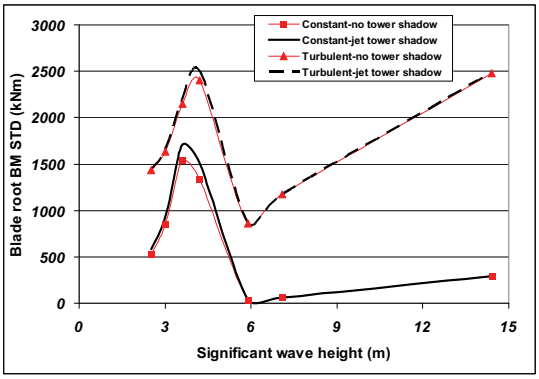

Figure 11: The standard deviation of the blade root bending moment (BM), tower shadow and turbulence effects on the wave-wind-induced dynamic response of a downwind TLS. The wind turbine is shut down for wind speeds higher than 25 m/sec. Significant wave heights refer to the load cases in Table 5 and the corresponding wind speeds.

Nacelle Surge Motion

Figure 12 shows the nacelle surge spectrum for the downwind TLS subjected to stochastic wave and wind actions for survival environmental conditions. The wave frequency part of the response is not affected very much by the wind action. The aerodynamic damping is active in reducing the pitch resonant response, which is clear when comparing the wave only and the wind-wave-induced pitch resonant response. The turbulent wind has energy in the low frequency region and can excite the resonant responses. The surge resonant response is excited due to the aerodynamic excitation for both turbulent and constant wind.

Figure 13 and 14 show the mean and standard deviation of the nacelle surge for different environmental conditions, respectively. Significant wave heights refer to the load cases in Table 5 and the corresponding wind speeds. The tower shadow and turbulence effects on the wave-wind-induced dynamic response of a downwind TLS are studied. The wind turbine is shut down for wind speeds higher than 25 m/sec. The results show that the mean of the nacelle surge motions are not affected very much by the turbulence and tower shadow. The maximum of the mean response in a 1-hour analysis is linked to the rated wind speed. However, the maximum of the standard deviation occurs in the survival conditions. The results show that the ratio of the standard deviation of the nacelle surge motion for turbulent and constant wind is up to 2.3 in the operational conditions.

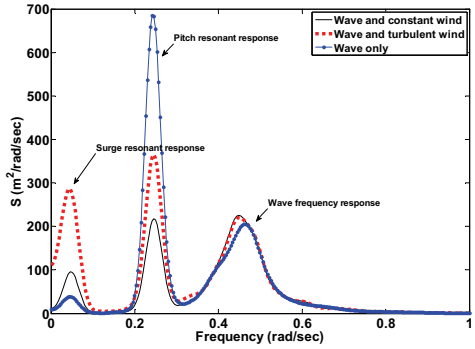

Figure 12: Nacelle surge spectrum for survival environmental conditions (V =49 m/sec, I =0.10, H_S =14.4 m and T_P =13.3 sec), wave-induced versus wave-wind-induced dynamic responses for constant and turbulent wind for a shutdown downwind TLS.

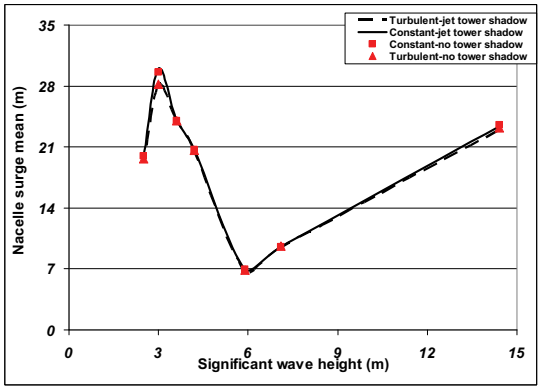

Figure 13: The mean of the nacelle surge to study the tower shadow and turbulence effects on the wave-wind-induced dynamic response of a downwind TLS. The wind turbine is shut down for wind speeds higher than 25 m/sec. Significant wave heights refer to the load cases in Table 5 and the corresponding wind speeds.

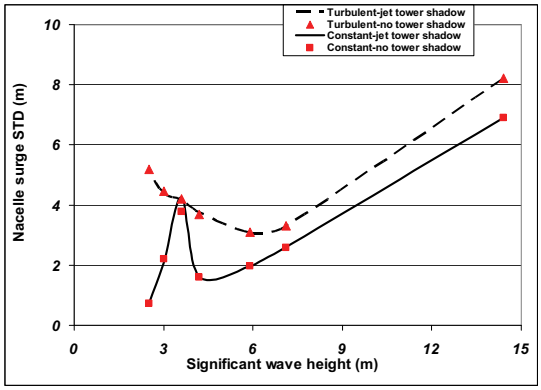

Figure 14: The standard deviation of the nacelle surge to study the tower shadow and turbulence effects on the wave-wind-induced dynamic response of a downwind TLS. The wind turbine is shut down for wind speeds higher than 25 m/sec. Significant wave heights refer to the load cases in Table 5 and the corresponding wind speeds.

Tension Response

Figure 15 shows the tension spectrum for the downwind TLS subjected to stochastic wave and wind actions for the over-rated wind speed case. The low frequency part of the response is not affected very much by the turbulence. The key frequencies in Figure 15 are similar to those in Figure 7. The heave resonant response increased due to the turbulent wind effects and hence the extra aerodynamic loads; see Figure 9. One option to remove such a huge heave resonant response is increasing the hydrodynamic damping in the heave direction, i.e., by adding some heave damper plates. The other option is to increase the heave natural frequency, i.e., above 5 rad/sec, to decrease the turbulence effects.

Figure 16 and 17 show the mean value and standard deviation of the tension for different environmental conditions. Significant wave heights refer to the load cases in Table 5 and the corresponding wind speeds. The tower shadow and turbulence effects on the wave-wind-induced dynamic response of a downwind TLS are studied. The wind turbine is shut down for wind speeds higher than 25 m/sec. The results show that the mean of the tension response are not affected very much by the turbulence and tower shadow. The maximum of the mean response in the 1-hour analysis is linked to the rated wind speed. However, the maximum of the standard deviation occurs in the survival conditions. The results show that the ratio of the standard deviation of the tension response for the turbulent and constant wind is up to 1.4 in the operational conditions.

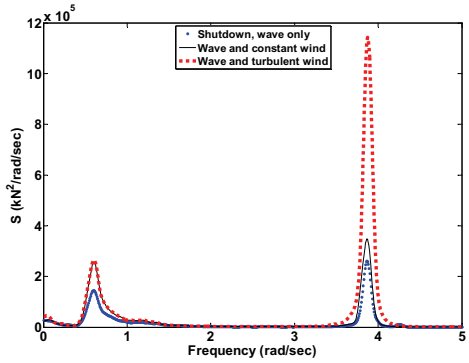

Figure 15: Tension spectrum for over-rated wind speed case (V =17 m/sec, I =0.15, H_S =4.2 m and T_P =10.5), wave-induced versus wave-wind-induced dynamic response for constant and turbulent wind for a downwind TLS.

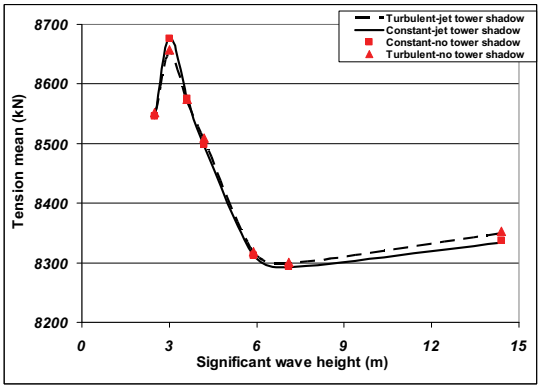

Figure 16: The mean value of the tension to study the tower shadow and turbulence effects on the wave-wind-induced dynamic response of a downwind TLS. The wind turbine is shut down for wind speeds higher than 25 m/sec. Significant wave heights refer to the load cases in Table 5 and the corresponding wind speeds.

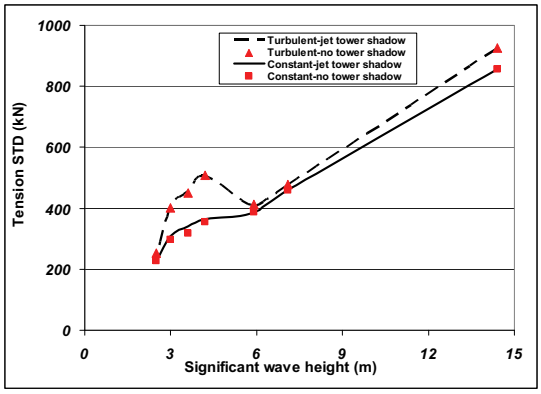

Figure 17: The standard deviation of the tension to study the tower shadow and turbulence effects on the wave-wind-induced dynamic response of a downwind TLS. The wind turbine is shut down for wind speeds higher than 25 m/sec. Significant wave heights refer to the load cases in Table 5 and the corresponding wind speeds.

Generated Power

Tables 7 and 8 list the mean value and standard deviation of the electrical power for TLS with the downwind rotor configuration subjected to wave-wind actions. The tower shadow and turbulence have small effects on the mean of the power. However, the effect of the turbulence on the standard deviation of the power is greater. The relative magnitude of the tower shadow effects on the responses compared to turbulence is less.

Table 7: The mean value of electrical power (MW) for TLS with a downwind rotor subjected to wave and wind actions. Wind velocities refer to the load cases in Table 5 and the corresponding wave conditions.

Wind velocity (m/sec)	Constant -no tower shadow	Constant -jet tower shadow	Turbulent -no tower shadow	Turbulent -jet tower shadow
8	1.77	1.75	1.76	1.74
11.2	4.44	4.43	4.21	4.18
14	5.00	4.98	4.87	4.86
17	5.00	5.00	5.01	5.01

Table 8: The standard deviation of electrical power (MW) for TLS with a downwind rotor subjected to wave and wind actions. Wind velocities refer to the load cases in Table 5 and the corresponding wave conditions.

Wind velocity (m/sec)	Constant -no tower shadow	Constant -jet tower shadow	Turbulent -no tower shadow	Turbulent -jet tower shadow
8	0.03	0.03	0.55	0.54
11.2	0.65	0.65	0.92	0.92
14	0.26	0.34	0.52	0.53
17	0.13	0.13	0.29	0.30

Bending moment at the tower-spar interface

The effects of turbulence and tower shadow on the bending moment response at the tower-spar interface are also studied. Figure 18 shows the bending moment spectrum for a downwind TLS subjected to stochastic wave and wind actions in survival environmental conditions. The wave-induced and wind-wave-induced responses for a constant and turbulent wind are compared. The wave frequency responses are not affected by the aerodynamic actions. The aerodynamic damping in wind-wave-induced cases helps to reduce the pitch resonant response. The elastic response for the wave only case is higher than those values for the wind-wave-induced cases due to the positive aerodynamic damping.

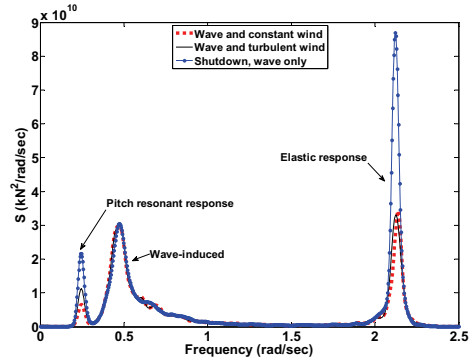

Figure 18: Spectrum of the bending moment at the tower-spar interface for survival environmental conditions (V =49 m/sec, I =0.10, H_S =14.4 m and T_P =13.3 sec), wave-induced versus wave-wind-induced dynamic response for constant and turbulent wind for a shutdown downwind TLS.

Figures 19 and 20 show the mean value and standard deviation of the bending moment at the tower-spar interface for different load cases. The turbulent wind and constant wind actions considering the effects of the tower shadow are studied. The results show that the structural responses are not affected significantly by the tower shadow and turbulence effects in the present case study.

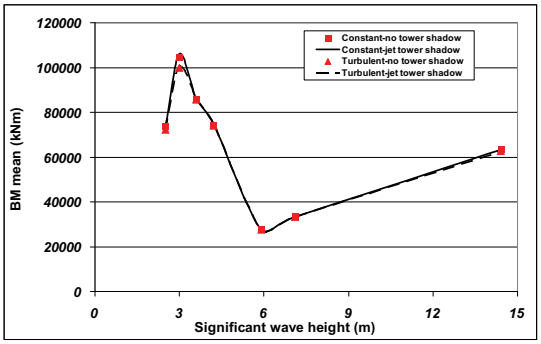

Figure 19: The mean value of the bending moment at the tower-spar interface to study the tower shadow and turbulence effects on the wave-wind-induced dynamic response of a downwind TLS. The wind turbine is shutdown for wind speeds higher than 25 m/sec. Significant wave heights refer to the load cases in Table 5 and the corresponding wind speeds.

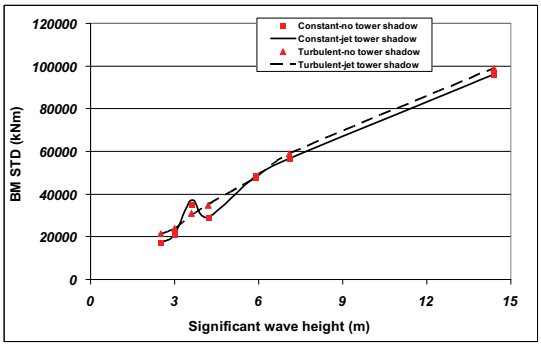

Figure 20: The standard deviation of the bending moment at the tower-spar interface to study the tower shadow and turbulence effects on the wave-wind-induced dynamic response of a downwind TLS. The wind turbine is shutdown for wind speeds higher than 25 m/sec. Significant wave heights refer to the load cases in Table 5 and the corresponding wind speeds.

Extreme value and normalised maximum responses

The extreme value responses depend on the concept and offshore site. Proper extreme value estimation using extrapolation based on the previous study [6] is applied herein. Five identical and independent 1-hour simulations are used. The maximum responses corresponding to an up-crossing rate of 0.0001 are found to be close to the most probable 3-hour extreme value. A previous study showed that the uncertainty of such an extrapolation is less than 2%. The maximum responses for the bending moment (BBM) at the blade root, bending moment (BM) at the tower-spar interface, shear force (SF) at the tower-spar interface, nacelle surge (NS) and Tension (TE) are listed in Table 9. Wind speed (V) refers to the load cases in Table 5. The statistical characteristics are based on five 1-hour samples. The maximum responses correspond to an up-crossing rate of 0.0001 and are obtained by extrapolation. The extreme value of the responses occurs in survival conditions, except that, for the blade root bending moment (BBM), the extreme value response under the survival and operational conditions are close. The ratio of the responses to the 100-year environmental conditions and to the load case associated with the rated wind speed can be as high as 2.6, 3.2, 1.3 and 1.2 for the bending moment (BM), shear force (SF), nacelle surge (NS) and tension (TE) responses, respectively. This finding shows that, for this floating wind turbine, the extreme value of responses can occur under survival conditions. However, land-based wind turbine extreme values are linked to the rated wind speed and occur under operational conditions.

The extreme value response can be roughly estimated as $\mu_x + k\sigma_x$, where μ_x is the mean value, σ_x is the standard deviation and k is the normalised maximum response ($\frac{x_{\max} - \mu_x}{\sigma_x}$). The normalised maximum responses for different load cases for the TLS subjected to stochastic wind and waves are discussed below. To draw more generalised conclusions, it is possible to present normalised responses. The normalised maximum of the responses for different load cases, considering turbulent winds, are presented in Figure 21.

Table 9: Maximum of the bending moment (BBM) at the blade root, bending moment (BM) at the tower-spar interface, shear force (SF) at the tower-spar interface, nacelle surge (NS) and tension (TE). The wind speed (V) refers to the load cases in Table 5. The statistical characteristics are based on five 1-hour samples. The maximum responses correspond to an up-crossing rate of 0.0001 and are obtained by extrapolation.

V (m/sec)	BBM (kNm)	BM (kNm)	SF (kN)	NS (m)	TE (kN)
8	11784	154163	1327	34	9764
11.2	13306	183495	1591	41	10193
14	14207	204589	1871	38	10276
17	14380	215765	1953	34	10440
25	3994	217404	2214	18	9681
30	5129	262168	2741	24	9810
49	11849	470096	5103	53	11899

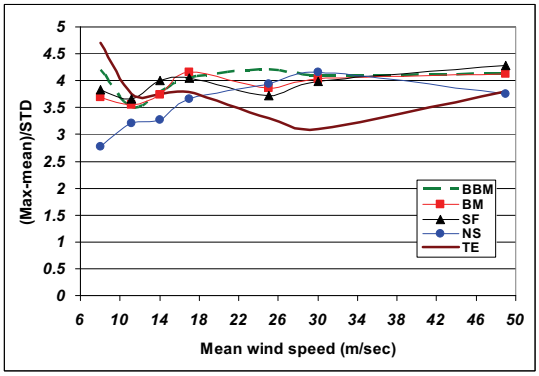

Figure 21: Normalised maximum of the bending moment (BBM) at the blade root, bending moment (BM) at the tower-spar interface, shear force (SF) at the tower-spar interface, nacelle surge (NS) and tension (TE). The wind speed (V) refers to the load cases in Table 5. The statistical characteristics are based on five 1-hour samples. The maximum responses correspond to an up-crossing rate of 0.0001 and are obtained by extrapolation.

Five identical and independent 1-hour integrated analyses for each load cases are simulated. The mean and standard deviation of the responses are obtained by averaging the mean and standard deviations of the five 1-hour ensembles. Extrapolation is used to reduce uncertainty in the estimated extreme values. The normalised maximum for the bending moment (BBM) at the blade root, bending moment (BM) at the tower-spar interface, shear force (SF) at the tower-spar interface, nacelle surge (NS) and tension (TE) are shown in Figure 21. For the present concept, the normalised responses corresponding to an up-crossing rate of 0.0001 vary between 3 and 5. Accepting the uncertainty involved in the present extrapolated maxima, these values provide insight regarding the responses of offshore wind turbines. However, the normalised responses depend on the concept, environmental conditions and offshore site.

CONCLUSIONS

This paper deals with the stochastic dynamic response of TLS wind turbines. The comparison of wave-induced and wind-wave-induced responses for a floating downwind TLS with parked and operating rotors in operational and survival conditions showed that:

1) The wave frequency responses are not affected very much by aerodynamic and controller actions.
2) For below-rated wind speeds, no negative damping occurs because the controller does not feather the blades for this wind speed region.
3) The surge resonant response governs the responses for the rated wind speed load case. The controller introduces some negative damping to surge resonant response for rated wind speeds.
4) The pitch resonant response is greatly affected by the negative damping of the collective blade pitch controller for over-rated wind speed region.
5) For survival cases, the aerodynamic damping helps to reduce the pitch motion resonance. In storm and hurricane conditions, the wave loading is dominant compared to the wind loads.

By tuning the controller gains, it is possible to prevent negative damping. In this study, the controller is tuned to have a natural frequency lower than the pitch resonant response frequency. The comparison of tuned and untuned controller showed that the deployment of the constant torque algorithm and tuning the controller gains helps to decrease the motion instabilities and improve the power production for the over-rated wind speed. At the rated wind speed, the response is governed by the surge resonance and the tuning effect is less effective. However, for the over-rated wind speed region,

because the response is governed by the pitch resonant motion, the tuning is very effective to remove the negative damping.

Comparison of statistical characteristics of responses for tuned and untuned controllers for the wind turbine subjected to wave and wind loads at over-rated wind speeds showed that the standard deviation (dynamic part) of the responses are decreased due to the removal of the negative damping. The ratio between the standard deviation of the power applying the untuned and tuned controllers for the over-rated wind speed case is 8.1. For the nacelle surge motion, the ratio of standard deviation with the untuned and tuned controllers is up to 14.5. Reducing the standard deviation of responses can help increase the fatigue life of the system. The results show that ameliorating the negative damping reduces the standard deviation of the structural dynamic responses up to 4.4 times.

The comparison of upwind and downwind configurations of floating TLS shows that the responses are very close for these turbines. However, some small differences are clear, which can be due to small modifications to the upwind turbine to make it a downwind turbine.

The effects of the turbulence and tower shadow on the different structural and motion responses are discussed in this paper. The results show that the global responses are less affected by the tower shadow. However, the blade root bending moment and the dynamic part of the responses are more affected. The relative magnitude of the turbulence effects is larger than the tower shadow effects. The ratio of the standard deviation of the bending moment at the blade root, nacelle surge motion and tension response for turbulent and constant wind speeds are 8.5, 2.3 and 1.4, respectively. The results show that the tower shadow does not significantly affect the mean value of the power and global responses.

It is necessary to note that the simplified tower shadow models are applied in the present research. In future, more advanced methods such as computational fluid dynamic (CFD) can be used to study the tower shadow effects for floating wind turbines. Generally, the influence from tower shadow is much less significant with turbulent wind loading compared to constant wind loading. The maximum velocity deficit will be much smaller for a floating wind turbine than a more stationary tower because the shadow and thus also the velocity deficit in time is being spread over a much larger area than the tower diameter due to the tower motion. For a bottom fixed turbine and a floating wind turbine the absolute contribution from the tower deficit is the almost the same. But, for a fixed turbine, the tower shadow has a relatively higher contribution to the total response standard deviation because the other contribution to the standard deviation is only from the turbulence. However, for a floating wind turbine wave-induced motions have a significant contribution to the standard deviation of the responses.

It is important to keep in mind that for land based wind turbines, the extreme response usually occurs in the operational cases related to rated wind speeds, but, for floating wind turbines, the extreme responses can occur in harsh environmental conditions when the rotor is parked. The ratio of the responses to 100-year environmental conditions and to the load case associated with the rated wind speed found to be as high as 2.6, 3.2, 1.3 and 1.2 for the bending moment (BM), shear force (SF), nacelle surge (NS) and tension (TE) responses, respectively.

It is noted that the maximum response in a 3-hour period can be estimated as the mean value plus k times the standard deviation. For the TLS-type wind turbine studied here, the k corresponding to up-crossing rate of 0.0001 varies between 3 and 5.

FURTHER WORK

In this research, collective blade pitch control is applied. Due to the lack of yaw stiffness and a proper yaw controller, the yaw motion is constrained. More advanced control algorithms such as an individual blade pitch controller for the tension leg spar wind turbine concept are needed to stabilise the yaw motion. Further research is needed to investigate the proper yaw stiffness and the selection of the yaw bearing (top of the tower, spar-tower interface or leg-spar joint). Further studies are needed to examine the responses in fault conditions. The tower shadow models used in the preset study are simplified models representing the velocity deficit due to the tower presence. In future, more advanced numerical methods, for i.e. computational fluid dynamics (CFD) can be used to study more precisely the tower shadow effects especially for downwind floating wind turbines.

ACKNOWLEDGEMENTS

The first author would like to thank Dr. Jason Jonkman from NREL, USA and Torben J. Larsen from Risø DTU, Denmark for discussions regarding downwind turbines. The

authors would like to thank Prof. Jørgen Amdahl from NTNU and Dr. Tore Holmas from Virtual Prototyping for discussions regarding the SWAY. The authors would also like to acknowledge the financial support from the Norwegian Research Council, which has been granted through the Centre for Ships and Ocean Structures (CeSOS).

REFERENCES

[1] Karimirad M., Gao Z. and Moan T., "Dynamic Motion Analysis of Catenary Moored Spar Wind Turbine in Extreme Environmental Condition", Proceeding of the European Offshore Wind Conference, EOW2009, September 2009, Stockholm, Sweden

[2] Holmas T. and Amdahl J., "Design of Floating Wind Turbines'', Computational Methods in Marine Engineering III, Published by CIMNE, Trondheim, Norway, 2009

[3] Meissonnier Q., Karimirad M., Gao Z. and Moan T., "Hydro-elastic Code-to-Code Comparison for a Tension Leg Spar Type Floating Wind Turbine", Submitted to Journal of Marine Structures

[4] Faltinsen O. M., "Sea Loads on Ships and Offshore Structures", Cambridge University Press, UK, 1995

[5] Karimirad M. and Moan T., "Wave and Wind Induced Dynamic Response of Catenary Moored Spar Wind Turbine'', Submitted to the Journal of Waterway, Port, Coastal, and Ocean Engineering, ASCE

[6] Karimirad M. and Moan T., "Extreme Dynamic Structural Response Analysis of Catenary Moored Spar Wind Turbine in Harsh Environmental Conditions", Submitted to Journal of Offshore Mechanics and Arctic Engineering (JOMAE), ASME

[7] Larsen T. J., "HAWC2, the User's Manual'', Version 3-9, Risø National Laboratory, DTU, Denmark, 2009

[8] Leishman J. G. and Beddoes T. S. "A Generalised Model for Unsteady Airfoil Behaviour and Dynamic Stall Using the Indicial Method'', Annual Forum of the American Helicopter Society, Washington D.C., USA, 1986

[9] Karimirad M. and Moan T., "Effect of Aerodynamic and Hydrodynamic Damping on Dynamic Response of a Spar Type Floating Wind Turbine '', European Wind Energy Conference EWEC 2010, Warsaw, Poland, 2010

[10] Burton T., Sharpe D., Jenkins N. and Bossanyi E., "Wind Energy Handbook'', John Wiley and Sons Ltd, Chichester, England, 2008

[11] Madsen H. Aa., Johansen J., Sørensen N. N., Larsen G. C. and Hansen M. H. "Simulation of Low Frequency Noise From a Downwind Wind Turbine Rotor'', Aerospace Sciences Meeting and Exhibit, Reno, Nevada, USA, 2007

[12] Jonkman J., Butterfield S., Musial W., and Scott G., "Definition of a 5-MW Reference Wind Turbine for Offshore System Development'', NREL/TP-500-38060. NREL, USA, 2009

[13] Karimirad M. and Moan T., "Ameliorating the Negative Damping in the Dynamic Responses of a Downwind Tension Leg Spar Type Offshore Wind Turbine'', Submitted to European Wind Energy Conference (EWEC2011), Brussels, Belgium, 2011

[14] Larsen T. J. and Hanson T. D., "A method to avoid negative damped low frequent tower vibrations for a floating, pitch controlled wind turbine'', Journal of Physics, The Science of Making Torque from Wind, IOP Publishing, Conference Series75 (2007) 012073, 2007

[15] WAFO, "WAFO theory manual'', Centre for Mathematical Sciences, Lund University, Sweden, 2000

[16] Johannessen K., Meling T. S. and Haver S., "Joint distribution for wind and wave in the Northern North Sea'', ISOPE, Stavanger, Norway, 2001

Previous Ph.D. theses and reports published at the Marine Technology Department, Norwegian University of Science and Technology (NTNU)

R A P P O R T E R
UTGITT VED
INSTITUTT FOR MARIN TEKNIKK
(tidligere: FAKULTET FOR MARIN TEKNIKK)
NORGES TEKNISK-NATURVITENSKAPELIGE UNIVERSITET

Report No.	Author	Title
	Kavlie, Dag	Optimization of Plane Elastic Grillages, 1967
	Hansen, Hans R.	Man-Machine Communication and Data-Storage Methods in Ship Structural Design, 1971
	Gisvold, Kaare M.	A Method for non-linear mixed -integer programming and its Application to Design Problems, 1971
	Lund, Sverre	Tanker Frame Optimalization by means of SUMT-Transformation and Behaviour Models, 1971
	Vinje, Tor	On Vibration of Spherical Shells Interacting with Fluid, 1972
	Lorentz, Jan D.	Tank Arrangement for Crude Oil Carriers in Accordance with the new Anti-Pollution Regulations, 1975
	Carlsen, Carl A.	Computer-Aided Design of Tanker Structures, 1975
	Larsen, Carl M.	Static and Dynamic Analysis of Offshore Pipelines during Installation, 1976
UR-79-01	Brigt Hatlestad, MK	The finite element method used in a fatigue evaluation of fixed offshore platforms. (Dr.Ing. Thesis)
UR-79-02	Erik Pettersen, MK	Analysis and design of cellular structures. (Dr.Ing. Thesis)
UR-79-03	Sverre Valsgård, MK	Finite difference and finite element methods applied to nonlinear analysis of plated structures. (Dr.Ing. Thesis)
UR-79-04	Nils T. Nordsve, MK	Finite element collapse analysis of structural members considering imperfections and stresses due to fabrication. (Dr.Ing. Thesis)
UR-79-05	Ivar J. Fylling, MK	Analysis of towline forces in ocean

		towing systems. (Dr.Ing. Thesis)
UR-80-06	Nils Sandsmark, MM	Analysis of Stationary and Transient Heat Conduction by the Use of the Finite Element Method. (Dr.Ing. Thesis)
UR-80-09	Sverre Haver, MK	Analysis of uncertainties related to the stochastic modeling of ocean waves. (Dr.Ing. Thesis)
UR-81-15	Odland, Jonas	On the Strength of welded Ring stiffened cylindrical Shells primarily subjected to axial Compression
UR-82-17	Engesvik, Knut	Analysis of Uncertainties in the fatigue Capacity of Welded Joints
UR-82-18	Rye, Henrik	Ocean wave groups
UR-83-30	Eide, Oddvar Inge	On Cumulative Fatigue Damage in Steel Welded Joints
UR-83-33	Mo, Olav	Stochastic Time Domain Analysis of Slender Offshore Structures
UR-83-34	Amdahl, Jørgen	Energy absorption in Ship-platform impacts
UR-84-37	Mørch, Morten	Motions and mooring forces of semi submersibles as determined by full-scale measurements and theoretical analysis
UR-84-38	Soares, C. Guedes	Probabilistic models for load effects in ship structures
UR-84-39	Aarsnes, Jan V.	Current forces on ships
UR-84-40	Czujko, Jerzy	Collapse Analysis of Plates subjected to Biaxial Compression and Lateral Load
UR-85-46	Alf G. Engseth, MK	Finite element collapse analysis of tubular steel offshore structures. (Dr.Ing. Thesis)
UR-86-47	Dengody Sheshappa, MP	A Computer Design Model for Optimizing Fishing Vessel Designs Based on Techno-Economic Analysis. (Dr.Ing. Thesis)
UR-86-48	Vidar Aanesland, MH	A Theoretical and Numerical Study of Ship Wave Resistance. (Dr.Ing. Thesis)
UR-86-49	Heinz-Joachim Wessel, MK	Fracture Mechanics Analysis of Crack

		Growth in Plate Girders. (Dr.Ing. Thesis)
UR-86-50	Jon Taby, MK	Ultimate and Post-ultimate Strength of Dented Tubular Members. (Dr.Ing. Thesis)
UR-86-51	Walter Lian, MH	A Numerical Study of Two-Dimensional Separated Flow Past Bluff Bodies at Moderate KC-Numbers. (Dr.Ing. Thesis)
UR-86-52	Bjørn Sortland, MH	Force Measurements in Oscillating Flow on Ship Sections and Circular Cylinders in a U-Tube Water Tank. (Dr.Ing. Thesis)
UR-86-53	Kurt Strand, MM	A System Dynamic Approach to One-dimensional Fluid Flow. (Dr.Ing. Thesis)
UR-86-54	Arne Edvin Løken, MH	Three Dimensional Second Order Hydrodynamic Effects on Ocean Structures in Waves. (Dr.Ing. Thesis)
UR-86-55	Sigurd Falch, MH	A Numerical Study of Slamming of Two-Dimensional Bodies. (Dr.Ing. Thesis)
UR-87-56	Arne Braathen, MH	Application of a Vortex Tracking Method to the Prediction of Roll Damping of a Two-Dimension Floating Body. (Dr.Ing. Thesis)
UR-87-57	Bernt Leira, MK	Gaussian Vector Processes for Reliability Analysis involving Wave-Induced Load Effects. (Dr.Ing. Thesis)
UR-87-58	Magnus Småvik, MM	Thermal Load and Process Characteristics in a Two-Stroke Diesel Engine with Thermal Barriers (in Norwegian). (Dr.Ing. Thesis)
MTA-88-59	Bernt Arild Bremdal, MP	An Investigation of Marine Installation Processes – A Knowledge - Based Planning Approach. (Dr.Ing. Thesis)
MTA-88-60	Xu Jun, MK	Non-linear Dynamic Analysis of Space-framed Offshore Structures. (Dr.Ing. Thesis)
MTA-89-61	Gang Miao, MH	Hydrodynamic Forces and Dynamic Responses of Circular Cylinders in Wave Zones. (Dr.Ing. Thesis)
MTA-89-62	Martin Greenhow, MH	Linear and Non-Linear Studies of Waves and Floating Bodies. Part I and Part II. (Dr.Techn. Thesis)

MTA-89-63	Chang Li, MH	Force Coefficients of Spheres and Cubes in Oscillatory Flow with and without Current. (Dr.Ing. Thesis
MTA-89-64	Hu Ying, MP	A Study of Marketing and Design in Development of Marine Transport Systems. (Dr.Ing. Thesis)
MTA-89-65	Arild Jæger, MH	Seakeeping, Dynamic Stability and Performance of a Wedge Shaped Planing Hull. (Dr.Ing. Thesis)
MTA-89-66	Chan Siu Hung, MM	The dynamic characteristics of tilting-pad bearings
MTA-89-67	Kim Wikstrøm, MP	Analysis av projekteringen for ett offshore projekt. (Licenciat-avhandling)
MTA-89-68	Jiao Guoyang, MK	Reliability Analysis of Crack Growth under Random Loading, considering Model Updating. (Dr.Ing. Thesis)
MTA-89-69	Arnt Olufsen, MK	Uncertainty and Reliability Analysis of Fixed Offshore Structures. (Dr.Ing. Thesis)
MTA-89-70	Wu Yu-Lin, MR	System Reliability Analyses of Offshore Structures using improved Truss and Beam Models. (Dr.Ing. Thesis)
MTA-90-71	Jan Roger Hoff, MH	Three-dimensional Green function of a vessel with forward speed in waves. (Dr.Ing. Thesis)
MTA-90-72	Rong Zhao, MH	Slow-Drift Motions of a Moored Two-Dimensional Body in Irregular Waves. (Dr.Ing. Thesis)
MTA-90-73	Atle Minsaas, MP	Economical Risk Analysis. (Dr.Ing. Thesis)
MTA-90-74	Knut-Aril Farnes, MK	Long-term Statistics of Response in Non-linear Marine Structures. (Dr.Ing. Thesis)
MTA-90-75	Torbjørn Sotberg, MK	Application of Reliability Methods for Safety Assessment of Submarine Pipelines. (Dr.Ing. Thesis)
MTA-90-76	Zeuthen, Steffen, MP	SEAMAID. A computational model of the design process in a constraint-based logic programming environment. An example from the offshore domain. (Dr.Ing. Thesis)

MTA-91-77	Haagensen, Sven, MM	Fuel Dependant Cyclic Variability in a Spark Ignition Engine - An Optical Approach. (Dr.Ing. Thesis)
MTA-91-78	Løland, Geir, MH	Current forces on and flow through fish farms. (Dr.Ing. Thesis)
MTA-91-79	Hoen, Christopher, MK	System Identification of Structures Excited by Stochastic Load Processes. (Dr.Ing. Thesis)
MTA-91-80	Haugen, Stein, MK	Probabilistic Evaluation of Frequency of Collision between Ships and Offshore Platforms. (Dr.Ing. Thesis)
MTA-91-81	Sødahl, Nils, MK	Methods for Design and Analysis of Flexible Risers. (Dr.Ing. Thesis)
MTA-91-82	Ormberg, Harald, MK	Non-linear Response Analysis of Floating Fish Farm Systems. (Dr.Ing. Thesis)
MTA-91-83	Marley, Mark J., MK	Time Variant Reliability under Fatigue Degradation. (Dr.Ing. Thesis)
MTA-91-84	Krokstad, Jørgen R., MH	Second-order Loads in Multidirectional Seas. (Dr.Ing. Thesis)
MTA-91-85	Molteberg, Gunnar A., MM	The Application of System Identification Techniques to Performance Monitoring of Four Stroke Turbocharged Diesel Engines. (Dr.Ing. Thesis)
MTA-92-86	Mørch, Hans Jørgen Bjelke, MH	Aspects of Hydrofoil Design: with Emphasis on Hydrofoil Interaction in Calm Water. (Dr.Ing. Thesis)
MTA-92-87	Chan Siu Hung, MM	Nonlinear Analysis of Rotordynamic Instabilities in Highspeed Turbomachinery. (Dr.Ing. Thesis)
MTA-92-88	Bessason, Bjarni, MK	Assessment of Earthquake Loading and Response of Seismically Isolated Bridges. (Dr.Ing. Thesis)
MTA-92-89	Langli, Geir, MP	Improving Operational Safety through exploitation of Design Knowledge - an investigation of offshore platform safety. (Dr.Ing. Thesis)
MTA-92-90	Sævik, Svein, MK	On Stresses and Fatigue in Flexible Pipes. (Dr.Ing. Thesis)
MTA-92-91	Ask, Tor Ø., MM	Ignition and Flame Growth in Lean Gas-Air Mixtures. An Experimental Study

		with a Schlieren System. (Dr.Ing. Thesis)
MTA-86-92	Hessen, Gunnar, MK	Fracture Mechanics Analysis of Stiffened Tubular Members. (Dr.Ing. Thesis)
MTA-93-93	Steinebach, Christian, MM	Knowledge Based Systems for Diagnosis of Rotating Machinery. (Dr.Ing. Thesis)
MTA-93-94	Dalane, Jan Inge, MK	System Reliability in Design and Maintenance of Fixed Offshore Structures. (Dr.Ing. Thesis)
MTA-93-95	Steen, Sverre, MH	Cobblestone Effect on SES. (Dr.Ing. Thesis)
MTA-93-96	Karunakaran, Daniel, MK	Nonlinear Dynamic Response and Reliability Analysis of Drag-dominated Offshore Platforms. (Dr.Ing. Thesis)
MTA-93-97	Hagen, Arnulf, MP	The Framework of a Design Process Language. (Dr.Ing. Thesis)
MTA-93-98	Nordrik, Rune, MM	Investigation of Spark Ignition and Autoignition in Methane and Air Using Computational Fluid Dynamics and Chemical Reaction Kinetics. A Numerical Study of Ignition Processes in Internal Combustion Engines. (Dr.Ing. Thesis)
MTA-94-99	Passano, Elizabeth, MK	Efficient Analysis of Nonlinear Slender Marine Structures. (Dr.Ing. Thesis)
MTA-94-100	Kvålsvold, Jan, MH	Hydroelastic Modelling of Wetdeck Slamming on Multihull Vessels. (Dr.Ing. Thesis)
MTA-94-102	Bech, Sidsel M., MK	Experimental and Numerical Determination of Stiffness and Strength of GRP/PVC Sandwich Structures. (Dr.Ing. Thesis)
MTA-95-103	Paulsen, Hallvard, MM	A Study of Transient Jet and Spray using a Schlieren Method and Digital Image Processing. (Dr.Ing. Thesis)
MTA-95-104	Hovde, Geir Olav, MK	Fatigue and Overload Reliability of Offshore Structural Systems, Considering the Effect of Inspection and Repair. (Dr.Ing. Thesis)
MTA-95-105	Wang, Xiaozhi, MK	Reliability Analysis of Production Ships with Emphasis on Load Combination and Ultimate Strength. (Dr.Ing. Thesis)

MTA-95-106	Ulstein, Tore, MH	Nonlinear Effects of a Flexible Stern Seal Bag on Cobblestone Oscillations of an SES. (Dr.Ing. Thesis)
MTA-95-107	Solaas, Frøydis, MH	Analytical and Numerical Studies of Sloshing in Tanks. (Dr.Ing. Thesis)
MTA-95-108	Hellan, Øyvind, MK	Nonlinear Pushover and Cyclic Analyses in Ultimate Limit State Design and Reassessment of Tubular Steel Offshore Structures. (Dr.Ing. Thesis)
MTA-95-109	Hermundstad, Ole A., MK	Theoretical and Experimental Hydroelastic Analysis of High Speed Vessels. (Dr.Ing. Thesis)
MTA-96-110	Bratland, Anne K., MH	Wave-Current Interaction Effects on Large-Volume Bodies in Water of Finite Depth. (Dr.Ing. Thesis)
MTA-96-111	Herfjord, Kjell, MH	A Study of Two-dimensional Separated Flow by a Combination of the Finite Element Method and Navier-Stokes Equations. (Dr.Ing. Thesis)
MTA-96-112	Æsøy, Vilmar, MM	Hot Surface Assisted Compression Ignition in a Direct Injection Natural Gas Engine. (Dr.Ing. Thesis)
MTA-96-113	Eknes, Monika L., MK	Escalation Scenarios Initiated by Gas Explosions on Offshore Installations. (Dr.Ing. Thesis)
MTA-96-114	Erikstad, Stein O., MP	A Decision Support Model for Preliminary Ship Design. (Dr.Ing. Thesis)
MTA-96-115	Pedersen, Egil, MH	A Nautical Study of Towed Marine Seismic Streamer Cable Configurations. (Dr.Ing. Thesis)
MTA-97-116	Moksnes, Paul O., MM	Modelling Two-Phase Thermo-Fluid Systems Using Bond Graphs. (Dr.Ing. Thesis)
MTA-97-117	Halse, Karl H., MK	On Vortex Shedding and Prediction of Vortex-Induced Vibrations of Circular Cylinders. (Dr.Ing. Thesis)
MTA-97-118	Igland, Ragnar T., MK	Reliability Analysis of Pipelines during Laying, considering Ultimate Strength under Combined Loads. (Dr.Ing. Thesis)
MTA-97-119	Pedersen, Hans-P., MP	Levendefiskteknologi for fiskefartøy.

		(Dr.Ing. Thesis)
MTA-98-120	Vikestad, Kyrre, MK	Multi-Frequency Response of a Cylinder Subjected to Vortex Shedding and Support Motions. (Dr.Ing. Thesis)
MTA-98-121	Azadi, Mohammad R. E., MK	Analysis of Static and Dynamic Pile-Soil-Jacket Behaviour. (Dr.Ing. Thesis)
MTA-98-122	Ulltang, Terje, MP	A Communication Model for Product Information. (Dr.Ing. Thesis)
MTA-98-123	Torbergsen, Erik, MM	Impeller/Diffuser Interaction Forces in Centrifugal Pumps. (Dr.Ing. Thesis)
MTA-98-124	Hansen, Edmond, MH	A Discrete Element Model to Study Marginal Ice Zone Dynamics and the Behaviour of Vessels Moored in Broken Ice. (Dr.Ing. Thesis)
MTA-98-125	Videiro, Paulo M., MK	Reliability Based Design of Marine Structures. (Dr.Ing. Thesis)
MTA-99-126	Mainçon, Philippe, MK	Fatigue Reliability of Long Welds Application to Titanium Risers. (Dr.Ing. Thesis)
MTA-99-127	Haugen, Elin M., MH	Hydroelastic Analysis of Slamming on Stiffened Plates with Application to Catamaran Wetdecks. (Dr.Ing. Thesis)
MTA-99-128	Langhelle, Nina K., MK	Experimental Validation and Calibration of Nonlinear Finite Element Models for Use in Design of Aluminium Structures Exposed to Fire. (Dr.Ing. Thesis)
MTA-99-129	Berstad, Are J., MK	Calculation of Fatigue Damage in Ship Structures. (Dr.Ing. Thesis)
MTA-99-130	Andersen, Trond M., MM	Short Term Maintenance Planning. (Dr.Ing. Thesis)
MTA-99-131	Tveiten, Bård Wathne, MK	Fatigue Assessment of Welded Aluminium Ship Details. (Dr.Ing. Thesis)
MTA-99-132	Søreide, Fredrik, MP	Applications of underwater technology in deep water archaeology. Principles and practice. (Dr.Ing. Thesis)
MTA-99-133	Tønnessen, Rune, MH	A Finite Element Method Applied to Unsteady Viscous Flow Around 2D Blunt Bodies With Sharp Corners. (Dr.Ing.

		Thesis)
MTA-99-134	Elvekrok, Dag R., MP	Engineering Integration in Field Development Projects in the Norwegian Oil and Gas Industry. The Supplier Management of Norne. (Dr.Ing. Thesis)
MTA-99-135	Fagerholt, Kjetil, MP	Optimeringsbaserte Metoder for Ruteplanlegging innen skipsfart. (Dr.Ing. Thesis)
MTA-99-136	Bysveen, Marie, MM	Visualization in Two Directions on a Dynamic Combustion Rig for Studies of Fuel Quality. (Dr.Ing. Thesis)
MTA-2000-137	Storteig, Eskild, MM	Dynamic characteristics and leakage performance of liquid annular seals in centrifugal pumps. (Dr.Ing. Thesis)
MTA-2000-138	Sagli, Gro, MK	Model uncertainty and simplified estimates of long term extremes of hull girder loads in ships. (Dr.Ing. Thesis)
MTA-2000-139	Tronstad, Harald, MK	Nonlinear analysis and design of cable net structures like fishing gear based on the finite element method. (Dr.Ing. Thesis)
MTA-2000-140	Kroneberg, André, MP	Innovation in shipping by using scenarios. (Dr.Ing. Thesis)
MTA-2000-141	Haslum, Herbjørn Alf, MH	Simplified methods applied to nonlinear motion of spar platforms. (Dr.Ing. Thesis)
MTA-2001-142	Samdal, Ole Johan, MM	Modelling of Degradation Mechanisms and Stressor Interaction on Static Mechanical Equipment Residual Lifetime. (Dr.Ing. Thesis)
MTA-2001-143	Baarholm, Rolf Jarle, MH	Theoretical and experimental studies of wave impact underneath decks of offshore platforms. (Dr.Ing. Thesis)
MTA-2001-144	Wang, Lihua, MK	Probabilistic Analysis of Nonlinear Wave-induced Loads on Ships. (Dr.Ing. Thesis)
MTA-2001-145	Kristensen, Odd H. Holt, MK	Ultimate Capacity of Aluminium Plates under Multiple Loads, Considering HAZ Properties. (Dr.Ing. Thesis)
MTA-2001-146	Greco, Marilena, MH	A Two-Dimensional Study of Green-Water Loading. (Dr.Ing. Thesis)

MTA-2001-147	Heggelund, Svein E., MK	Calculation of Global Design Loads and Load Effects in Large High Speed Catamarans. (Dr.Ing. Thesis)
MTA-2001-148	Babalola, Olusegun T., MK	Fatigue Strength of Titanium Risers – Defect Sensitivity. (Dr.Ing. Thesis)
MTA-2001-149	Mohammed, Abuu K., MK	Nonlinear Shell Finite Elements for Ultimate Strength and Collapse Analysis of Ship Structures. (Dr.Ing. Thesis)
MTA-2002-150	Holmedal, Lars E., MH	Wave-current interactions in the vicinity of the sea bed. (Dr.Ing. Thesis)
MTA-2002-151	Rognebakke, Olav F., MH	Sloshing in rectangular tanks and interaction with ship motions. (Dr.Ing. Thesis)
MTA-2002-152	Lader, Pål Furset, MH	Geometry and Kinematics of Breaking Waves. (Dr.Ing. Thesis)
MTA-2002-153	Yang, Qinzheng, MH	Wash and wave resistance of ships in finite water depth. (Dr.Ing. Thesis)
MTA-2002-154	Melhus, Øyvin, MM	Utilization of VOC in Diesel Engines. Ignition and combustion of VOC released by crude oil tankers. (Dr.Ing. Thesis)
MTA-2002-155	Ronæss, Marit, MH	Wave Induced Motions of Two Ships Advancing on Parallel Course. (Dr.Ing. Thesis)
MTA-2002-156	Økland, Ole D., MK	Numerical and experimental investigation of whipping in twin hull vessels exposed to severe wet deck slamming. (Dr.Ing. Thesis)
MTA-2002-157	Ge, Chunhua, MK	Global Hydroelastic Response of Catamarans due to Wet Deck Slamming. (Dr.Ing. Thesis)
MTA-2002-158	Byklum, Eirik, MK	Nonlinear Shell Finite Elements for Ultimate Strength and Collapse Analysis of Ship Structures. (Dr.Ing. Thesis)
IMT-2003-1	Chen, Haibo, MK	Probabilistic Evaluation of FPSO-Tanker Collision in Tandem Offloading Operation. (Dr.Ing. Thesis)
IMT-2003-2	Skaugset, Kjetil Bjørn, MK	On the Suppression of Vortex Induced Vibrations of Circular Cylinders by Radial Water Jets. (Dr.Ing. Thesis)
IMT-2003-3	Chezhian, Muthu	Three-Dimensional Analysis of

		Slamming. (Dr.Ing. Thesis)
IMT-2003-4	Buhaug, Øyvind	Deposit Formation on Cylinder Liner Surfaces in Medium Speed Engines. (Dr.Ing. Thesis)
IMT-2003-5	Tregde, Vidar	Aspects of Ship Design: Optimization of Aft Hull with Inverse Geometry Design. (Dr.Ing. Thesis)
IMT-2003-6	Wist, Hanne Therese	Statistical Properties of Successive Ocean Wave Parameters. (Dr.Ing. Thesis)
IMT-2004-7	Ransau, Samuel	Numerical Methods for Flows with Evolving Interfaces. (Dr.Ing. Thesis)
IMT-2004-8	Soma, Torkel	Blue-Chip or Sub-Standard. A data interrogation approach of identity safety characteristics of shipping organization. (Dr.Ing. Thesis)
IMT-2004-9	Ersdal, Svein	An experimental study of hydrodynamic forces on cylinders and cables in near axial flow. (Dr.Ing. Thesis)
IMT-2005-10	Brodtkorb, Per Andreas	The Probability of Occurrence of Dangerous Wave Situations at Sea. (Dr.Ing. Thesis)
IMT-2005-11	Yttervik, Rune	Ocean current variability in relation to offshore engineering. (Dr.Ing. Thesis)
IMT-2005-12	Fredheim, Arne	Current Forces on Net-Structures. (Dr.Ing. Thesis)
IMT-2005-13	Heggernes, Kjetil	Flow around marine structures. (Dr.Ing. Thesis
IMT-2005-14	Fouques, Sebastien	Lagrangian Modelling of Ocean Surface Waves and Synthetic Aperture Radar Wave Measurements. (Dr.Ing. Thesis)
IMT-2006-15	Holm, Håvard	Numerical calculation of viscous free surface flow around marine structures. (Dr.Ing. Thesis)
IMT-2006-16	Bjørheim, Lars G.	Failure Assessment of Long Through Thickness Fatigue Cracks in Ship Hulls. (Dr.Ing. Thesis)
IMT-2006-17	Hansson, Lisbeth	Safety Management for Prevention of

		Occupational Accidents. (Dr.Ing. Thesis)
IMT-2006-18	Zhu, Xinying	Application of the CIP Method to Strongly Nonlinear Wave-Body Interaction Problems. (Dr.Ing. Thesis)
IMT-2006-19	Reite, Karl Johan	Modelling and Control of Trawl Systems. (Dr.Ing. Thesis)
IMT-2006-20	Smogeli, Øyvind Notland	Control of Marine Propellers. From Normal to Extreme Conditions. (Dr.Ing. Thesis)
IMT-2007-21	Storhaug, Gaute	Experimental Investigation of Wave Induced Vibrations and Their Effect on the Fatigue Loading of Ships. (Dr.Ing. Thesis)
IMT-2007-22	Sun, Hui	A Boundary Element Method Applied to Strongly Nonlinear Wave-Body Interaction Problems. (PhD Thesis, CeSOS)
IMT-2007-23	Rustad, Anne Marthine	Modelling and Control of Top Tensioned Risers. (PhD Thesis, CeSOS)
IMT-2007-24	Johansen, Vegar	Modelling flexible slender system for real-time simulations and control applications
IMT-2007-25	Wroldsen, Anders Sunde	Modelling and control of tensegrity structures. (PhD Thesis, CeSOS)
IMT-2007-26	Aronsen, Kristoffer Høye	An experimental investigation of in-line and combined inline and cross flow vortex induced vibrations. (Dr. avhandling, IMT)
IMT-2007-27	Gao, Zhen	Stochastic Response Analysis of Mooring Systems with Emphasis on Frequency-domain Analysis of Fatigue due to Wide-band Response Processes (PhD Thesis, CeSOS)
IMT-2007-28	Thorstensen, Tom Anders	Lifetime Profit Modelling of Ageing Systems Utilizing Information about Technical Condition. (Dr.ing. thesis, IMT)
IMT-2008-29	Berntsen, Per Ivar B.	Structural Reliability Based Position Mooring. (PhD-Thesis, IMT)
IMT-2008-30	Ye, Naiquan	Fatigue Assessment of Aluminium Welded Box-stiffener Joints in Ships

		(Dr.ing. thesis, IMT)
IMT-2008-31	Radan, Damir	Integrated Control of Marine Electrical Power Systems. (PhD-Thesis, IMT)
IMT-2008-32	Thomassen, Paul	Methods for Dynamic Response Analysis and Fatigue Life Estimation of Floating Fish Cages. (Dr.ing. thesis, IMT)
IMT-2008-33	Pákozdi, Csaba	A Smoothed Particle Hydrodynamics Study of Two-dimensional Nonlinear Sloshing in Rectangular Tanks. (Dr.ing.thesis, IMT)
IMT-2007-34	Grytøyr, Guttorm	A Higher-Order Boundary Element Method and Applications to Marine Hydrodynamics. (Dr.ing.thesis, IMT)
IMT-2008-35	Drummen, Ingo	Experimental and Numerical Investigation of Nonlinear Wave-Induced Load Effects in Containerships considering Hydroelasticity. (PhD thesis, CeSOS)
IMT-2008-36	Skejic, Renato	Maneuvering and Seakeeping of a Singel Ship and of Two Ships in Interaction. (PhD-Thesis, CeSOS)
IMT-2008-37	Harlem, Alf	An Age-Based Replacement Model for Repairable Systems with Attention to High-Speed Marine Diesel Engines. (PhD-Thesis, IMT)
IMT-2008-38	Alsos, Hagbart S.	Ship Grounding. Analysis of Ductile Fracture, Bottom Damage and Hull Girder Response. (PhD-thesis, IMT)
IMT-2008-39	Graczyk, Mateusz	Experimental Investigation of Sloshing Loading and Load Effects in Membrane LNG Tanks Subjected to Random Excitation. (PhD-thesis, CeSOS)
IMT-2008-40	Taghipour, Reza	Efficient Prediction of Dynamic Response for Flexible amd Multi-body Marine Structures. (PhD-thesis, CeSOS)
IMT-2008-41	Ruth, Eivind	Propulsion control and thrust allocation on marine vessels. (PhD thesis, CeSOS)
IMT-2008-42	Nystad, Bent Helge	Technical Condition Indexes and Remaining Useful Life of Aggregated Systems. PhD thesis, IMT
IMT-2008-43	Soni, Prashant Kumar	Hydrodynamic Coefficients for Vortex

		Induced Vibrations of Flexible Beams, PhD thesis, CeSOS
IMT-2009-43	Amlashi, Hadi K.K.	Ultimate Strength and Reliability-based Design of Ship Hulls with Emphasis on Combined Global and Local Loads. PhD Thesis, IMT
IMT-2009-44	Pedersen, Tom Arne	Bond Graph Modelling of Marine Power Systems. PhD Thesis, IMT
IMT-2009-45	Kristiansen, Trygve	Two-Dimensional Numerical and Experimental Studies of Piston-Mode Resonance. PhD-Thesis, CeSOS
IMT-2009-46	Ong, Muk Chen	Applications of a Standard High Reynolds Number Model and a Stochastic Scour Prediction Model for Marine Structures. PhD-thesis, IMT
IMT-2009-47	Hong, Lin	Simplified Analysis and Design of Ships subjected to Collision and Grounding. PhD-thesis, IMT
IMT-2009-48	Koushan, Kamran	Vortex Induced Vibrations of Free Span Pipelines, PhD thesis, IMT
IMT-2009-49	Korsvik, Jarl Eirik	Heuristic Methods for Ship Routing and Scheduling. PhD-thesis, IMT
IMT-2009-50	Lee, Jihoon	Experimental Investigation and Numerical in Analyzing the Ocean Current Displacement of Longlines. Ph.d.-Thesis, IMT.
IMT-2009-51	Vestbøstad, Tone Gran	A Numerical Study of Wave-in-Deck Impact usin a Two-Dimensional Constrained Interpolation Profile Method, Ph.d.thesis, CeSOS.
IMT-2009-52	Bruun, Kristine	Bond Graph Modelling of Fuel Cells for Marine Power Plants. Ph.d.-thesis, IMT
IMT-2009-53	Holstad, Anders	Numerical Investigation of Turbulence in a Sekwed Three-Dimensional Channel Flow, Ph.d.-thesis, IMT.
IMT-2009-54	Ayala-Uraga, Efren	Reliability-Based Assessment of Deteriorating Ship-shaped Offshore Structures, Ph.d.-thesis, IMT
IMT-2009-55	Kong, Xiangjun	A Numerical Study of a Damaged Ship in Beam Sea Waves. Ph.d.-thesis,

		IMT/CeSOS.
IMT-2010-56	Kristiansen, David	Wave Induced Effects on Floaters of Aquaculture Plants, Ph.d.-thesis, IMT/CeSOS.
IMT-2010-57	Ludvigsen, Martin	An ROV-Toolbox for Optical and Acoustic Scientific Seabed Investigation. Ph.d.-thesis IMT.
IMT-2010-58	Hals, Jørgen	Modelling and Phase Control of Wave-Energy Converters. Ph.d.thesis, CeSOS.
IMT-2010- 59	Shu, Zhi	Uncertainty Assessment of Wave Loads and Ultimate Strength of Tankers and Bulk Carriers in a Reliability Framework. Ph.d. Thesis, IMT.
IMT-2010-60	Shao, Yanlin	Numerical Potential-Flow Studies on Weakly-Nonlinear Wave-Body Interactions with/without Small Forward Speed, Ph.d.thesis, IMT.
IMT-2010-61	Califano, Andrea	Dynamic Loads on Marine Propellers due to Intermittent Ventilation. Ph.d.thesis, IMT.
IMT-2010-62	El Khoury, George	Numerical Simulations of Massively Separated Turbulent Flows, Ph.d.-thesis, IMT
IMT-2010-63	Seim, Knut Sponheim	Mixing Process in Dense Overflows with Emphasis on the Faroe Bank Channel Overflow. Ph.d.thesis, IMT
IMT-2010-64	Jia, Huirong	Structural Analysis of Intect and Damaged Ships in a Collission Risk Analysis Perspective. Ph.d.thesis CeSoS.
IMT-2010-65	Jiao, Linlin	Wave-Induced Effects on a Pontoon-type Very Large Floating Structures (VLFS). Ph.D.-thesis, CeSOS.
IMT-2010-66	Abrahamsen, Bjørn Christian	Sloshing Induced Tank Roof with Entrapped Air Pocket. Ph.d.thesis, CeSOS.